Fast Electromagnetic Simulation for Interconnects on High Speed Circuits

By

Houfei Chen

A dissertation submitted in partial fulfillment of the requirements for the degree of

Doctor of Philosophy

University of Washington

2002

Program Authorized to Offer Degree: Department of Electrical Engineering

Doctoral Dissertation

In presenting this dissertation in partial fulfillment of the requirements for the Doctoral degree at the University of Washington, I agree that the Library shall make its copies freely available for inspection. I further agree that extensive copying of the dissertation is allowable only for scholarly purposes, consistent with "fair use" as prescribed in the U.S. Copyright Law. Requests for copying or reproduction of this dissertation may be referred to Bell and Howell Information and Learning, 300 North Zeeb Road, P.O. Box 1346, Ann Arbor, MI 48106-1346, or to the author.

Signature 

Date July 25, 2002

University of Washington
Graduate School

This is to certify that I have examined this copy of a doctoral dissertation by

Houfei Chen

and have found that it is complete and satisfactory in all respects,
and that any and all revisions required by the final
examining committee have been made.

Chair of Supervisory Committee:

Leung Tsang

Reading Committee:

Leung Tsang

Vikram Jandhyala

Qin Li

Date: July 29, 2002

University of Washington

Abstract

Fast Electromagnetic Simulation for Interconnects on High Speed Circuits

by Houfei Chen

Chairperson of the Supervisory Committee

Professor Leung Tsang

Department of Electrical Engineering

This research work carries out the analysis of microstrip with gap discontinuity and bypass capacitors on the ground plane. The full wave approach is based on integral equations using the spatial domain Green's function in layered medium. Method of moment solution is obtained with RWG basis function and Galerkin testing. The method is applied to gaps with bypass capacitors in single and double layer structure. Simulation results were obtained for various values and locations of bypass capacitors and for the case of a second reference plane.

This research work presents a full wave modeling technique for vertical vias in multi-layered integrated circuits. The analysis of the interior problem is based upon the cylindrical wave expansion of the magnetic field Green's function; the multiple interaction among vias is modeled by the Foldy-Lax scattering formula. Multi-layered effects are considered using cascaded network of the single-layered components. The exterior problem is analyzed using MOM approach and combined with interior problem into a system of equation to facilitate solution of large number of vias. Problems of several thousand vias are analyzed with moderate CPU and memory requirement. Numerical results are obtained for different via configurations and for large range of frequency. Also illustrated are results for differential signaling with surrounding idle and shorting vias.

The exterior structure of via is further formulated using more rigorous approach. Compared with traces with known characteristic impedance which fails to take into account the corner and pad effect, and compared with thin wire approximation, which is improper for some layout dimensions and also fails to consider the pad effect, this formulation considers the actual layout of the exterior structure thus gives a more reliable simulation. Simulation results are given for reflection characteristic under different pad radius.

This research work also presents the spatial domain layer-medium Green's functions that are used in modeling the gap discontinuity and the exterior structure of via. The Green's functions are calculated by integrating along the Sommerfeld integration path. Convergence of the integration can be facilitated by higher-order asymptotic extractions.

Table of Contents

List of Figures

List of Tables

ACKNOWLEDGEMENTS

I would like to take this opportunity to thank a number of individuals for their assistance in the course of conducting this research work and pursuing this degree. First I wish to express my deep gratitude to my advisor, Prof. Leung Tsang, for his guidance and help throughout this research work. His diligence and expertise in research work shows me the quality of a real scholar and encourages me from time to time. As a mentor, he teaches me well and from those I learned from him, I may benefit for a lifetime.

I would like to thank the rest of my reading committee, Prof. Vikram Jandhyala, for his advice on the exterior formulation of via, Dr. Qin Li, for his help on the simulation of shorting vias and differential signaling, and the discussion with them also benefits me a lot during the research work. I would also like to thank my colleague, Chungchi Huang, for his help and discussion on the layer-medium Green's function.

Finally I would like to thank Washington Technology Center (WTC) and Hyperlynx for their financial support for this research work.

DEDICATION

To my parents and wife

1 Introduction

Continuous advances being made in circuit density and speed, at both the chip level, package level and board level, are placing increasing demands on the simulation techniques on interconnects and discontinuity. If improperly constructed, IC interconnects and discontinuity can degenerate digital-signal quality, induce coupling between signals, and produce radiation at levels that cause the systems in which they are embedded to fail completely. At each level of the design period, engineers need simulation techniques that can predict phenomenons like crosstalk, ringing, ground bounce, reflection, radiation etc. and give design rules which can prevent or reduce this kind of effect. Due to the high speed (up to 15GHz) we are talking about here, besides the traditional circuit level simulation, more simulations are needed that include electromagnetic effects. Some examples are Hspice and Cadence. Both of them are circuit simulation software, but with quasi-static electromagnetic analysis like transmission line model and capacitance extraction.

Circuit models which utilizes quasistatic parameters can no longer well describe the whole structure and its behavior as frequency increases. Although electromagnetic analysis has been introduced into simulation software, however, there is a general need in industry for more accurate and faster models for different kinds of discontinuity and interconnections. Presently at low frequency, one can still omit a via or a gap in simulation and yet get a reasonably good product based on such simulation. But as frequency increases, the structure no longer functions according to the circuit simulations. Even for single component like a diode and MOS transistor, it is necessary now to use rigorous electromagnetic analysis to obtain accurate device modeling parameter for circuit simulation software.

Some electromagnetic analyses have already been used in circuit simulation. Among them, some methods are quite accurate, yet computational intensive and slow, like FDTD (Finite Difference Time Domain method)[1]-[4]. Some are simple yet not accurate enough for densely packed high frequency circuits, e.g. the quasi-static analysis of transmission line model [5][6] and LCR (Inductance, Capacitance and Resistance) extraction [7]-[12]. There is a definite need for fast and accurate electromagnetic analysis. It is hard to find a general purpose simulation technique which is fast and accurate for all kinds of discontinuity, although this kind of technique will be most favorable. Normally, the choice of

electromagnetic simulation approach is structure and geometry dependent.

Due to the fast computer development in the recent decades, most of the discontinuity structures can be and have already been well formulated by general numerical methods like FDTD, MoM (Method of Moment) [13]-[18] and FEM (Finite Element Method) [19]-[23], the procedures are quite general and most of them have already been incorporated into varies commercial software. But as the density and complexity of the circuit increases, pure numerical methods suffer from large memory requirement and relatively slow simulation speed. In a word, the increase of the computer speed and memory cannot keep up with the increase of the complexity of the problems. So in this thesis, most of the research effort are put on the development of fast electromagnetic solver. By examining carefully the numerical and analytical nature of the problem at hand, also by appropriate use of electromagnetic theorems and decomposition of the problems, semi-analytical approaches can be developed which greatly increase the computational speed while reserves the same level of accuracy as pure numerical solver.

In chapter 2 of the thesis, gap discontinuity on the reference plane with bypass capacitors is analyzed. Quasi-static approach gives the low frequency parameters of the discontinuity including extra capacitance and extra inductance. Potential distribution at the gap and current distribution on the ground plane are also presented which shows intuitive characteristics of the discontinuity. In the MoM solution of the integral equation, CG-FFT method is implemented to reduce the computational time from N^3 to $CN\log_2 N$. For high frequency, full wave approach is presented utilizing reciprocity theorem, equivalence principle and spatial domain layered medium Green's function. The analysis shows the resonance effect and it also simulates the effect of the value and location of the bypass capacitors.

In chapter 3, the propagation characteristics of single vertical vias are analyzed for through-hole, single-layered and multi-layered geometry. In the formulation, cylindrical wave expansion of Green's function is carried out to facilitate the analysis considering the cylindrical shape of the via. The exterior structure is analyzed separately by decomposition of the problem, the result of which can also be used in chapter 4 for multiple via coupling cases. It gives a straight forward yet rigorous analysis compared with existing literatures. Vias with different parameters are simulated and their propagation and loss characteristics

are presented.

In chapter 4, the propagation characteristics of multiple vertical vias are analyzed by utilizing the cylindrical wave expansion used in chapter 3 and foldy-lax multiple scattering formulation which characterize the exciting, incident and scattered wave from each via cylinder. Compared with existing literatures, this approach is much straight forward and can account for all orders of coupling among large number of vias. It also has the ability to simulate unsymmetrical via structure. Due to the semi-analytical nature of this approach, and by using iterative approach in the final matrix equation (which incorporates the exterior structure of the via), a problem with the scale of thousands of vias can be solved in the time of one minutes. The simulation result shows clearly that the existence of surrounding vias can have significant effect on the coupling between the two active vias. Results are also shown for the simulation of thousands of passive vias or shorting vias and the effect of surrounding vias on common mode and differential mode in differential signaling.

In chapter 5, the exterior problem of the via is analyzed more thoroughly using the spatial domain layer-medium green's function. Unlike in chapter 3 and 4, where the exterior problem is simplified by thin wire approximation, here it accurately models the microstrip structure and also the pad discontinuity at the corner. EFIE (Electric Field Integral Equation) is established on the surface of the structure and RWG function is used as basis function on the microstrip, pad and also on the vertical section of the exterior part of via. Matrix pencil method is used to extract out the scattering parameter for the exterior discontinuity. Compared with thin wire approximation, this gives much better result for low frequency and thin layer thickness (where thin wire approximation no longer stands). Due to the decomposition we mentioned in chapter 3, the solution of the exterior problem is completely separated with the interior problem, which enables us to elaborate the exterior solution without changing the formulation of the interior problem.

2 Gap discontinuity with bypass capacitors in layered geometry

Consider a microstripline above a ground plane that has a gap. There can be a second ground plane below the first one and there can be bypass capacitors in the gap (Figure 1). The top layer above the microstripline is air, the middle layer between the microstripline and ground plane is dielectric material with a relative dielectric constant of ε_{r1}, the layer below the ground plane can be air or dielectric material.

2.1 Static analysis of the gap discontinuity

In this section, quasi-static analysis is proposed for gap discontinuity on the ground plane, for low frequency range. This analysis is valid at DC and low frequencies when the wavelength is much larger than the dimension of the discontinuity. Although this kind of analysis looks preliminary compared with full wave analysis and may not bear good result in high frequency range, it gives important information for circuit behavior at DC and low frequencies. It also gives circuit characteristics at low frequency which sometimes will help the modelling and prediction of circuit behavior at high frequency range. Even in high speed circuit, high frequency component only happens at signal transition, like rising and falling edges, but it also have stable period which has plenty of DC term in signal spectrum. So even in high speed circuit, quasi-static approaches are still widely used [24]-[27] due to the necessity to analyze the DC and low frequency characteristics of the discontinuity which sometimes may not be obtained by high frequency electromagnetic solver. By using quasi-static approach, the capacitance and inductance of the discontinuity are ready to be extracted which can be used in circuit simulator.

We know as the frequency goes to zero, charges and currents are decoupled and Maxwells equations give rise to two independent systems of equations, namely electrostatic and magnetostatic systems.

2.1.1 Electrostatic analysis

Formulation: For electrostatic case (Figure 2), in region 1:

$$\nabla^2\phi_1 = -\frac{\rho_v}{\varepsilon_1} \quad (1)$$

$$\nabla^2 g_{D1}(\overline{r},\overline{r}') = -\delta(\overline{r}-\overline{r}') \quad (2)$$

In region 2:

$$\nabla^2\phi_2 = 0 \quad (3)$$

$$\nabla^2 g_{D2}(\overline{r},\overline{r}') = -\delta(\overline{r}-\overline{r}') \quad (4)$$

Apply Green's theorem

$$\iiint d\overline{r}(\psi_2\nabla^2\psi_1 - \psi_1\nabla^2\psi_2) = \iint d\overline{S}\cdot(\psi_2\overline{\nabla}\psi_1 - \psi_1\overline{\nabla}\psi_2) \quad (5)$$

in region 1 by setting

$$\psi_1 = \phi_1 \quad (6)$$

$$\psi_2 = g_{D1}(\overline{r},\overline{r}') \quad (7)$$

we have:

$$\phi_1(\overline{r}') = \int_{V_1} d\overline{r} g_{D1}(\overline{r},\overline{r}')\frac{\rho_v(\overline{r})}{\varepsilon_1} + \int_{S_g} dS\phi_1(\overline{r})\frac{\partial g_D}{\partial n} \quad (8)$$

which suggests that the potential in region 1 is due to the charge in region 1 and the equivalent source at the aperture.

Similarly apply Green's theorem in region 2 and we have:

$$\phi_2(\overline{r}') = \int_{S_g} dS\phi_2(\overline{r})\frac{\partial g_{D2}}{\partial n} \quad (9)$$

which suggests that the potential in region 2 is due to the equivalent source at the aperture only.

Integral Equation: We set up integral equations by enforcing boundary conditions on the microstrip and at the aperture:

1) The potential on the microstrip should be constant (assume 1 volt);

2) The normal component of $\overline{D}$ continues at the aperture.

And we have the following integral equation for the electrostatic case:

$$1 = \int_{V_1} d\overline{r} g_{D1}(\overline{r}, \overline{r}') \frac{\rho_v(\overline{r})}{\varepsilon_1} + \int_{S_g} dS \phi_1(\overline{r}) \frac{\partial g_{D1}}{\partial n} \tag{10}$$

$$\varepsilon_1 \left(\int_{V_1} d\overline{r} \frac{\partial g_{D1}(\overline{r}, \overline{r}')}{\partial n'} \frac{\rho_v(\overline{r})}{\varepsilon_1} + \int_{S_g} dS \phi_1(\overline{r}) \frac{\partial^2 g_{D1}}{\partial n \partial n'} \right) = \varepsilon_2 \int_{S_g} dS \phi_2(\overline{r}) \frac{\partial g_{D2}}{\partial n \partial n'} \tag{11}$$

Method of Moment is used to solve the integral equation (10) and (11). The unknowns are the charges on the microstrip and the potentials at the aperture.

Notice that the total charge density is nonzero all along the trace, and it is impossible to use it as unknown for the integral equation, otherwise we will have infinite number of unknowns on the microstrip. We divide the total charge density into two parts: 1) the extra charge density which is due to the discontinuity and 2) the normal charge density of a uniform microstripline which is known given the voltage on the microstrip. We use the extra charge density as the unknown and this charge density will reduce to zero at a short distance away from the gap discontinuity. The effect of the normal charge density due to the microstrip line can be pre-calculated and taken into account in the integral equation (10) and (11).

Results and Discussion: Solving the integral equations will give the extra charge density on the trace and the potential distribution at the gap (figure 3). It shows clearly that the extra charge density concentrates near the discontinuity and reduces to zero at some distance away from the gap. The potential distribution at the gap also concentrates right under the trace and reduces to zero away from the trace. This suggests that the far end of the gap area can be looked as filled with PEC and have a potential of zero. This assumption is further confirmed by the numerical simulation result (table 1) which shows that the extra capacitance does not change much with the length (the direction across the trace) of the gap, but rather sensitive to the width (the direction along the trace) of the gap. The far

end of the gap has a near zero potential, increasing the length of the gap almost makes no change to the total potential distribution.

2.1.2 Magnetostatic analysis

Formulation: The magnetic scalar potential ϕ in region 1 and region 2 are:

$$\begin{aligned}\phi_1 &= \frac{J_s dy'}{2\pi}(\tan^{-1}(\frac{y-y'}{z}) - \tan^{-1}(\frac{y-y'}{z+2h})) \\ &\quad + \iint dy'dz' \frac{2m(y',z')}{4\pi\sqrt{(x+h)^2+(y-y')^2+(z-z')^2}} \qquad (12)\\ \phi_2 &= -\iint dy'dz' \frac{2m(y',z')}{4\pi\sqrt{(x+h)^2+(y-y')^2+(z-z')^2}} \qquad (13)\end{aligned}$$

where we see that ϕ_1 is due to two sources: J_s, the current distribution on the microstrip and m, the equvalent magnetic charge at the aperture, and ϕ_2 is only due to the equivalent magnetic charge at the aperture.

Enforce the boundary condition at the aperture which is the continuity of magnetic scalar potential, we have the following integral equation:

$$\frac{J_s dy'}{2\pi}(\tan^{-1}(\frac{y-y'}{z+2h}) - \tan^{-1}(\frac{y-y'}{z})) = \iint dy'dz' \frac{4m(y',z')}{4\pi\sqrt{(x+h)^2+(y-y')^2+(z-z')^2}} \qquad (14)$$

The unknown is the magnetic charge density at the gap. J_s is known as the current distribution of a normal microstrip line.

Here we make the assumption that the current distribution on the microstrip line is unperturbed. The change in current distribution can be taken into account by making J_s unknown on the microstrip and solve for the perturbation of the current distribution, which requires another integral equation on the microstrip.

Solve equation (14) using method of moment will give the magnetic charge density at the gap after which we can obtain the magnetic field inside the structure and the current distribution on the ground plane.

Results and discussion: Figure 4 shows the current distribution on the ground plane, which shows that the current takes a detour around the gap and thus introduces extra

inductance due to the larger current loop area. Unlike the simulation result of extra capacitance, the value of the extra inductance has significant dependence on both the length and width of the gap. This is because both the length and width of the gap will increase the current loop area thus increase the extra inductance. The simulation results shown in table 2 tells that the extra inductance increases with either the length or the width of the gap.

2.1.3 CG (Conjugate Gradient) and FFT method for the MOM solution of integral equation

To reduce the computational time of the static analysis, first we introduce CG method [28] in the solution of the matrix equation. Compared with conventional matrix inversion, which has a computational time of the order of N^3 (N is the size of the square matrix and the computational time is mainly counted for the multiplication operations), CG method reduces the computational time to the order of CN^2, where C accounts for the iteration times and how many matrix times column vector operations in one iteration, N^2 is the computational time for the matrix times column vector operation.

To further reduce the computational time, we noticed that the distance invariant characteristics of the impedance matrix element. Because of this character, we implemented FFT method for matrix times column vector operation, which reduces the computational time from N^2 to $N \log_2 N$, thus the total computational time of CG-FFT is $CN \log_2 N$ for our static analysis.

2.2 Full wave analysis of the gap discontinuity with bypass capacitors

For higher frequencies, quasi-static analysis can no longer give reasonable results because of the increasing influence of wave effect. For such short wavelength, discontinuity can exhibit obvious wave phenomenon such as radiation and resonance. Full wave analysis is usually introduced to account for those wave effects at high frequency [29]-[33]. In this section, we introduce a full wave analysis for the gap discontinuity with bypass capacitors.

The approach is formulated using reciprocity theorem, equivalence principle and spatial domain magnetic field Green's function for the layered medium [34][35]. The MFIE (magnetic field integral equation) technique [36][37] was used to set up the integral equation. The

boundary condition for capacitor is derived from the discontinuity of tangential magnetic field due to the displacement current in the bypass capacitor. At last, Method of Moment solution was obtained for the integral equation using RWG basis function.

In the past analysis of microstrip problem, the layered medium Green's function used was either expressed using spectral domain Green's function [38]-[42] or in the spatial domain using mixed potential [43]-[46]. For the spectral domain approach, the evaluation of impedance matrix elements is slow due to two dimensional spectral domain integration and slow convergence of the integration. For the spatial domain approach using mixed potentials, because of the inherent doublet (one positive and one negative) in transferring the spatial derivatives to the basis and testing function, the method requires effectively taking the finite difference of layered medium Green's function. In this paper, we use spatial domain magnetic field Green's function. Recently, we showed that the electromagnetic fields Green's function in the spatial domain can be computed using extraction technique [34][47] and used to formulate integral equation. Also they can be used to compute the impedance matrix elements without need of mixed potential. In [48], it has been shown that the impedance matrix elements obtained from this approach are the same as those obtained by spectral domain approach. As for the MoM solution, we choose RWG basis function [49] that can be applied to arbitrary shape of discontinuity and when the bypass capacitors are present.

Numerical simulation results are also illustrated. Simulations were made on different kind of geometries, which includes: 1) gap without bypass capacitors nor second reference plane, 2) gap with various bypass capacitor values and locations, 3) gap with bypass capacitors and a second reference plane. Salient features of the simulation results give us the following conclusion: 1) When gap is wide, the current on the ground plane will have to take detour around the gap and result in large inductance. 2) A second reference plane can provide a path for the current and reduce the series impedance. 3) Bypass capacitors can reduce the impedance and also increases the resonant frequency of the gap. 4) The larger the capacitance, the greater the effect in reducing the impedance. However for low frequency, a large capacitor is required to provide the path for the current. 5) Bypass capacitor placed at the center (directly under the gap) produces larger inductance reduction

than capacitor placed on the side.

2.2.1 Formulation

Applying reciprocity theorem [50], the voltage reflection coefficient is:

$$R = -\frac{1}{2\sqrt{Z_c}} \iint_{S_g} dS\hat{z} \cdot \left(\overline{E}_g \times \overline{h}^m\right) \tag{15}$$

where S_g and Z_c are the surface of the gap and characteristic impedance of the microstripline, respectively. $\overline{E}_g$ is the electric field at the gap. $\overline{h}^m$ is the normalized modal solution of magnetic field inside the substrate due to the microstripline when there is no gap. The normalization is $\iint dydz \cdot \hat{x} \cdot (\overline{e}^m \times \overline{h}^m) = 1$. It is calculated by using the Method of Moment to solve for the microstripline current distribution and then obtain the magnetic field from the current distribution on the microstripline.

The equivalence principle is used to replace the unknown gap electric field by equivalent magnetic surface current $\overline{M}_s = -\overline{E} \times \hat{n}$. For the case when there are no bypass capacitors, the integral equation is set up by enforcing the continuity of the magnetic fields above and below the gap.

a) Fields above the gap:

$$\overline{H}_a(\overline{r}) = (1 - R)\frac{1}{\sqrt{Z_c}}\overline{h}^m(\overline{r}) + \iint dx'dy'\overline{\overline{G}}^{HMa}(\overline{r}, \overline{r}') \cdot \overline{M}_s(\overline{r}') \tag{16}$$

$\overline{\overline{G}}^{HMa}(\overline{r}, \overline{r}')$ are the tangential components of the dyadic Green's function of the magnetic field created by magnetic surface current. In $\overline{\overline{G}}^{HMa}(\overline{r}, \overline{r}')$, the superscript a represents "above the gap". The spatial domain magnetic field Green's function can be expressed such that it depends on ρ and has simple dependence on ϕ. $\overline{\overline{G}}^{HMa}(\overline{r}, \overline{r}')$ can be decomposed into primary and response field, the primary field is 2 times the homogeneous medium Green's function (the factor of 2 is because of image theorem), and the response field is the response for the layered medium.

$$\overline{\overline{G}}^{HMa}(\overline{r}, \overline{r}') = \overline{\overline{G}}_P^{HM}(\overline{r}, \overline{r}') + \overline{\overline{G}}_R^{HMa}(\overline{r}, \overline{r}') \tag{17}$$

$$\overline{\overline{G}}_P^{HM}\left(\overline{r},\overline{r}'\right) = -j2\omega\varepsilon_1\left(\overline{\overline{I}}+\frac{1}{k_1^2}\nabla_s\nabla_s\right)\frac{e^{-jk_1\rho}}{4\pi\rho} \tag{18}$$

$$\begin{aligned}\overline{\overline{G}}_R^{HMa}\left(\overline{r},\overline{r}'\right) &= \widehat{x}\widehat{x}g_{Rxx}^a\left(x-x',y-y'\right)\\ &\quad+\left(\widehat{x}\widehat{y}+\widehat{y}\widehat{x}\right)g_{Rxy}^a\left(x-x',y-y'\right)\\ &\quad+\widehat{y}\widehat{y}g_{Ryy}^a\left(x-x',y-y'\right)\end{aligned} \tag{19}$$

$$g_{Rxx}^a\left(x-x',y-y'\right) = \sin^2\phi W_{R\rho}^a(\rho)-\cos^2\phi W_{R\phi}^a(\rho) \tag{20}$$

$$g_{Rxy}^a\left(x-x',y-y'\right) = -\sin\phi\cos\phi\left(W_{R\rho}^a(\rho)+W_{R\phi}^a(\rho)\right) \tag{21}$$

$$g_{Ryy}^a\left(x-x',y-y'\right) = \cos^2\phi W_{R\rho}^a(\rho)-\sin^2\phi W_{R\phi}^a(\rho) \tag{22}$$

where $k_1=\omega\sqrt{\mu\varepsilon_1}$ is the wave number of the dielectric material, ω is the angular frequency. $x-x'=\rho\cos\phi$, $y-y'=\rho\sin\phi$. $\nabla_s=\widehat{x}\frac{\partial}{\partial x}+\widehat{y}\frac{\partial}{\partial y}$ is transverse del operator. $W_{R\rho}^a(\rho)$ and $W_{R\phi}^a(\rho)$ are in the form of Sommerfeld Integral:

$$\begin{aligned}W_{R\rho}^a(\rho) &= -\frac{\omega\varepsilon_1}{\pi}\int_{SIP}dk_\rho\frac{k_\rho}{k_{1z}}\\ &\quad\left[J_1'\left(k_\rho\rho\right)\frac{R_{10}^{TM}e^{-2jk_{1z}h_1}}{1-R_{10}^{TM}e^{-2jk_{1z}h_1}}-\frac{k_{1z}^2}{k_1^2}\frac{J_1\left(k_\rho\rho\right)}{k_\rho\rho}\frac{R_{10}^{TE}e^{-2jk_{1z}h_1}}{1+R_{10}^{TE}e^{-2jk_{1z}h_1}}\right]\end{aligned} \tag{23}$$

$$\begin{aligned}W_{R\phi}^a(\rho) &= -\frac{\omega\varepsilon_1}{\pi}\int_{SIP}dk_\rho\frac{k_\rho}{k_{1z}}\\ &\quad\left[-\frac{J_1\left(k_\rho\rho\right)}{k_\rho\rho}\frac{R_{10}^{TM}e^{-2jk_{1z}h_1}}{1-R_{10}^{TM}e^{-2jk_{1z}h_1}}+\frac{k_{1z}^2}{k_1^2}J_1'\left(k_\rho\rho\right)\frac{R_{10}^{TE}e^{-2jk_{1z}h_1}}{1+R_{10}^{TE}e^{-2jk_{1z}h_1}}\right]\end{aligned} \tag{24}$$

where

$$R_{10}^{TM} = \frac{\varepsilon_0k_{1z}-\varepsilon_1k_z}{\varepsilon_0k_{1z}+\varepsilon_1k_z} \tag{25}$$

$$R_{10}^{TE} = \frac{k_{1z}-k_z}{k_{1z}-k_z} \tag{26}$$

$$k_z = \sqrt{k^2-k_\rho^2} \tag{27}$$

$$k_{1z} = \sqrt{k_1^2-k_\rho^2} \tag{28}$$

$k=\omega\sqrt{\mu\varepsilon_0}$ is the wave number of the free space, J_1 is the Bessel function and SIP stands for Sommerfeld Integration Path.

They can be evaluated by using extraction as stated in [34] and [35]. Because $W_{R\rho}^a(\rho)$ and

$W^a_{R\phi}(\rho)$ depend only on ρ, they can be tabulated and looked up when evaluating impedance matrix elements. Note that the primary field is singular at $\overline{r} = \overline{r}'$ while the response is not.

b) Fields below the gap:

$$\overline{H}_b(\overline{r}) = -\iint dx'dy'\overline{\overline{G}}^{HMb}(\overline{r},\overline{r}') \cdot \overline{M}_s(\overline{r}') \tag{29}$$

The integral equation is obtained by enforcing the continuity of the tangential magnetic fields above and below the gap, which is $\overline{H}_a(\overline{r}) = \overline{H}_b(\overline{r})$.

$$-\iint dx'dy'(\overline{\overline{G}}^{HMb}(\overline{r},\overline{r}') + \overline{\overline{G}}^{HMa}(\overline{r},\overline{r}')) \cdot \overline{M}_s(\overline{r}') = (1-R)\frac{1}{\sqrt{Z_c}}\overline{h}_{inc}(\overline{r}) \tag{30}$$

From equation (15) and (30), the unknown magnetic surface current $\overline{M}_s$ and reflection coefficient R can be solved. After the reflection coefficient R is found, the equivalent series impedance Z_e of the gap can be calculated from [50]

$$Z_e = Z_c\frac{2R}{1-R} \tag{31}$$

2.2.2 Boundary condition for bypass capacitors

To model the effect of the bypass capacitors, we use the equivalent model in figure 5 and apply the integral form of Ampere's law $\oint \overline{H} \cdot \overline{dl} = \iint \varepsilon \frac{\partial \overline{E}}{\partial t} \cdot \hat{n}da$ to the capacitor cell, which will give:

$$W_c(H_{2y} - H_{1y}) = j\omega\varepsilon E_x \delta W_c \tag{32}$$

where δ is the thickness of the capacitor cell in z direction, and W_c is the width of the capacitor cell in y direction. This is a simple approximation to simulate the effect of a capacitor at the gap. A cell like this will give a capacitance of $C_c = \varepsilon\frac{\delta W_c}{W_g}$.

Equation (32) can be written as:

$$W_c(H_{2y} - H_{1y}) = j\omega C_c E_x W_g = j\omega C_c V \tag{33}$$

where V is the voltage across the gap. Equation (33) states that the discontinuity of the magnetic fields above and below the capacitor cell equals the displacement current

in the capacitor. Also note that $E_x = M_{sy}$. Only the $\widehat{y}$ component of magnetic field is discontinuous.

Let

$$\begin{aligned} C(x,y) &= \frac{C_c W_q}{W_c} \quad \text{for capacitor cell} \\ &= 0 \qquad \text{otherwise} \end{aligned} \tag{34}$$

We get the boundary condition for the tangential magnetic field as:

$$\overline{H}_{1t} - \overline{H}_{2t} = -j\omega C(x,y)\widehat{y}M_{sy} \tag{35}$$

The integral equation for gap with bypass capacitor is:

$$-\iint dx'dy'(\overline{\overline{G}}^{HMb}(\overline{r},\overline{r}') + \overline{\overline{G}}^{HMa}(\overline{r},\overline{r}'))\cdot\overline{M}_s(\overline{r}') - j\omega C(x,y)\widehat{y}M_{sy}(\overline{r}) = (1-R)\frac{1}{\sqrt{Z_c}}\overline{h}^m(\overline{r}) \tag{36}$$

This is the general form of integral equation for gap discontinuity which will reduce to (30) simply by setting $C(x,y) = 0$.

Basis function for MoM In solving the integral equations using the MOM method, complete domain basis function [51] as well as RWG basis function was investigated. Complete domain basis function has the advantages of being simple and fast, but it is less accurate and rigorous at high frequency and cannot be applied to arbitrary shapes of discontinuity or with the existence of bypass capacitors. On the other hand, being a vector basis function, the RWG basis function has the advantage of being accurate and stable at high frequency, and it can be applied to arbitrary shapes of discontinuity as well as the existence of bypass capacitors. The disadvantage of RWG function is its relatively low computational speed. Here we choose RWG basis function.

2.2.3 Results and discussion

Normalized impedance was obtained for a frequency range from 100MHz to 10GHz, resonant effect was observed from the numerical simulation. Gap with bypass capacitors and second

ground plane was modeled by using RWG basis function. The effect of different values and locations of bypass capacitors was investigated; numerical results were obtained for the serial impedance and the resonant frequency.

In figure 1, region 0 is air, the parameters used in simulations are dielectric permittivity $\varepsilon_1 = 2.2\varepsilon_0$ in region 1, stripline width $W_s = 0.3cm$, gap width $W_g = 0.05cm$ in x direction, gap length $L_g = 8cm$ in y direction. The thickness of the dielectric layer above the first reference/ground plane is $h_1 = 0.1cm$. We consider the cases with and without the second reference/ground plane. For the case without the second reference/ground plane , the medium below the first reference/ground plane is air with $\varepsilon_r = 1$. For the case when the second reference/ground plane is present, the separation between the first and second reference/ground plane is $h_2 = 0.1cm$, the medium between these two planes has relative dielectric permittivity of 2.2.

a) Gap without bypass capacitors and second reference plane: Figure 6 shows the normalized series impedance $Z_n = Z_e/Z_c$ of a gap in a single layer structure without bypass capacitors nor the second reference plane. The calculation was made with 511 RWG basis function in the y direction along the gap and with one cell in the x direction. The solution was stable with the variance of the number of basis function. RWG basis function gives more accurate results than one dimensional roof-top basis functions for this problem. For low frequency below 500 MHz, the resistance is small and the inductive reactance is linear with frequency. The series inductance can be extracted from the relation $Z_e \approx j\omega L_e$ which gives $L_e = 1.15nH$ for this case. As frequency increases, the resistance and the reactance increase until a resonance is reached. The resonance for this case occurs at $1.55GHz$.

b) Gap with various values of bypass capacitor placed at the center: Figure 7 and 8 show the normalized impedance Z_n of a gap with different values of bypass capacitor placed at the center (right under the microstripline). The second reference plane is absent in this case. Comparing the impedance and resonant frequency in figure 7,8 and figure 6, it can be seen that bypass capacitor can greatly reduce the series impedance of the gap. The resonant frequency is also increased. The larger the bypass capacitor, the smaller the impedance and the higher the resonant frequency. However, as the bypass capacitor increases beyond 0.01uF in this case, the resonance frequency approaches the limit of 2.95 GHz. With a

bypass capacitor at the center of the gap, most of the current will continue through the capacitor in the form of displacement current instead of detouring around the gap. This greatly reduces the inductance of the gap. The presence of the bypass capacitor at the center virtually separates the gap into two parts. thus decreases the gap length and results in a higher resonant frequency. Figure 7 also indicates that the resistance is also greatly reduced.

To further illustrate the effects of bypass capacitors we plot the electric field (magnetic surface current) at the gap as a function of y in figure 9. The bypass capacitor is at the center and the frequency is $1GHz$. We know that without the bypass capacitor. the electric field assumes the dependence of a half cycle cosine dependence. When the bypass capacitor is present. the electric field dips at the center. As the capacitance increases. the electric field at the center continues to decrease until it dips to zero. The electric field at the capacitor approaches 0 as in a conductor. In fact. at high frequency and for large capacitance. the capacitor cell behaves like a conductor.

c) Variation of locations of bypass capacitors: Here we compare with the case when there are two capacitors. one on each side of the gap. Figure 10 shows the imaginary part of the normalized impedance of a gap with 100pF capacitor at the center compared with two 50pF capacitors at each side. The location of the two bypass capacitors are respectively at -1.51 cm and 1.51 cm. The result shows that capacitor placed at the center is more effective in reducing inductance than capacitors placed on the two sides. This indicates that two bypass capacitors cannot be simply treated as two shunt capacitors with addition of capacitance. Figure 11 shows the electric field at a gap with two bypass capacitors on each side compared with one bypass capacitor at the center. The electric field dips at the locations of the bypass capacitors. Capacitor at the center has better effect in reducing inductance because the electric field of a gap reaches the maximum at the center and a capacitor at the center will bypass the displacement current more effectively. The h_y of the microstrip line reaches the maximum under the microstrip. Thus decreasing the E_x directly under the microstrip will result in the most reduction of the reflection coefficient.

d) Effect of a second reference plane: Figure 12 and 13 shows the real and imaginary part of the normalized impedance of a gap in a double layer structure when the second reference

plane is present. Compared with the normalized impedance of a gap in single layer structure in figure 6, we can see that the second reference plane helps to reduce the impedance of the gap even without the bypass capacitor. This is because the second reference plane also has bypass effect for the current because the current can reach across the gap in the form of displacement current by detouring to the second reference plane. The current on the first reference plane will go to the second reference plane when it meets the gap, and then go back to the first reference plane after it passes the gap. In fact, the first and second reference plane virtually form a parallel plate capacitor and bypasses current around the gap. However a bypass capacitor directly placed at the gap will have larger reduction in impedance as shown in figure 12 and 13.

e) Low frequency inductance extraction: Table 3 tabulates the low frequency inductance of each case. It is shown that same capacitor will have different effect on the reduction of gap inductance at different frequency range. We can see that at $500MHz$, a $125pF$ capacitor will reduce the inductance to $6.16pH$, while at $100MHz$, it will only reduce the inductance to $42.29pH$ and we need a $0.0125uF$ capacitor to reduce the inductance to $4.25pH$ at $100MHz$. Since the signals on the PCB have frequency components ranging from several hundred mega Hz to several giga Hz, it is necessary to use large capacitor to reduce the low frequency inductance.

2.2.4 Conclusion

A method has been presented to solve gap discontinuity in multi-layered structure with bypass capacitors taken into account. In the evaluation of impedance matrix elements in Method of Moment solution of integral equation, spatial domain magnetic field layer-medium Green's function has been used instead of spectral domain Green's function. Also with the introduction of bypass capacitors at the gap, RWG basis functions are used to represent the magnetic current at the gap. Gaps with different values and locations of bypass capacitors in a multi-layered structure are simulated. The combination of RWG basis function and spatial domain field Green's function in layered medium can be a powerful technique in analyzing all similar discontinuity in multi-layered high speed printed circuit board. The use of spatial domain electromagnetic fields Green's function can speed up the

evaluation in several orders of magnitude and make large number of basis function possible. This approach can find application in PCB simulation software for similar discontinuity problems.

Table 1: Excessive capacitance of gap

Gap Width	Gap Length	Excessive Capacitance
1mil	128mil	-5.63e-18
4mil	128mil	-8.87e-17
4mil	256mil	-8.86e-17

Table 2: Excessive inductance of gap

Gap Width	Gap Length	Excessive Inductance
1mil	128mil	1.86e-10
4mil	128mil	2.67e-10
4mil	256mil	5.65e-10

Table 3: Extracted inductance of gap for different bypass case

Inductance		100MHz	500MHz
w/o second ground	w/o bypass	105.7pH	115.5pH
	bypass of 1.25pF	104.1pH	81.03pH
	bypass of 125pF	42.29pH	6.163pH
	bypass of 0.0125uF	4.254pH	3.600pH
w/h second ground	w/o bypass	33.69pH	37.64pH
	bypass of 125pF	22.29pH	5.131pH

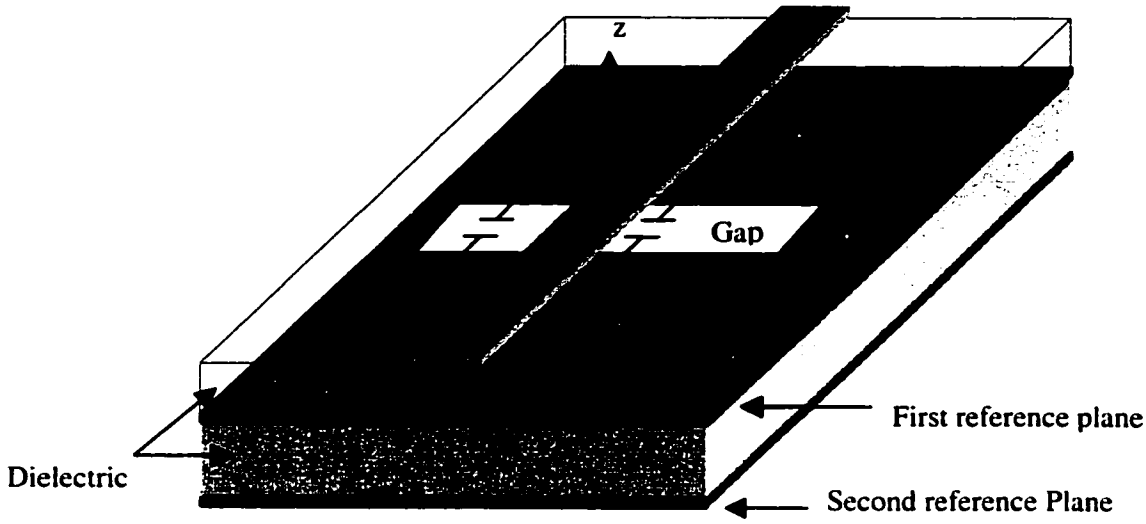

Figure 1: 3-D view of a gap with bypass capacitors in multi-layered structure

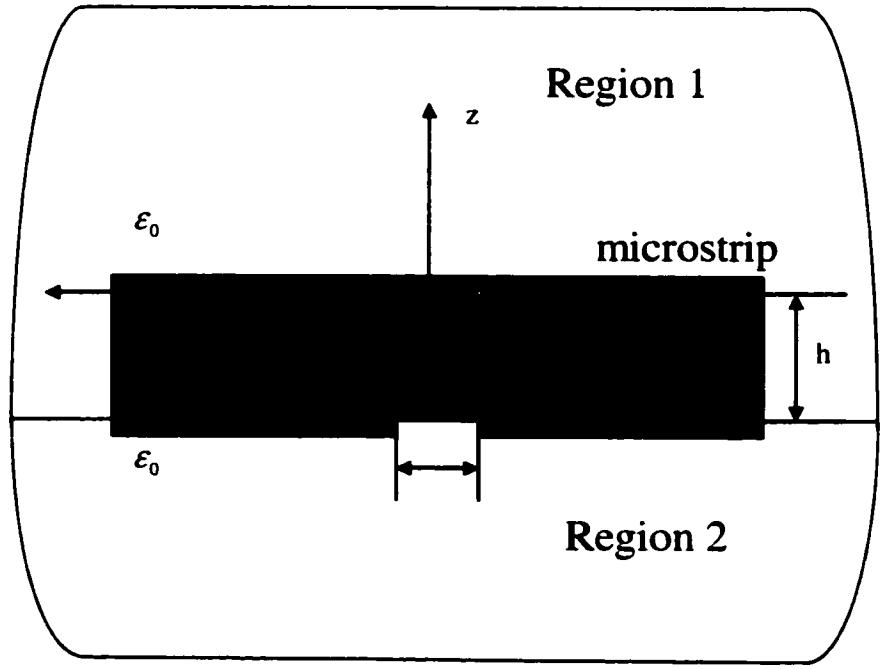

Figure 2: Apply Green's theorem in electrostatic analysis

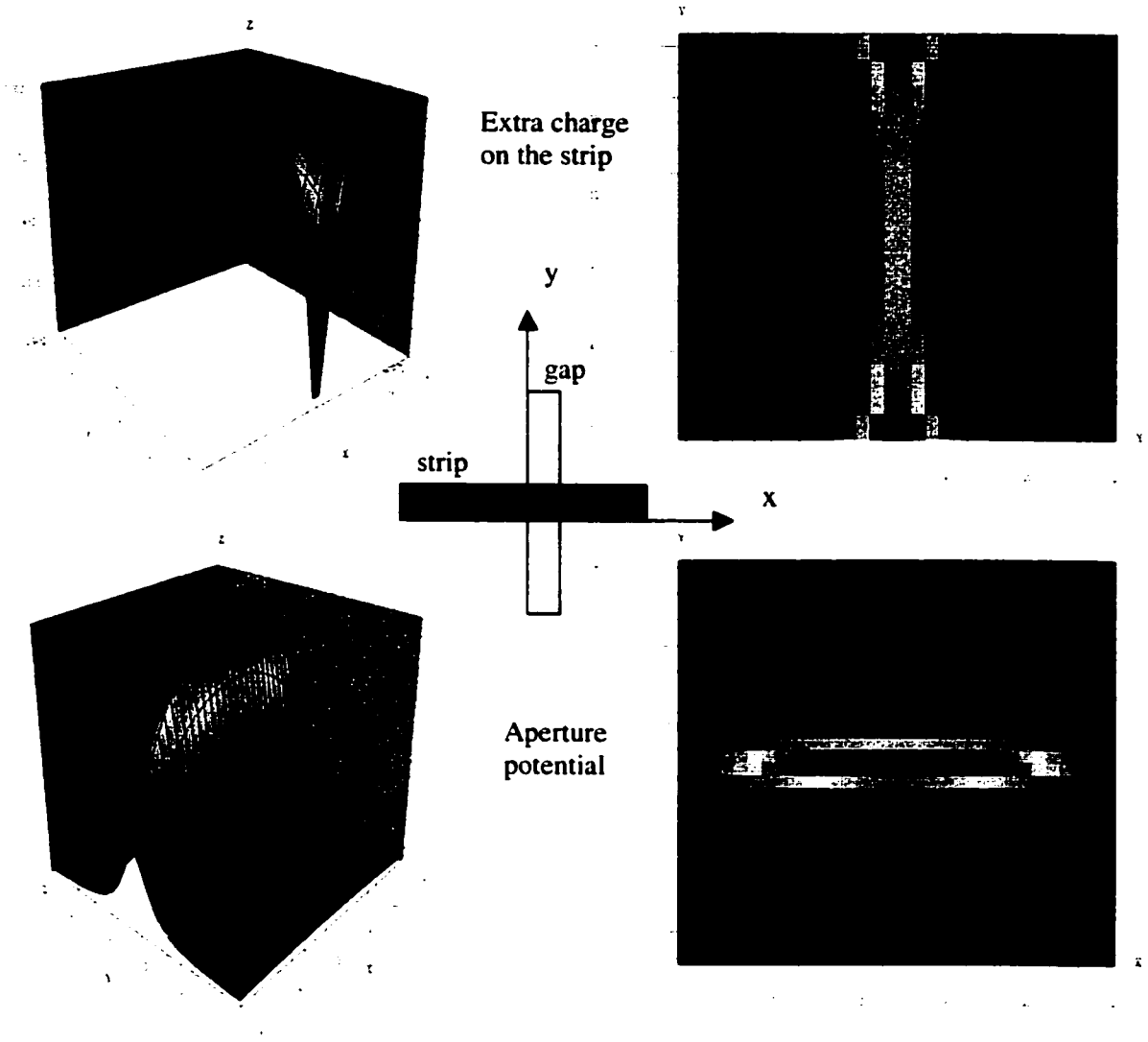

Figure 3: Charge density on the strip and potential distribution at the gap

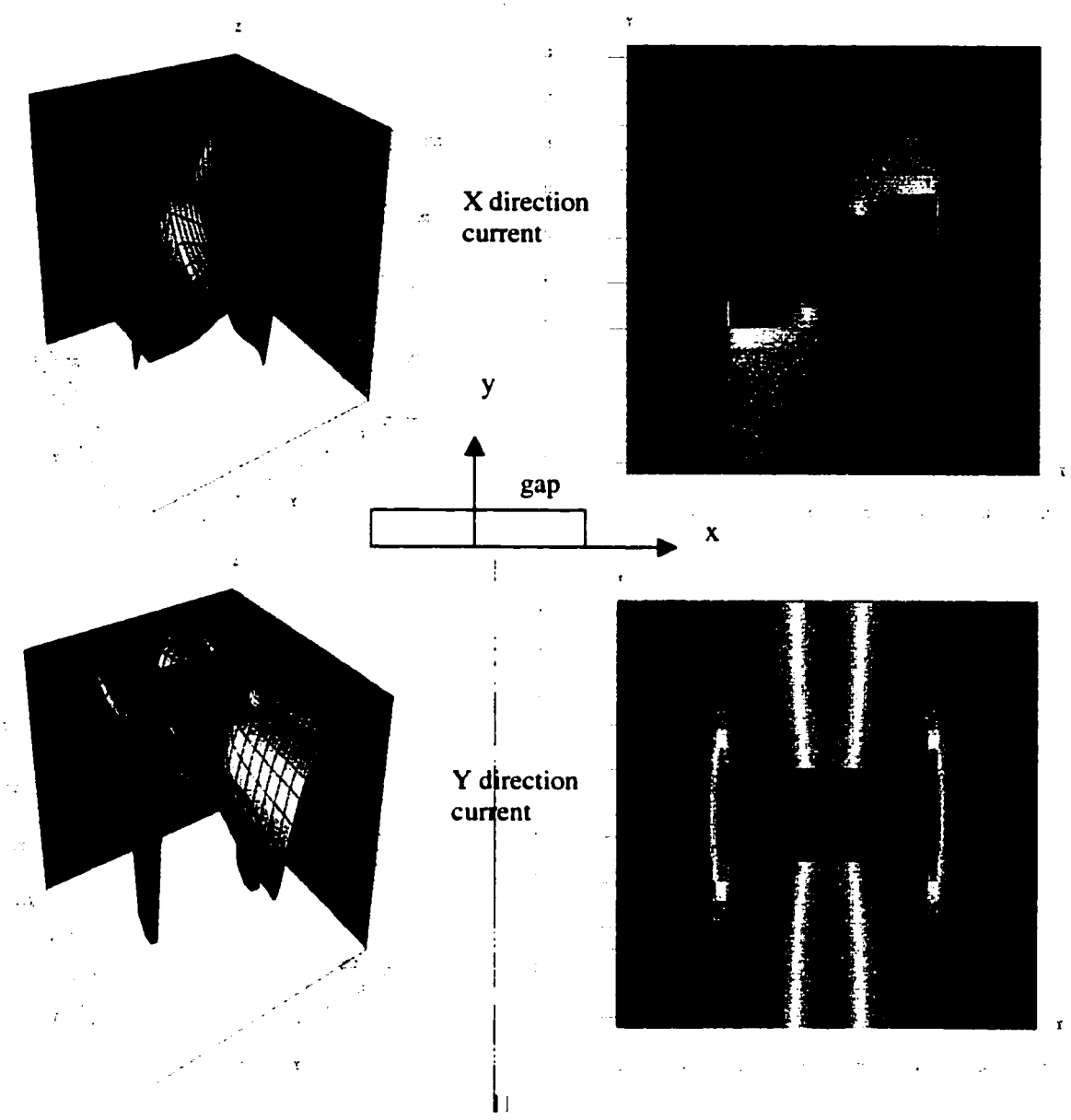

Figure 4: Current distribution on the ground plane

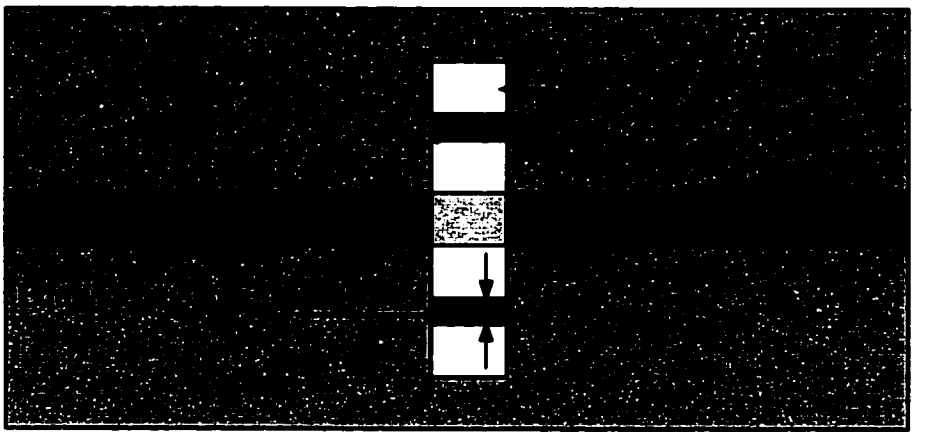

Figure 5: The equivalent modeling of bypass capacitors at the gap. The ratio in the figure does not reflect the real parameters.

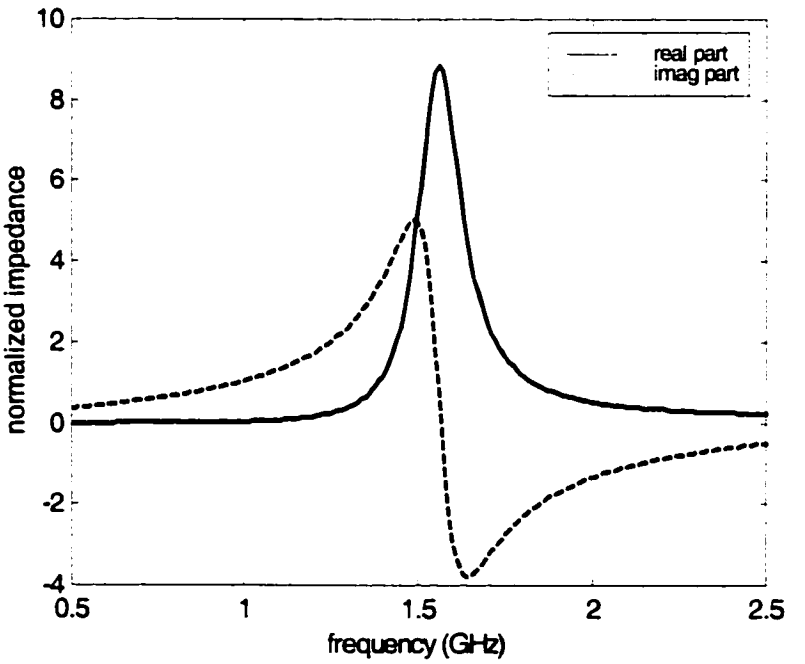

Figure 6: Normalized series impedance of a gap without bypass capacitors in single layer structure.

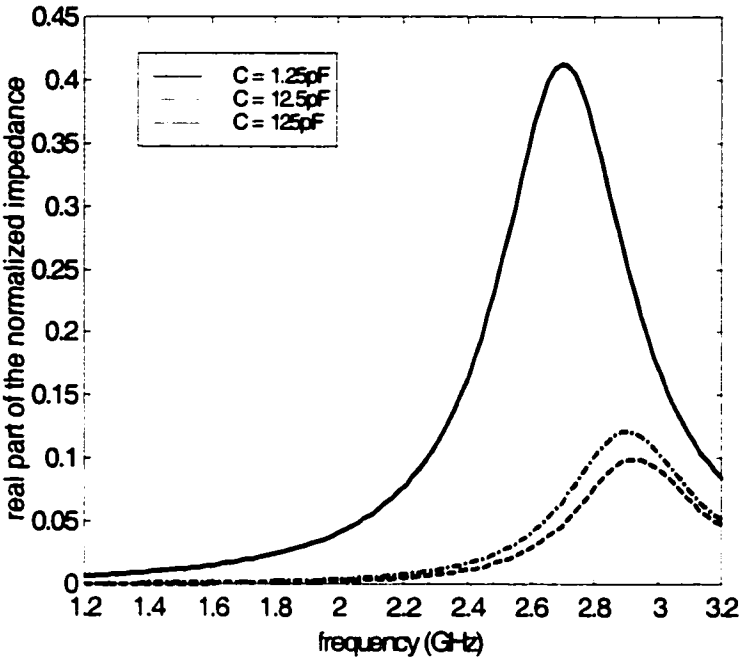

Figure 7: Real part of normalized impedance of a gap with different values of bypass capacitor at the center

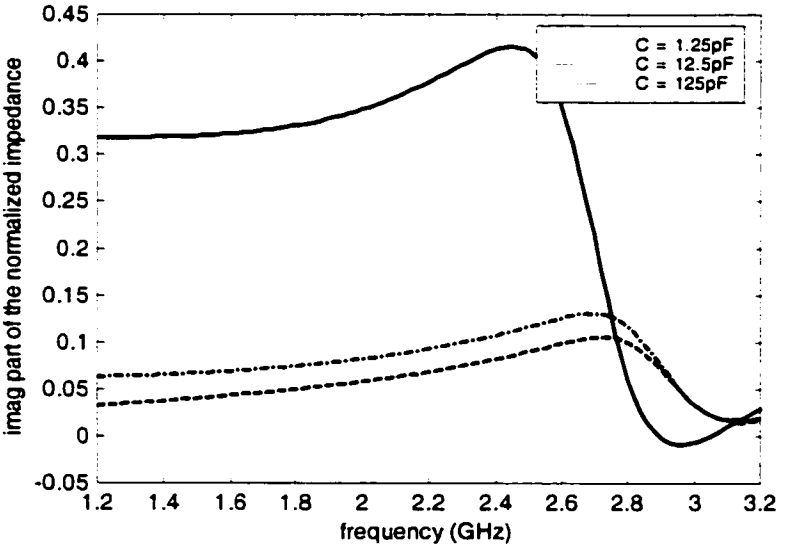

Figure 8: Imaginary part of normalized impedance of a gap with different values of bypass capacitor at the center

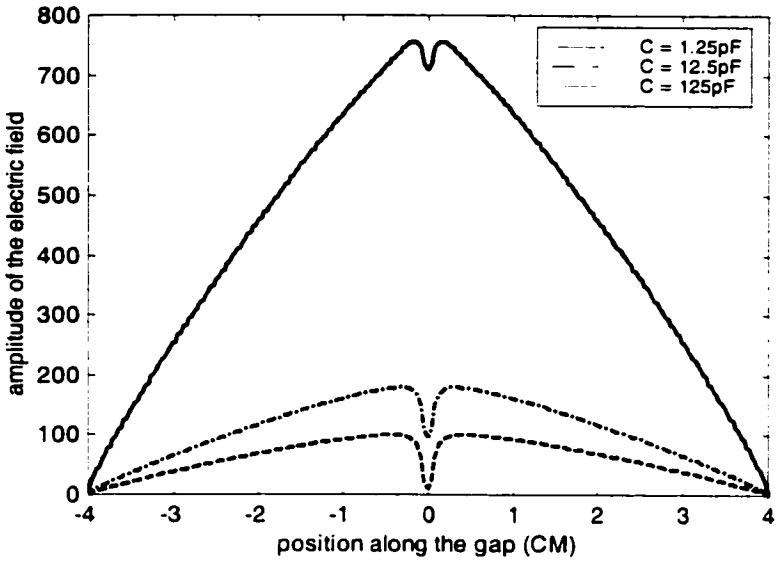

Figure 9: Electric field at the gap with different values of bypass capacitor at the center

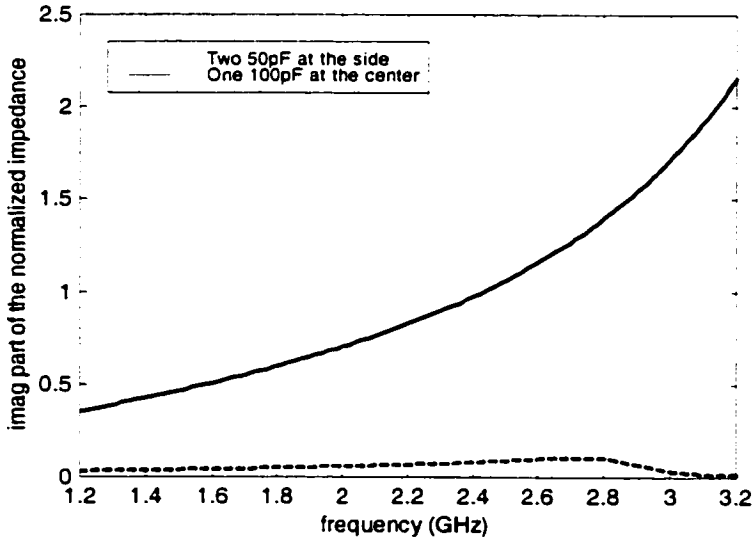

Figure 10: Imaginary part of normalized impedance of a gap with different locations of bypass capacitor

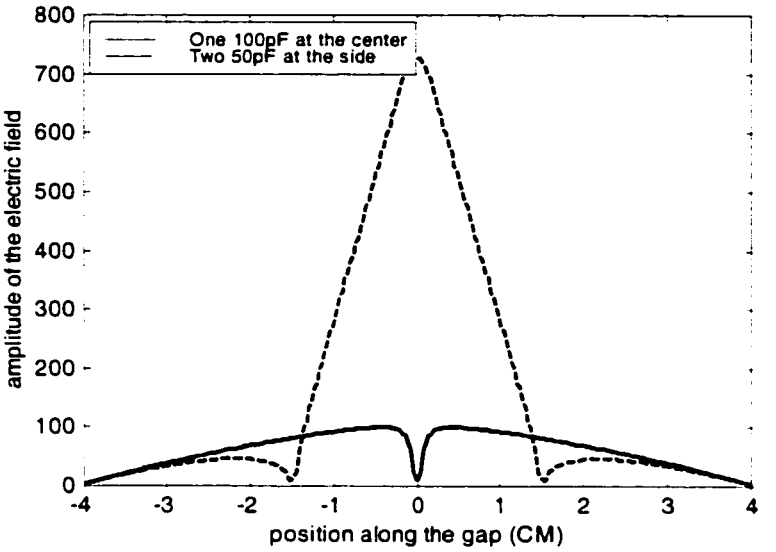

Figure 11: Electric field at the gap with different locations of bypass capacitor

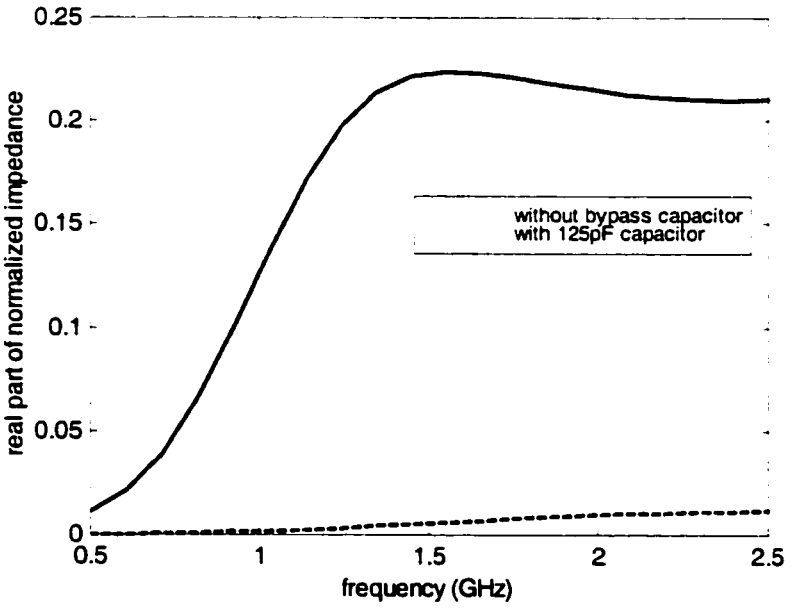

Figure 12: Real part of normalized impedance of a gap with a second ground/reference plane

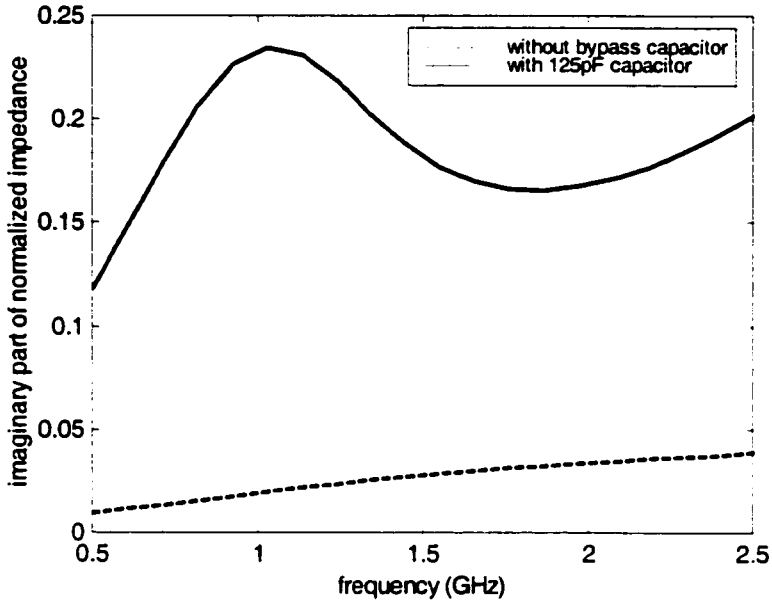

Figure 13: Imaginary part of normalized impedance of a gap with a second ground/reference plane

3 Single via structure

3.1 Introduction

In order to provide good routing in densely packaged integrated circuits, vias have been extensively used in high speed circuit to connect signal traces residing on different layers of a multi-layered printed circuit board or packaging structure. Because of the different impedance of vias with the signal traces, they will create reflection and radiation; also because of the special vertical via structure in multi-layered geometry, there is much radiation inside the parallel plate structure; and the long return path in vertical via structure often result in unwanted inductance which causes severe problems like ground bounce and mutual coupling. All these significant signal integrity problems happen in high-speed circuit design and need to be addressed appropriately.

In the past, different types of vias have been investigated using different methods. The inductance of a via connection of two striplines was analyzed [52] by using the partial electric element circuit (PEEC) model [53]. The capacitance and inductance of a through-hole via has been analyzed using quasi-static approach [54]-[56] or empirical formulas [57]. A circularly symmetric via has been modelled using quasi-static approach [58]. More recently, full wave analysis has been applied to through-hole via geometry [59]-[61]. The vertical via structure in multi-layered geometry has been analyzed using equivalent circuit and microwave network analysis [62][63]. Also a differential via pair has been analyzed in [64]. However some of these analysis are only for low frequency range, some are only for through-hole via instead of via in multi-layered structure, and some analysis need special feed-in assumption and symmetric structure.

In our formulation in this chapter, we analyze the vertical via in multi-layered structure. Using equivalence principle, the problem is decomposed into interior and exterior problem. The interior problem consists of magnetic sources between plane conductors and with cylindrical via structures [65]. The interior problem is solved using the dyadic magnetic field Green's function based on cylindrical wave expansion [?] that is suited for cylindrical vias. The via cylinders are modeled as scatterers inside parallel plate waveguide structure, and cylindrical wave expansion of Green's function is obtained for this structure. The Green's

function is further expanded into waveguide modes. Scattering of waves by the via is described by T-matrix coefficients. This is straight forward in physical meaning and can be further implemented later when dealing with multi-via structure.

For the multi-layered structure, it is decomposed into several single-layered via structure, the admittance matrix of each section obtained from single layer analysis is transfered to transfer matrix and these transfer matrices are cascaded together to give the final transfer matrix of the multi-layered via structure. Simple analytic formulas are also derived for the short via limit which indicates an inductance and a frequency dependent resistor.

The exterior structure of the via is analyzed using the method in [60] and combined with the interior structure formulation by relating the port voltages and currents. Comparing with the derivation in [65][62] and [63], the cylindrical wave expansion of Green's function approach is much straight forward in physical meaning and much more flexible in treating different size via coupling later because unlike even- and odd- mode analysis, it does not require symmetry in the structure. This approach also allows varies types of feed-in structure in that the decomposition of interior and exterior problem isolated the feed-in structure from the interior structure.

The cylindrical wave expansion of Green's function between two parallel plates is derived first. It is then used as primary wave for a cylindrical scatterer and gives the Green's function for a cylindrical scatterer between two parallel plates. Based on this, given voltage at the via aperture, a magnetic current ring source is used to excite cylindrical waves of magnetic field inside the parallel plate, and the currents on the via cylinders are obtained by doing contour integral of magnetic field around the via cylinder at interesting points. With current and voltage, the admittance matrix of a single via in single-layered structure is obtained. The analysis is quite straight forward in that it only utilizes the magnetic field Green's function and the definition of admittance. While in [62], the admittance was given after using image theorem and tricky setup of equivalent circuit and analysis of incident and reflected wave of coaxial cable.

Further more, we use the technique in [60] to analyze the exterior structure of the vertical via and combine it with our interior formulation to give the complete propagation characteristics of the entire structure. To verify the correctness of our formulation, the

admittance Y_{oc} and Y_{sc} of our formulation has been compared with those of [62] using their parameters. The results show very good agreements. Combining with the exterior structure, we give the scattering parameter of an entire via structure. Numerical results of the scattering parameters are illustrated for a large frequency range and for various multi-layered via configurations.

3.2 Formulation

Figure 14 shows several typical single vertical via structures on printed circuit board. To formulate the propagation characteristics of the entire via structure, we decompose it into interior and exterior problem as in figure 15 by sealing via apertures using equivalent magnetic current sources.

3.3 Interior Problem

To solve the interior problem as given in figure 15, the cylindrical wave expansion of dyadic magnetic field Green's function of a cylindrical scatterer in terms of waveguide modes is derived. The via cylinders are then modeled as conducting cylindrical scatterers between these two PECs. Based upon the Green's function, we excite the structure using a voltage source at the port, which is equivalent as a magnetic current ring source at the via aperture. The electric currents are then found on the surface of via cylinder by doing contour integral of magnetic field. In this way, the admittance matrix of the via is obtained which fully describes the interior structure of a single vertical via.

3.3.1 Cylindrical wave expansion of Dyadic Green's function Between Two PECs

Consider two perfect electric conductors at $z = d/2$ and $z = -d/2$. Let the magnetic current source z' be between the two PECs. Let us also consider the case when the magnetic current source sheet $\overline{M}_s$ flows in the horizontal plane.

$$\overline{H} = -j\omega\varepsilon \iint dx'dy' \overline{\overline{G}}(\overline{r},\overline{r}') \cdot \overline{M}_s(\overline{r}') \tag{37}$$

The Green's function is

$$\overline{\overline{G}} = \overline{\overline{G}}_P + \overline{\overline{G}}_R \tag{38}$$

where $\overline{\overline{G}}_P$ and $\overline{\overline{G}}_R$ are respectively the primary Green's function and the response Green's function. The Green's function of two parallel PECs [66][67] will be the primary field for this case as the source between two parallel plates generates the incident field onto the cylindrical scatterer.

In the following we use upper sign for $z < z'$, lower sign for $z > z'$, and let $\overline{\overline{I}}_t = \hat{x}\hat{x} + \hat{y}\hat{y}$ be the transverse dyad.

For $\rho < \rho'$,

$$\begin{aligned}
&\overline{\overline{G}}_P(\overline{r}, \overline{r}') \cdot \overline{\overline{I}}_t \\
= \; & -\frac{\eta}{4d} \sum_{n,\ell} \frac{(-1)^{n+\ell}}{k_{\rho\ell}^2} f_\ell \left(1 + e^{2jk_{z\ell}(z' \mp d/2)}\right) e^{-jk_{z\ell}(z' \mp d/2)} \\
& Rg\overline{H}_n^{TM}(k_{\rho\ell}, k_{z\ell}, \overline{\rho}, z \pm d/2)\overline{m}_{-n}(k_{\rho\ell}, k_{z\ell}, \overline{\rho}')e^{jn\phi'} \cdot \overline{\overline{I}}_t \\
& + \frac{j\eta}{4d} \sum_{n,\ell} \frac{(-1)^{n+\ell}}{k_{\rho\ell}^2} f_\ell \left(1 + e^{2jk_{z\ell}(z' \mp d/2)}\right) e^{-jk_{z\ell}(z' \mp d/2)} \\
& Rg\overline{H}_n^{TE}(k_{\rho\ell}, k_{z\ell}, \overline{\rho}, z \pm d/2)\overline{n}_{-n}(k_{\rho\ell}, k_{z\ell}, \overline{\rho}')e^{jn\phi'} \cdot \overline{\overline{I}}_t
\end{aligned} \tag{39}$$

For $\rho > \rho'$,

$$\begin{aligned}
&\overline{\overline{G}}_P(\overline{r}, \overline{r}') \cdot \overline{\overline{I}}_t \\
= \; & -\frac{\eta}{4d} \sum_{n,\ell} \frac{(-1)^{n+\ell}}{k_{\rho\ell}^2} f_\ell \left(1 + e^{2jk_z(z' \mp d/2)}\right) e^{-jk_z(z' \mp d/2)} \\
& \overline{H}_n^{TM}(k_{\rho\ell}, k_{z\ell}, \overline{\rho}, z \pm d/2) Rg\overline{m}_{-n}(k_{\rho\ell}, k_{z\ell}, \overline{\rho}')e^{jn\phi'} \cdot \overline{\overline{I}}_t \\
& + \frac{j\eta}{4d} \sum_{n,\ell} \frac{(-1)^{n+\ell}}{k_{\rho\ell}^2} f_\ell \left(1 + e^{2jk_z(z' \mp d/2)}\right) e^{-jk_z(z' \mp d/2)} \\
& \overline{H}_n^{TE}(k_{\rho\ell}, k_{z\ell}, \overline{\rho}, z \pm d/2) Rg\overline{n}_{-n}(k_{\rho\ell}, k_{z\ell}, \overline{\rho}')e^{jn\phi'} \cdot \overline{\overline{I}}_t
\end{aligned} \tag{40}$$

where

$$\begin{aligned} f_\ell &= \frac{1}{2} \quad \text{for } \ell = 0 \\ &= 1 \quad \text{for } \ell = 1, 2, ... \end{aligned} \tag{41}$$

$\eta = \sqrt{\mu/\varepsilon}$ is the wave impedance, and $k_{zl} = \frac{l\pi}{d}$, $l = 0, 1, 2, ...$

The magnetic modal solutions are defined as follows:

$$\begin{aligned} & Rg\overline{H}_n^{TE}(k_\rho, k_z, \overline{\rho}, z) \\ = \; & \frac{1}{2\eta}\left\{e^{-jk_z z} Rg\overline{n}_n(k_\rho, k_z, \overline{\rho}) - e^{jk_z z} Rg\overline{n}_n(k_\rho, -k_z, \overline{\rho})\right\} e^{-jn\phi} \\ = \; & \frac{e^{-jn\phi}}{\eta}\left\{ \begin{array}{c} -\widehat{\rho}\frac{jk_\rho k_z}{k} J_n'(k_\rho\rho)\cos(k_z z) - \widehat{\phi}\frac{nk_z}{k\rho} J_n(k_\rho\rho)\cos(k_z z) \\ -\widehat{z}\frac{k_\rho^2}{k} J_n(k_\rho\rho) j\sin(k_z z) \end{array} \right\} \end{aligned} \tag{42}$$

$$\begin{aligned} & Rg\overline{H}_n^{TM}(k_\rho, k_z, \overline{\rho}, z) \\ = \; & \frac{j}{2\eta}\left\{e^{-jk_z z} Rg\overline{m}_n(k_\rho, k_z, \overline{\rho}) + e^{jk_z z} Rg\overline{m}_n(k_\rho, -k_z, \overline{\rho})\right\} e^{-jn\phi} \\ = \; & \frac{j}{\eta}\left\{-\widehat{\rho}\frac{jn}{\rho} J_n(k_\rho\rho) - \widehat{\phi} k_\rho J_n'(k_\rho\rho)\right\} e^{-jn\phi}\cos(k_z z) \end{aligned} \tag{43}$$

where $k_\rho = \sqrt{k^2 - k_z^2}$ and Rg stands for regular with Bessel functions being used. Without the Rg, the corresponding functions are Hankel functions of the second kind.

The two vector cylindrical wave functions are,

$$\overline{m}_n(k_\rho, k_z, \overline{\rho}) = -\widehat{\rho}\frac{jn}{\rho} H_n^{(2)}(k_\rho\rho) - \widehat{\phi} k_\rho H_n^{(2)\prime}(k_\rho\rho) \tag{44}$$

$$\overline{n}_n(k_\rho, k_z, \overline{\rho}) = -\widehat{\rho}\frac{jk_\rho k_z}{k} H_n^{(2)\prime}(k_\rho\rho) - \widehat{\phi}\frac{nk_z}{k\rho} H_n^{(2)}(k_\rho\rho) + \widehat{z}\frac{k_\rho^2}{k} H_n^{(2)}(k_\rho\rho) \tag{45}$$

The summation of the modal solutions starts with $\ell = 0$ for TM waves, and starts with $\ell = 1$ for TE waves, and the summation of harmonics are for $n = -\infty$ to ∞.

3.3.2 Dyadic Green's function of a cylindrical scatterer between two PECs

The above is the cylindrical wave expansion of dyadic Green's function between two parallel PECs. To include vertical via into this structure, we model the vertical via as conducting scatterer and look into the Green's function of two parallel PECs with vertical conducting cylindrical scatterer. The Green's function of the previous section will be the primary Green's function for this case. The response Green's function for this case is due to the cylindrical scatterer.

Because the via cylinder (where the field points are on) always has a smaller radius than the via aperture (where the source points are on), we have $\rho < \rho'$ in the formulation.

First we consider the case of upper port where the source is at $z' = d/2$. We only need the Green's function for $z < z'$. Thus, letting $z' = d/2$, we have:

For $z < d/2$, $\rho < \rho'$, from equation (39):

$$\begin{aligned}
&\bar{\bar{G}}_P(\bar{r}, \bar{r}') \cdot \bar{\bar{I}}_t \\
= \; & -\frac{\eta}{2d} \sum_{n,\ell} \frac{(-1)^{n+\ell}}{k_{\rho\ell}^2} f_\ell \\
& Rg\overline{H}_n^{TM}(k_{\rho\ell}, k_{z\ell}, \bar{\rho}, z + d/2)\overline{m}_{-n}(k_{\rho\ell}, k_{z\ell}, \bar{\rho}')e^{-in\phi'} \cdot \bar{\bar{I}}_t \\
& -\frac{i\eta}{2d} \sum_{n,\ell} \frac{(-1)^{n+\ell}}{k_{\rho\ell}^2} f_\ell \\
& Rg\overline{H}_n^{TE}(k_{\rho\ell}, k_{z\ell}, \bar{\rho}, z + d/2)\overline{n}_{-n}(k_{\rho\ell}, k_{z\ell}, \bar{\rho}')e^{-in\phi'} \cdot \bar{\bar{I}}_t
\end{aligned} \tag{46}$$

For response Green's function, $Rg\overline{H}_n^{TM}$ has a scattering coefficient of $T_n^{(N)}$ for scattering by a cylinder. $Rg\overline{H}_n^{TE}$ has a scattering coefficient of $T_n^{(M)}$. Thus the response Green's

function of the cylinder is:

$$\begin{aligned}
&\bar{\bar{G}}_R(\bar{r},\bar{r}')\cdot\bar{\bar{I}}_t \\
= &-\frac{\eta}{2d}\sum_{n,\ell}\frac{(-1)^{n+\ell}}{k_{\rho\ell}^2}f_\ell \\
&T_n^{(N)}\overline{H}_n^{TM}(k_{\rho\ell},k_{z\ell},\bar{\rho},z+d/2)\overline{m}_{-n}(k_{\rho\ell},k_{z\ell},\bar{\rho}')e^{-in\phi'}\cdot\bar{\bar{I}}_t \\
&-\frac{i\eta}{2d}\sum_{n,\ell}\frac{(-1)^{n+\ell}}{k_{\rho\ell}^2}f_\ell \\
&T_n^{(M)}\overline{H}_n^{TE}(k_{\rho\ell},k_{z\ell},\bar{\rho},z+d/2)\overline{n}_{-n}(k_{\rho\ell},k_{z\ell},\bar{\rho}')e^{-in\phi'}\cdot\bar{\bar{I}}_t
\end{aligned} \tag{47}$$

$T_n^{(N)}$ and $T_n^{(M)}$ are obtained by forcing the boundary condition that the tangential electric field must be zero on the cylinder surface:

$$T_n^{(N)} = T_{-n}^{(N)} = -\frac{J_n(k_{\rho\ell}a)}{H_n^{(2)}(k_{\rho\ell}a)} \tag{48}$$

$$T_n^{(M)} = T_{-n}^{(M)} = -\frac{J_n'(k_{\rho\ell}a)}{H_n^{(2)\prime}(k_{\rho\ell}a)} \tag{49}$$

Next we consider the case for lower port where the source is at $z' = -d/2$. We only need the Green's function for $z > z'$. Thus, letting $z' = -d/2$, we have:

For $z > -d/2$, $\rho < \rho'$, from equation (39):

$$\begin{aligned}
&\bar{\bar{G}}(\bar{r},\bar{r}')\cdot\bar{\bar{I}}_t \\
= &-\frac{\eta}{2d}\sum_{n,\ell}\frac{(-1)^{n+\ell}}{k_{\rho\ell}^2}f_\ell \\
&Rg\overline{H}_n^{TM}(k_{\rho\ell},k_{z\ell},\bar{\rho},z-d/2)\overline{m}_{-n}(k_{\rho\ell},k_{z\ell},\bar{\rho}')e^{-in\phi'}\cdot\bar{\bar{I}}_t \\
&-\frac{i\eta}{2d}\sum_{n,\ell}\frac{(-1)^{n+\ell}}{k_{\rho\ell}^2}f_\ell \\
&Rg\overline{H}_n^{TE}(k_{\rho\ell},k_{z\ell},\bar{\rho},z-d/2)\overline{n}_{-n}(k_{\rho\ell},k_{z\ell},\bar{\rho}')e^{-in\phi'}\cdot\bar{\bar{I}}_t
\end{aligned} \tag{50}$$

The response Green's function of the cylinder can be written in a similar way as equation

(47):

$$
\begin{aligned}
& \bar{\bar{G}}_R(\bar{r},\bar{r}') \cdot \bar{\bar{I}}_t \\
= \; & -\frac{\eta}{2d}\sum_{n,\ell}\frac{(-1)^{n+\ell}}{k_{\rho\ell}^2} f_\ell \\
& T_n^{(N)}\overline{H}_n^{TM}(k_{\rho\ell},k_{z\ell},\bar{\rho},z-d/2)\overline{m}_{-n}(k_{\rho\ell},k_{z\ell},\bar{\rho}')e^{-\imath n\phi'}\cdot\bar{\bar{I}}_t \\
& -\frac{i\eta}{2d}\sum_{n,\ell}\frac{(-1)^{n+\ell}}{k_{\rho\ell}^2} f_\ell \\
& T_n^{(M)}\overline{H}_n^{TE}(k_{\rho\ell},k_{z\ell},\bar{\rho},z-d/2)\overline{n}_{-n}(k_{\rho\ell},k_{z\ell},\bar{\rho}')e^{-\imath n\phi'}\cdot\bar{\bar{I}}_t
\end{aligned}
\tag{51}
$$

3.3.3 Magnetic field and surface current density on the cylinder

For vertical via formulation, we let the source be at $\rho' > a$ where a is the radius of via cylinder. We have, for the magnetic field:

$$
\begin{aligned}
& \overline{H} \\
= \; & \frac{jk}{2d}\sum_{n,\ell}\frac{(-1)^{n+\ell}}{k_{\rho\ell}^2} f_\ell \begin{bmatrix} Rg\overline{H}_n^{TM}(k_{\rho\ell},k_{z\ell},\bar{\rho},z\pm d/2) \\ +T_n^{(N)}\overline{H}_n^{TM}(k_{\rho\ell},k_{z\ell},\bar{\rho},z\pm d/2) \end{bmatrix} \\
& \int d\bar{\rho}'\overline{m}_{-n}(k_{\rho\ell},k_{z\ell},\bar{\rho}')e^{jn\phi'_{\bar{\rho}'}}\cdot\overline{M}_s(\bar{\rho}') \\
& +\frac{k}{2d}\sum_{n,\ell}\frac{(-1)^{n+\ell}}{k_{\rho\ell}^2} f_\ell \begin{bmatrix} Rg\overline{H}_n^{TE}(k_{\rho\ell},k_{z\ell},\bar{\rho},z\pm d/2) \\ +T_n^{(M)}\overline{H}_n^{TE}(k_{\rho\ell},k_{z\ell},\bar{\rho},z\pm d/2) \end{bmatrix} \\
& \int d\bar{\rho}'\overline{n}_{-n}(k_{\rho\ell},k_{z\ell},\bar{\rho}')e^{jn\phi'_{\bar{\rho}'}}\cdot\overline{M}_s(\bar{\rho}')
\end{aligned}
\tag{52}
$$

Hence the surface current density on the surface of the cylinder is obtained by setting

$\rho = a$:

$$\begin{aligned}
&\overline{J}_s \\
&= \frac{jk}{2d}\sum_{n,\ell}\frac{(-1)^{n+\ell}}{k_{\rho\ell}^2} f_\ell \overline{J}_{sn}^{TM}(k_\rho, k_z, z \pm d/2) \\
&\int d\overline{\rho}' \overline{m}_{-n}(k_{\rho\ell}, k_{z\ell}, \overline{\rho}') e^{jn\phi'_{\overline{\rho}'}} \cdot \overline{M}_s(\overline{\rho}') \\
&+\frac{k}{2d}\sum_{n,\ell}\frac{(-1)^{n+\ell}}{k_{\rho\ell}^2} f_\ell \overline{J}_{sn}^{TE}(k_\rho, k_z, z \pm d/2) \\
&\int d\overline{\rho}' \overline{n}_{-n}(k_{\rho\ell}, k_{z\ell}, \overline{\rho}') e^{jn\phi'_{\overline{\rho}'}} \cdot \overline{M}_s(\overline{\rho}')
\end{aligned} \tag{53}$$

where the modal solutions of surface current density are

$$\overline{J}_{sn}^{TE}(k_\rho, k_z, z) = \frac{-\frac{2j}{\eta\pi k_\rho a} e^{-jn\phi}}{H_n^{(2)\prime}(k_\rho a)} \left[-\widehat{z}\frac{nk_z}{ka}\cos(k_z z) + \widehat{\phi}\frac{k_\rho^2}{k} j \sin(k_z z) \right] \tag{54}$$

$$\overline{J}_{sn}^{TM}(k_\rho, k_z, z) = \widehat{z}\frac{\frac{2}{\eta\pi a}}{H_n^{(2)}(k_\rho a)} \{\cos k_z z\} e^{-jn\phi} \tag{55}$$

3.3.4 Admittance matrix of a single via:

To obtain the admittance matrix of a single via, we excite the structure using voltage sources and obtain the corresponding current on the cylinder at each port. For a voltage source at the aperture, it is equivalent to a magnetic current ring source due to equivalence principle:

$$\overline{M} = \overline{E} \times \widehat{n} \tag{56}$$

where $\widehat{n}$ is the normal unit vector to the aperture surface.

Assume the via cylinder centers at $\overline{\rho} = 0$, then for the upper source V_u at $z' = d/2$, the magnetic current ring source is:

$$\overline{M}_{su}(\overline{\rho}') = -\frac{V_u}{|\overline{\rho}'| \ln\frac{b}{a}} \widehat{\phi}'_{\overline{\rho}'}, \quad \text{for } a \le |\overline{\rho}'| \le b \tag{57}$$

For the lower source V_b at $z' = -d/2$, the magnetic current ring source is:

$$\overline{M}_{sb}\left(\overline{\rho}'\right) = -\frac{V_b}{|\overline{\rho}'| \ln \frac{b}{a}} \widetilde{\phi}'_{\overline{\rho}'}, \quad \text{for } a \leq |\overline{\rho}'| \leq b \tag{58}$$

Substitute the above equations into equation (53) to calculate surface current density $\overline{J}_s$. We have:

$$\begin{aligned} & \int d\overline{\rho}' \overline{n}_{-n}(k_{\rho\ell}, k_{z\ell}, \overline{\rho}') e^{jn\phi'_{\overline{\rho}'}} \cdot \overline{M}_s\left(\overline{\rho}'\right) \\ = & -\frac{2\pi V}{\ln \frac{b}{a}} \delta_{n0} \left[H_0^{(2)}\left(k_{\rho\ell} b\right) - H_0^{(2)}\left(k_{\rho\ell} a\right)\right] \end{aligned} \tag{59}$$

where $V = V_u$ for $\overline{M}_{su}$ and $V = V_b$ for $\overline{M}_{sb}$. The Kronecker delta δ_{n0} is because there is no azimuthal dependence of the source.

Also because $\overline{n}_0(k_{\rho\ell}, k_{z\ell}, \overline{\rho}') = 0$, we have:

$$\int d\overline{\rho}' \overline{n}_{-n}(k_{\rho\ell}, k_{z\ell}, \overline{\rho}') e^{jn\phi'_{\overline{\rho}'}} \cdot \overline{M}_s\left(\overline{\rho}'\right) = 0 \tag{60}$$

which indicates that for a magnetic current ring source which is azimuthally symmetrical, only TM mode will be excited in this structure.

The surface current on the cylinder in the positive z direction is:

$$\begin{aligned} I_s &= 2\pi a \overline{J}_s \cdot \hat{z} \\ &= -\frac{jk}{\eta d} \frac{4\pi V}{\ln \frac{b}{a}} \sum_{\ell} \frac{(-1)^{\ell}}{k_{\rho\ell}^2} f_{\ell} \frac{1}{H_0^{(2)}(k_\rho a)} \left\{\cos k_z\left(z \pm d/2\right)\right\} \\ &\quad \left[H_0^{(2)}\left(k_{\rho\ell} b\right) - H_0^{(2)}\left(k_{\rho\ell} a\right)\right] \end{aligned} \tag{61}$$

The admittance matrix of a two-port network is defined as:

$$\begin{bmatrix} I_u \\ I_b \end{bmatrix} = \begin{bmatrix} Y_{11} & Y_{12} \\ Y_{21} & Y_{22} \end{bmatrix} \begin{bmatrix} V_1 \\ V_2 \end{bmatrix} \tag{62}$$

where: $I_u = -I_s(z = d/2)$, $I_b = I_s(z = -d/2)$ and $V_1 = V_u$, $V_2 = V_b$.

From equation (61), we can easily obtain:

$$Y_{11} = (\frac{4\pi\omega\varepsilon j}{d\ln\frac{b}{a}})\sum_{l}\frac{f_\ell}{k_{\rho\ell}^2}\left[\frac{H_0^{(2)}(k_{\rho\ell}b)}{H_0^{(2)}(k_{\rho\ell}a)}-1\right] \quad (63)$$

$$Y_{12} = (\frac{4\pi\omega\varepsilon j}{d\ln\frac{b}{a}})\sum_{l}\frac{(-1)(-1)^l f_\ell}{k_{\rho\ell}^2}\left[\frac{H_0^{(2)}(k_{\rho\ell}b)}{H_0^{(2)}(k_{\rho\ell}a)}-1\right] \quad (64)$$

and due to symmetry:

$$Y_{21} = Y_{12} \quad (65)$$

$$Y_{22} = Y_{11} \quad (66)$$

3.4 Exterior Problem

We solve the exterior problem using MOM techniques following [60][61]. The exterior part of a vertical via could be modeled as a thin wire terminated with a hole on the ground plane [60][61]. This problem could be further decomposed into a short circuit problem and a wire antenna problem (figure 16).

In short circuit problem, incident wave is excited at one end of the wire with amplitude of A. Integral equation is then set up on the surface of the wire by enforcing the tangential electric field equal to zero on the wire surface. The basis function used here is piecewise sinusoidal basis function, and half sinusoidal basis function at each end. After the current distribution on the wire is obtained, the reflected wave amplitude B is extracted out using matrix pencil method. The current at the short circuit end I_{sc} due to unit incident wave is calculated.

Similar technique is used for the wire antenna problem, with an additional voltage source V (equivalent magnetic current source) at the via aperture as the driven source for antenna. Using this excitation, we calculate the transmitted wave B and the current at the input end I. Analyzing these two problems and synthesizing them will give the following matrix

equation relating the incident, reflected waves at the port and the port voltage and current:

$$\begin{bmatrix} B \\ I \end{bmatrix} = \begin{bmatrix} \Gamma_{sc} & T_{ant} \\ I_{sc} & Y_{ant} \end{bmatrix} \begin{bmatrix} A \\ V \end{bmatrix} \tag{67}$$

Here Y_{ant} is the input admittance of the wire antenna in figure 16; T_{ant} is the amplitude of the transmitted wave in wire antenna with a unit voltage source across the aperture; Γ_{sc} is the reflection coefficient of the short circuit problem in figure 16; I_{sc} is the current at the short circuit end in figure 16 when the structure is excited with a unit incident wave. A and B are the amplitudes of incident and reflected waves at the port, V and I are the port voltage and current at the via aperture. In this chapter, the exterior problem is the same as reference [60][61]. It consists of a wire bent at the pad and the height is labeled as h.

3.5 The combination of interior and exterior problem

The combination of the solution of the interior and exterior structure is carried out by relating the port voltage and current at the via aperture. Due to the decomposition technique we used here, interior and exterior problem are completely isolated with each other, which allows us to take care of each other separately and if necessary, modify and refine each problem without affecting the other. Also because of the relation between the interior and exterior problem is based on voltage and currents, we don't need to worry about the higher order modes which usually happends at network junction, those have already been taken care of in each sub-problem.

3.5.1 Single-layered via

By solving the interior problem in figure 15, the port voltage and current are related by the admittance matrix:

$$\begin{bmatrix} I_u \\ I_b \end{bmatrix} = \begin{bmatrix} Y_{11} & Y_{12} \\ Y_{21} & Y_{22} \end{bmatrix} \begin{bmatrix} V_u \\ V_b \end{bmatrix} \tag{68}$$

By solving the exterior problem in figure 15, we have the following matrix equation for

upper port 1:

$$\begin{bmatrix} B_1 \\ I_1 \end{bmatrix} = \begin{bmatrix} \Gamma_{sc1} & T_{ant1} \\ I_{sc1} & Y_{ant1} \end{bmatrix} \begin{bmatrix} A_1 \\ V_1 \end{bmatrix} \tag{69}$$

and the following matrix equation for lower port 2:

$$\begin{bmatrix} B_2 \\ I_2 \end{bmatrix} = \begin{bmatrix} \Gamma_{sc2} & T_{ant2} \\ I_{sc2} & Y_{ant2} \end{bmatrix} \begin{bmatrix} A_2 \\ V_2 \end{bmatrix} \tag{70}$$

From figure 15. we have the following relation of the voltages and currents of the interior and exterior problem:

$$I_u = -I_1 \tag{71}$$

$$I_b = -I_2 \tag{72}$$

$$V_u = V_1 \tag{73}$$

$$V_b = V_2 \tag{74}$$

In order to obtain the scattering parameters of a single vertical via structure. we give a unit incident wave at port 1. $A_1 = 1$. and have port 2 terminated with matched load. which means $A_2 = 0$. Combining equations (68).(69) and (70). we have the following matrix equation for the entire via structure:

$$\begin{bmatrix} 1 & 0 & -T_{ant1} & 0 & 0 & 0 \\ 0 & 1 & -Y_{ant1} & 0 & 0 & 0 \\ 0 & 0 & 0 & 1 & 0 & -T_{ant2} \\ 0 & 0 & 0 & 0 & 1 & -Y_{ant2} \\ 0 & 1 & Y_{11} & 0 & 0 & Y_{12} \\ 0 & 0 & Y_{21} & 0 & 1 & Y_{22} \end{bmatrix} \begin{bmatrix} B_1 \\ I_1 \\ V_1 \\ B_2 \\ I_2 \\ V_2 \end{bmatrix} = \begin{bmatrix} \Gamma_{sc1} \\ I_{sc1} \\ 0 \\ 0 \\ 0 \\ 0 \end{bmatrix} \tag{75}$$

Solving equation (75) gives the reflected wave B_1 at port 1 and transmitted wave B_2 at

port 2, and the scattering parameters of the structure are given as follows:

$$S_{11} = B_1/A_1 = B_1 \tag{76}$$

$$S_{12} = B_2/A_1 = B_2 \tag{77}$$

For a symmetric via structure, $S_{21} = S_{12}$, $S_{22} = S_{11}$; for an asymmetric via structure, S_{21} and S_{22} can also be easily obtained by the same process by exciting the structure at port 2 and have port 1 terminated with matched load.

3.5.2 Multi-layered via

For multi-layered geometry, we decompose the structure into several single-layered vertical via and cascade these single-layered structure in the means of transfer matrix. We first convert the admittance matrix of a single-layered via to its corresponding transfer matrix.

For admittance matrtix, we have:

$$\begin{bmatrix} I_u \\ I_b \end{bmatrix} = \begin{bmatrix} Y_{11} & Y_{12} \\ Y_{21} & Y_{22} \end{bmatrix} \begin{bmatrix} V_1 \\ V_2 \end{bmatrix} \tag{78}$$

For transfer matrix, we have:

$$\begin{bmatrix} V_2 \\ I_b' \end{bmatrix} = \begin{bmatrix} A_{11} & A_{12} \\ A_{21} & A_{22} \end{bmatrix} \begin{bmatrix} V_1 \\ I_u \end{bmatrix} \tag{79}$$

Here $I_b = I_b'$ according to the definition of admittance and transfer matrix.

The conversion from Y matrix elements to A matrix elements is as follows:

$$A_{11} = -\frac{Y_{11}}{Y_{12}} \tag{80}$$

$$A_{12} = \frac{1}{Y_{12}} \tag{81}$$

$$A_{21} = -Y_{21} + \frac{Y_{22}Y_{11}}{Y_{12}} \tag{82}$$

$$A_{22} = -\frac{Y_{22}}{Y_{12}} \tag{83}$$

For multi-layered geometry, we can have:

$$\begin{bmatrix} V_{n2} \\ I'_{nb} \end{bmatrix} = \overline{\overline{A}}_n \overline{\overline{A}}_{n-1} \ldots \overline{\overline{A}}_1 \begin{bmatrix} V_1 \\ I_u \end{bmatrix} \tag{84}$$

and $\overline{\overline{A}} = \overline{\overline{A}}_n \overline{\overline{A}}_{n-1} \ldots \overline{\overline{A}}_1$ is the total transfer matrix for the multi-layered vertical via structure.

To obtain the scattering parameters of the multi-layered via, the total transfer matrix $\overline{\overline{A}}$ is converted back to the admittance matrix $\overline{\overline{Y}}$ and equation (75) is again used to calculate the scattering parameters. The conversion from Y matrix elements to A matrix elements is as follows:

$$Y_{11} = -\frac{A_{11}}{A_{12}} \tag{85}$$

$$Y_{12} = \frac{1}{A_{12}} \tag{86}$$

$$Y_{21} = -A_{21} + \frac{A_{22}A_{11}}{A_{12}} \tag{87}$$

$$Y_{22} = -\frac{A_{22}}{A_{12}} \tag{88}$$

3.6 Analytic formula for short via limit

For the case of short via limit in which the layer thickness is much smaller than the operating wavelength ($kd << 1$), there can be analytic formula derived for the vertical via. Because the short via limit is actually most of the cases in real PCB and eletronic packaging structure, the analytic formula gives intuitive characteristics of the via structure and helps engineer in the prototype of digital design without sophisticated simulation tools.

Note here that d is the layer thickness and not the via length as there are sections of via outside the layered structure. The section of the via outside the layers is included in the exterior problem. Also assume that the via radius and via aperture radius are much smaller than the operating wavelength ($ka << 1, kb << 1$). Then we retain only the $\ell = 0$ term in equation (63) and (64) for admittance.

Using a small argument approximation for the Hankel function in equation (63) and

(64), we have:

$$\begin{aligned} Y_{11} &= Y_{22} = -Y_{12} = -Y_{21} \\ &= -\frac{2\pi j}{\omega\mu d\left[-\log\left(\frac{\gamma ka}{2}\right) - j\frac{\pi}{2}\right]} \end{aligned} \tag{89}$$

where $\gamma = 1.781$. This can be expressed in terms of a simple series impedance for the short vertical via structure:

$$Z = j\omega\frac{\mu d}{2\pi}\left[-\log\left(\frac{\gamma ka}{2}\right) - j\frac{\pi}{2}\right] = j\omega L + R \tag{90}$$

Note that the inductance L and the resistance R given above are frequency dependent.

For the case of multi-layered via, using the transfer matrix cascading approach, we find out that if the total length of the entire via through all the layers is still much smaller than operating wavelength, then the above analytic formula is still valid with d replaced by the sum of the lengths of via section in different layers, which means d corresponds to the total length of the via inside the layers. In fact, short via limit is actually quasi-static limit in that the discontinuity (the vertical via in this case) dimension (here d, b and a) is much smaller than the operating wavelength. And in quasi-static limit we know that the magnetic field inside parallel plate structure is nearly the same as a vertical cylinder, thus a single-layered via of length d has nearly the same effect as a multi-layered via of total length d. Notice again this is only for short via limit where quasi-static applys.

3.7 Results and Discussion:

Figure 17 shows the scattering parameters of a single-layered vertical via. Comparison was made between the approach in this paper and the approach mentioned in [62]. The reason we only compare for single-layered structure is because multi-layered structure can be decomposed into single-layered structure, also the simulation of exterior structure has been totally separated from the simulation of interior structure. To make the comparison, we use the same configuration as the reference with a coaxial cable as the exterior problem. The parameters are: the inner radius of the via $a = 0.457\ mm$, the outer radius of the

via $b = 1.524\ mm$, the layer thickness of each layer $d = 1.524\ mm$, with a layer relative dielectric constant of $\varepsilon_r = 2.2$. The coaxial cable has the same inner and outer radius as the via and it also has a relative dielectric constant of $\varepsilon_r = 2.2$.

There are also other intermediate results can be used for comparison. For example, in our approach, it is also very convenient to obtain short circuit admittance and open circuit admittance. Simply apply an odd excitation voltage at both ports, we will get the short circuit admittance Y_{sc}, and apply an even excitation voltage at both ports, we will get the open circuit admittance Y_{oc}.

Figure 18 shows the propagation characteristics of a through hole via, a single-layered vertical via and a 9-layer vertical via. The inner radius of the via $a = 5\ mil$, the outer radius of the via $b = 15\ mil$, the layer thickness of each layer $d = 10\ mil$, with a layer relative dielectric constant of $\varepsilon_r = 2.2$. For the exterior parameter, the wire radius is the same as the via inner radius, the wire bend is at $h = 40\ mil$. Figure 19 shows the loss comparison of these three kinds of vias. The loss is defined as $L = 1 - |S_{11}|^2 - |S_{21}|^2$. Loss is due to a) radiation by the wire along the planar waveguide, b) discontinuity at the wire bend and the via aperture, c) parallel plate waveguide modes excited between metal layers. We can see clearly that a through hole via has the least radiation loss; a single-layered vertical via has more radiation loss because of the parallel plate waveguide effect of the interior structure; a 9-layer vertical via has the most radiation loss among the three due to the large number of parallel plate waveguide it passes through all the way.

Figure 20 shows the loss comparison of a 9-layer vertical via with different layer thickness. The parameters used in the simulation are the same as in figure 18, except the layer thickness of each layer $d = 10, 12, 15\ mil$ respectively. The comparison shows that radiation loss of a 9-layer vertical via increases as the layer thickness increases. Figure 21 shows the propagation characteristics of this 9-layer via with different layer thickness. The comparison shows that the transmission decreases as the layer thickness increases.

Figure 22 shows the loss comparison of a vertical via with different number of layers. The parameter used in the simulation are the same as in figure 18, except the number of layers is 1,6 and 9 respectively. The comparison shows that the radiation loss of vertical via increases significantly as the number of layers increases. This is because the more layers

there are, the more energy will be radiated out through the parallel plate waveguide. Figure 23 shows the propagation characteristics of vertical via with different number of layers. It shows clearly that the transmission decreases as the number of layer increases.

Figure 24 and 25 shows the comparison of propagation characteristics of a 9-layer vertical via with different outer radius. The parameters used in the simulation are the same as in figure 18, except that the outer radius of the via $b = 12, 15, 18$ *mil* respectively. The comparison shows that radiation loss decreases as the outer radius of the via increases, but it is not so significant as changing the layer thickness or changing the number of layers as we see in figure 20 and 22. This is because the radiation loss in vertical via structure is mainly due to the parallel plate waveguide effect of the two reference planes. Changing the layer thickness or changing the number of layers directly changes the configuration of the waveguide while changing outer radius of the via only affects the capacitance formed by the reference plane and the inner cylinder, which has rather more clear effect on the reflection characteristics as we see in figure 25, the reflection decreases as the outer radius increases. Also the comparison shows that the transmission increases as the outer radius of the via increases.

Figure 26 and 27 shows the comparison of propagation characteristics of a 9-layer vertical via with different inner radius. The parameters used in the simulation are the same as in figure 18, except the inner radius of the via $a = 5, 8, 11$ *mil* respectively. The comparison shows that radiation loss increases as the inner radius of the via increases. For the same reason mentioned above, the effect is not so significant as changing the layer thickness or changing the number of layers. Also the comparison shows that the reflection increases as the inner radius increase while the transmission decreases as the inner radius of the via increases. Together with the above analysis about the outer radius, we can see that changing the inner radius has the opposite effect as changing the outer radius, which suggests that the propagation characteristics actually relates with the ratio of the inner and outer radius.

3.8 Conclusion

A semi-analytical method is presented in this chapter for via discontinuity in high speed circuit from very low frequency to very high frequency. For high frequency, besides TEM

mode, it can consider higher order modes of cylindrical wave as well. The same derivation can be applied to further extend the structure to multiple cylindrical scatterers as treated in chapter 4, the following chapter. For the case of feeding with a coaxial cable, results are in good comparison with reference [62].

The via problem represents major coupling because waves decay as the square root of distance away from the via because of the excitation of plane waveguide modes that are above cutoff.

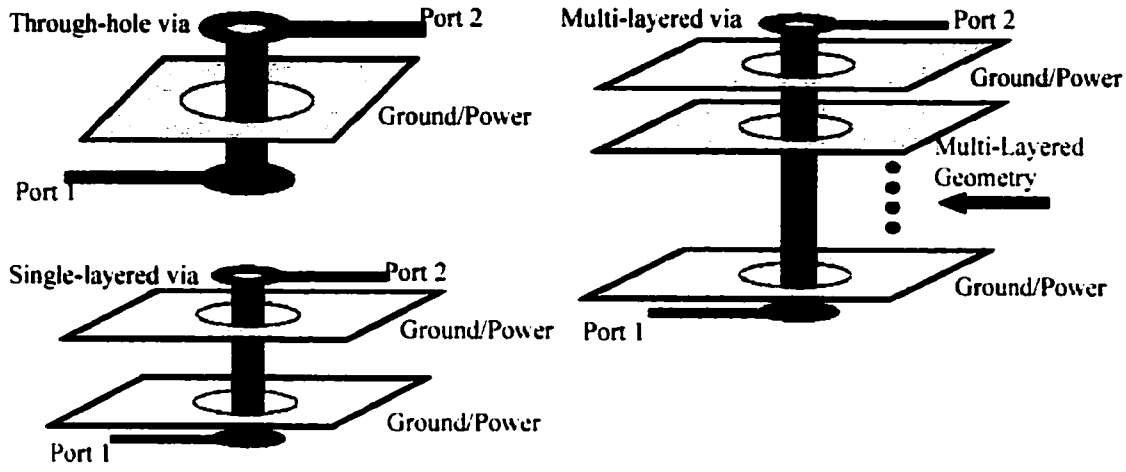

Figure 14: Vertical vias on printed circuit board

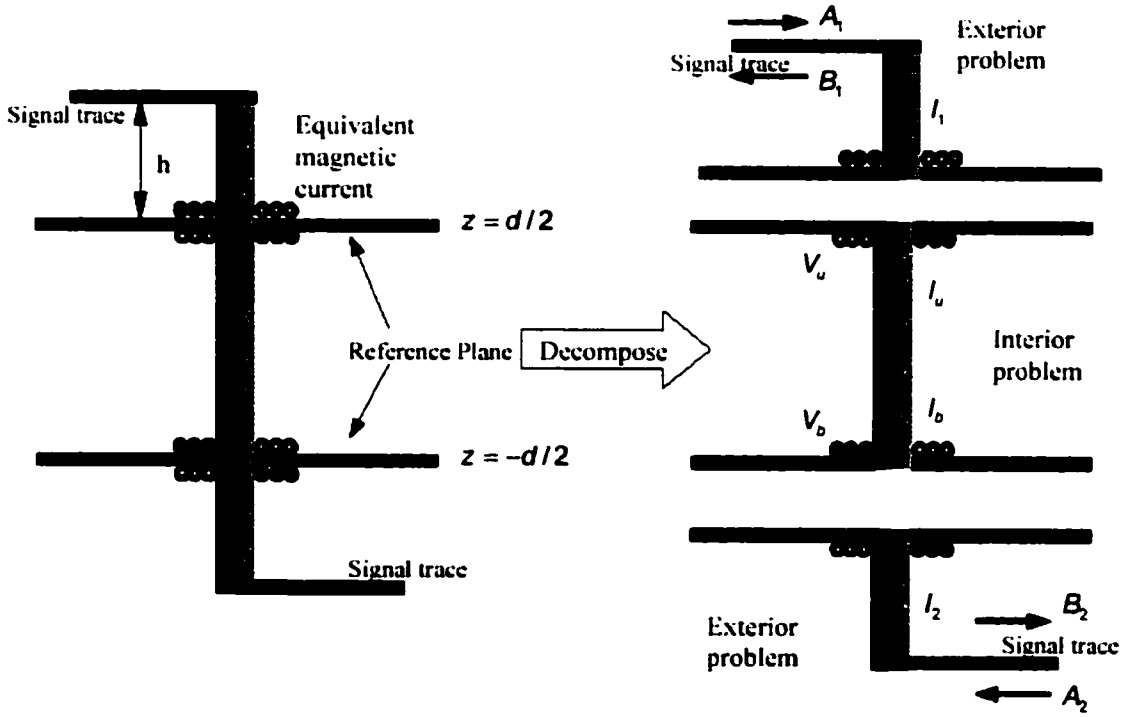

Figure 15: Decomposition of vertical via

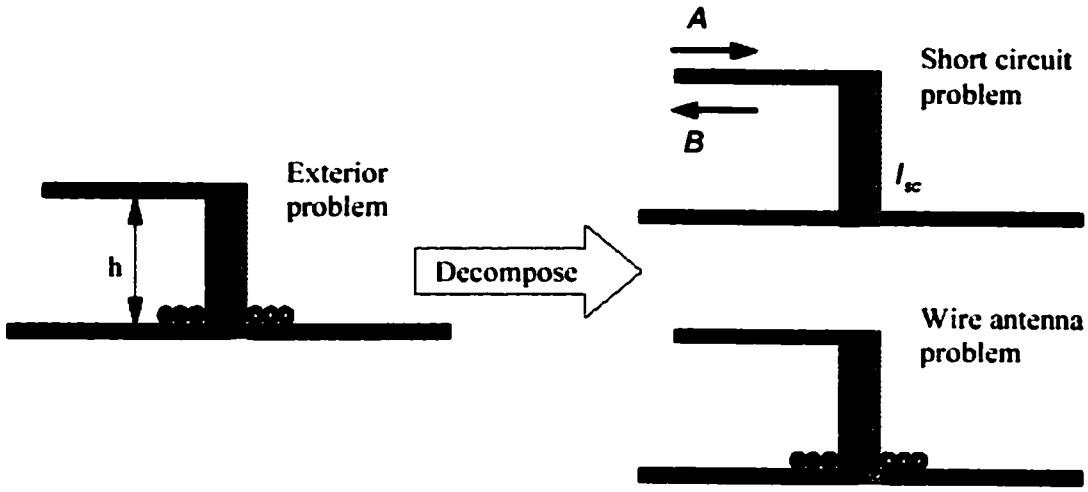

Figure 16: Decomposition of exterior problem

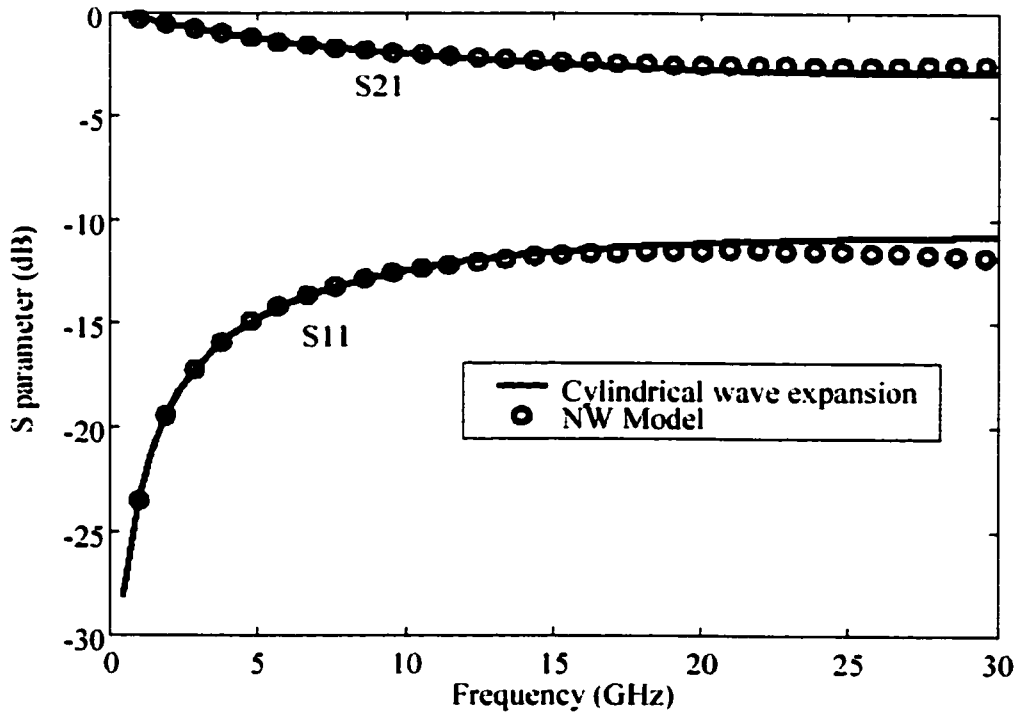

Figure 17: S parameter comparison between two approaches

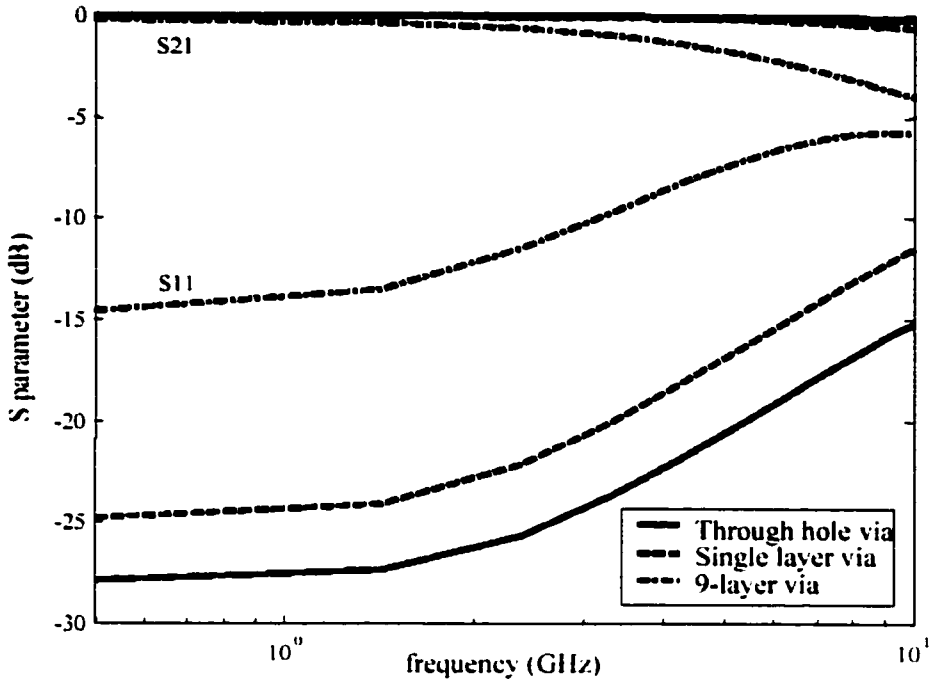

Figure 18: S parameter of 3 kind of vias

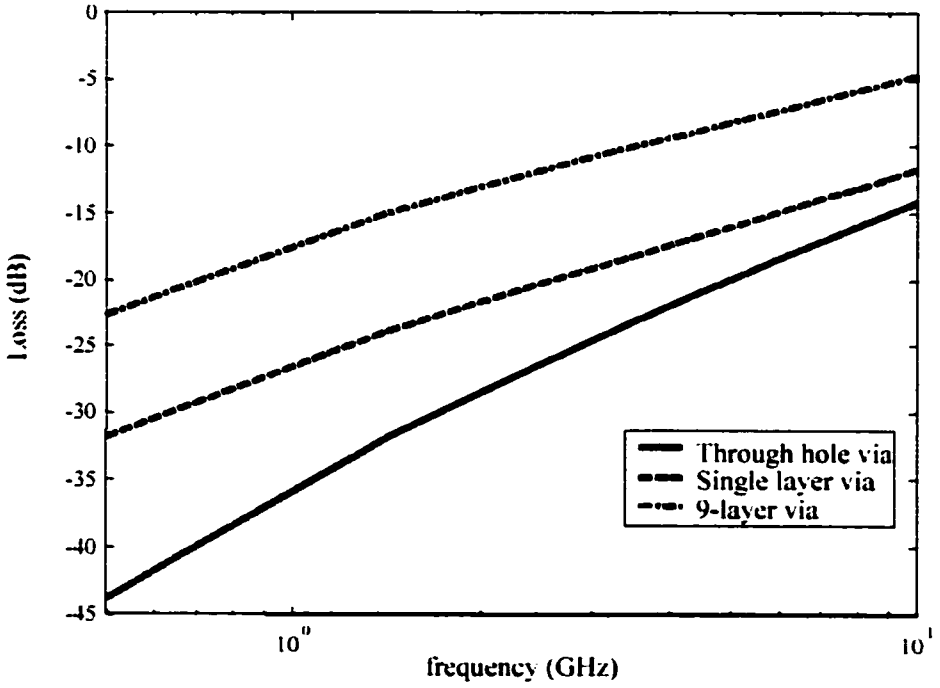

Figure 19: Loss comparison of 3 kinds of vias

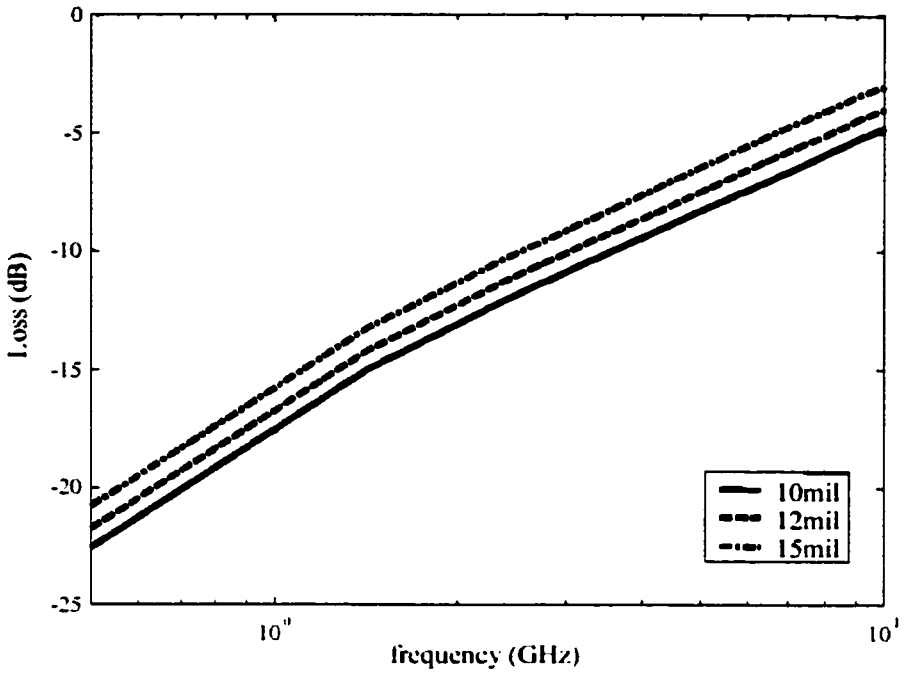

Figure 20: Loss comparison of 9-layer via with different layer thickness

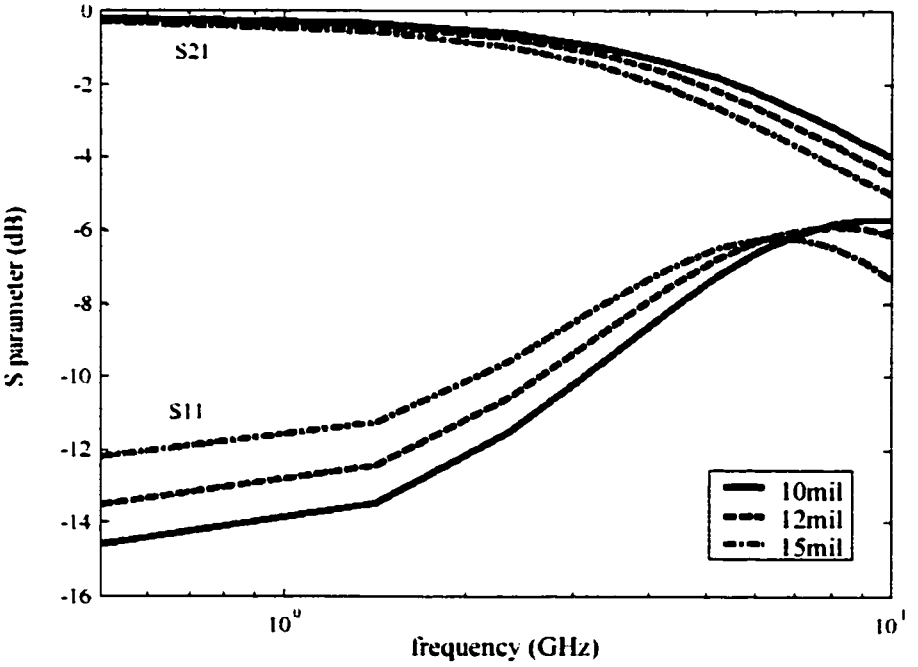

Figure 21: S parameter of 9-layer via with different layer thickness

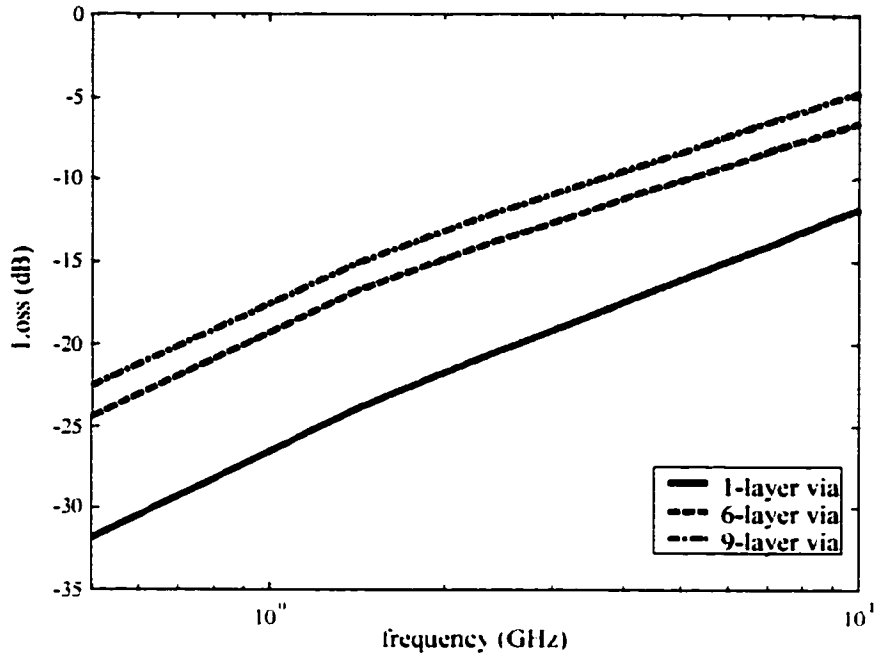

Figure 22: Loss comparison of via with different layer number

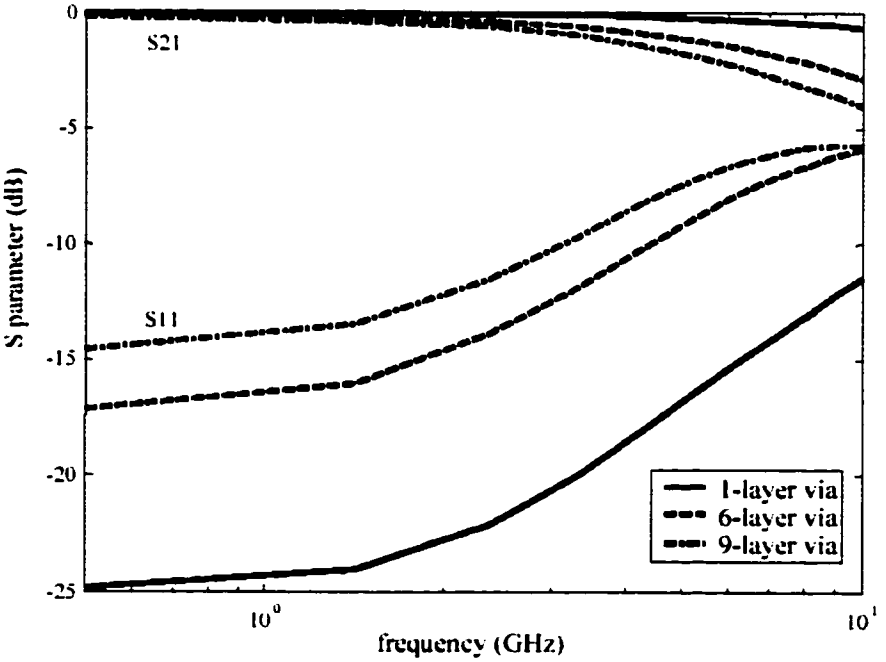

Figure 23: S parameter of via with different layer number

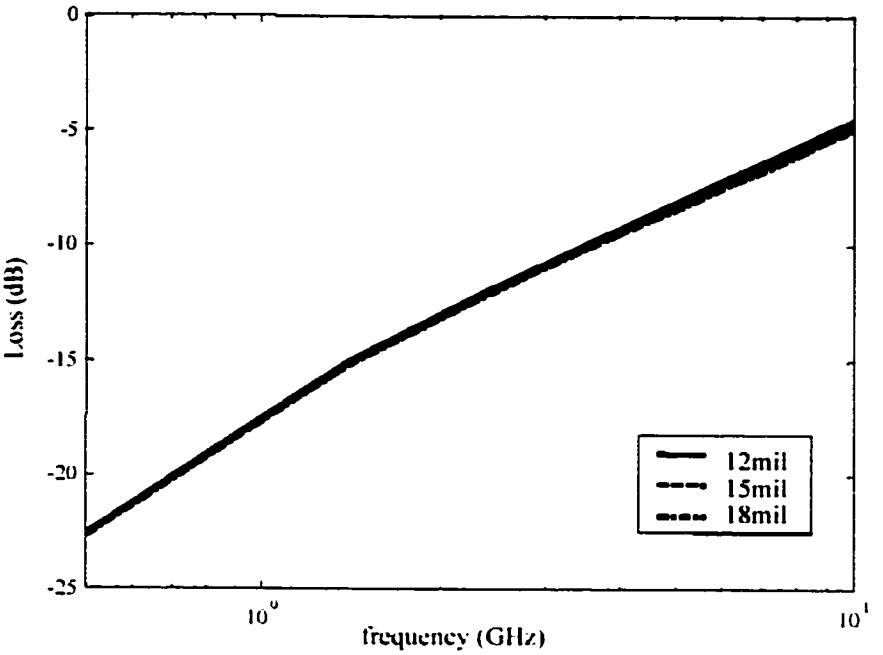

Figure 24: Loss comparison of 9 layer via with different outer radius

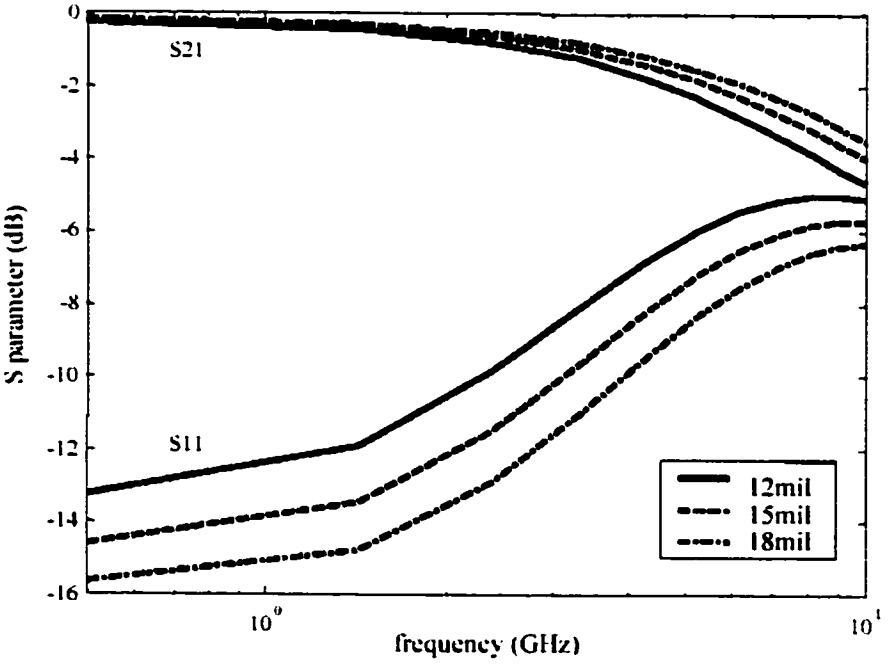

Figure 25: S parameter of 9 layer via with different outer radius

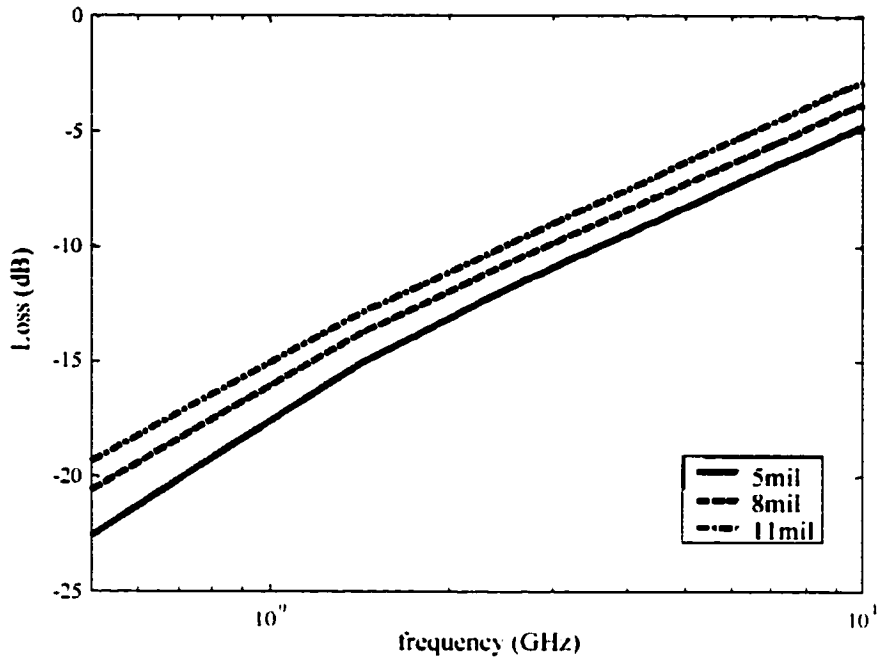

Figure 26: Loss comparison of 9-layer via with different inner radius

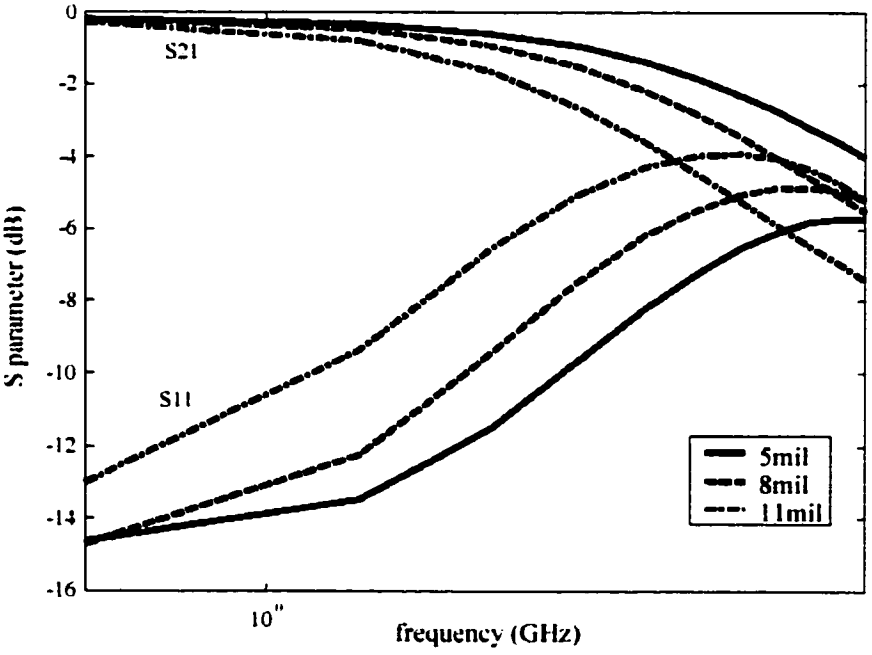

Figure 27: S parameter of 9 layer via with different inner radius

4 Modeling of multiple scattering among vias using Foldy-Lax Equations

4.1 Introduction

The single via analysis in chapter 3 gives reflection, transmission and loss characteristics of single vertical via in multi-layer structure, but in high density circuits, the mutual coupling among vias could be quite strong due to the nature of multi-layered geometry. The parallel reference planes in multi-layered geometry introduce parallel plate waveguide effect, which means the signal (current or voltage) on the active via cylinders will excite waveguide modes along the plane and thus affect other active or passive vias. The induced current/voltage on other via cylinders will in turn affect the original active vias. The coupling through parallel plate waveguide mode generally decays slowly as the square root of distance and poses a significant challenge to reliable, high-speed IC operation. Numerous problems arising therefrom (such as larger delays, loss of signal integrity and false switching of devices) can lead to the malfunctioning of overall systems. In this chapter, we present a semi-analytical approach to model this kind of multiple coupling among large number of vertical vias in layered geometry.

In the past, different types of vias have been investigated using various methods. The capacitance and inductance of a through hole via has been analyzed using quasi-static approach [52]-[57][58] and full wave approach [59]-[61]. Vertical via structure in multi-layered geometry has been analyzed using equivalent circuit and microwave network analysis [62]. The coupling noise among vias could have considerable effect on the overall performance of the system, such as the traces controlling other devices which may false switch devices under coupling noise. Thus the effect of coupling noise must be accounted for in any system simulation for the simulation to predict true hardware performance.

An attempt to account for coupling noise between coupled vias is shown in [63]. The electromagnetic coupling between two adjacent vias in a multi-layered integrated circuit was analyzed by means of equivalent magnetic frill array models [63] incorporated with the even- and odd-mode approach.

A typical multi-via structure is shown in figure 28. Following the previous chapter 3,

we decompose the problem into exterior and interior problem (figure 29) by sealing the via apertures using equivalent magnetic sources. The interior problem consists of a large number of vertical cylinders placed in parallel plate waveguide. The exterior problem consists of coupled transmission lines bent into vertical vias outside the parallel plate waveguide. In a recent paper [69], we solve the interior problem by using Foldy-Lax equations in vector cylindrical waves and waveguide modes. The Foldy-Lax equations are used to study the multiple scattering among the cylindrical vias excited by the magnetic current sources.

In this chapter, we solve the exterior problem by extending the MOM approach of reference [60]. The exterior and interior problem are then combined by equating port voltages and currents. A matrix equation is obtained for the combined interior and exterior problem and solved by iterative method. The solution gives the overall propagation characteristics of the structure. The procedure can simulate cases of several thousand vias with moderate CPU and memory requirements. Recently, differential signaling has drawn considerable interest because of significant less radiation loss. In the chapter we also illustrate results for common and differential modes in differential signaling, and the effect of adjacent idle vias and shorting vias with number of up to thousands.

In the second section of this chapter we summarize the formulation of the interior problem of multiple scattering using Foldy-Lax equations. Magnetic current ring sources are used as excitations. The port currents are expressed in terms of the solutions of the Foldy-Lax equations. In section 3, we extend the MOM approach of reference [60] to treat the exterior problem of coupled transmission lines bent into vertical vias outside the parallel plate waveguide. In section 4, matrix equations are derived to represent the combined exterior and interior problem and iterative method is applied to calculate the solution. In section 5, we illustrate results for the problem of thousands of vias in differential signaling and the effect of shorting vias.

4.2 Formulation of Interior Problem

4.2.1 Multiple Scattering Among Vias using Foldy Lax equations

In the interior problem, we consider coupling among all the vias. Consider two perfect electric conductors at $z = d/2$ and $z = -d/2$. In the multiple via coupling problem, equiv-

alence principle is invoked with equivalent magnetic sources at $z' = \pm d/2$. Consider N via cylinders between the two parallel plates centered at $\overline{\rho}_1, \overline{\rho}_2 \ldots\ldots \overline{\rho}_N$ and magnetic surface current density $\overline{M}_s = \overline{M}_{su}$ at $(\overline{\rho}', z' = d/2)$ and $\overline{M}_s = \overline{M}_{sb}$ at $(\overline{\rho}', z' = -d/2)$. The multiple scattering can be formulated in terms of Foldy-Lax multiple scattering equations. We use the upper sign for results with source $\overline{M}_{su}$ at $(\overline{\rho}', z' = d/2)$ and lower sign for results with source $\overline{M}_{sb}$ at $(\overline{\rho}', z' = -d/2)$. After multiple scattering, the final exciting field of cylinder p is:

$$\begin{aligned} \overline{H}_{ex}^{(p)} &= \sum_{m,\ell} w_{\ell m}^{TM(p)} Rg\overline{H}_m^{TM}(k_{\rho\ell}, k_{z\ell}, \overline{\rho} - \overline{\rho}_p, z \pm d/2) \\ &\quad + \sum_{m,\ell} w_{\ell m}^{TE(p)} Rg\overline{H}_m^{TE}(k_{\rho\ell}, k_{z\ell}, \overline{\rho} - \overline{\rho}_p, z \pm d/2) \end{aligned} \tag{91}$$

where $w_{\ell m}^{TM(p)}$ and $w_{\ell m}^{TE(p)}$ are exciting field coefficients to be solved using Foldy-Lax equations. In the interior problem, the vias are coupled because the excited waveguide mode amplitude decays with the square root of distance from the via.

The Foldy-Lax multiple scattering equations state that the final exciting field of cylinder q is equal to the incident field plus the scattered fields from all other cylinders except the scattered field from itself. The scattered field incident from cylinder p to cylinder q can be re-expressed by using translation addition theorem for modal solution $\overline{H}_n^{TE}$ and $\overline{H}_n^{TM}$ [68].

The Foldy-Lax multiple scattering equations are in the following form:

$$\begin{aligned} & w_{\ell n}^{TM(q)} \\ &= a_{\ell n}^{TM(q)} + \sum_{\substack{p=1 \\ p\neq q}}^{N} \sum_{m=-\infty}^{\infty} H_{n-m}^{(2)}(k_{\rho\ell} \left|\overline{\rho}_p - \overline{\rho}_q\right|) e^{j(n-m)\phi_{\overline{\rho}_p\overline{\rho}_q}} T_m^{(N)} w_{\ell m}^{TM(p)} \end{aligned} \tag{92}$$

$$\begin{aligned} & w_{\ell n}^{TE(q)} \\ &= a_{\ell n}^{TE(q)} + \sum_{\substack{p=1 \\ p\neq q}}^{N} \sum_{m=-\infty}^{\infty} H_{n-m}^{(2)}(k_{\rho\ell} \left|\overline{\rho}_p - \overline{\rho}_q\right|) e^{j(n-m)\phi_{\overline{\rho}_p\overline{\rho}_q}} T_m^{(M)} w_{\ell m}^{TE(p)} \end{aligned} \tag{93}$$

where $a_{\ell n}^{TM(q)}$ and $a_{\ell n}^{TE(q)}$ are the incident fields of the magnetic current source onto cylinder

q and can be calculated by using the primary Green's function derived in the previous section. Notice that in the Foldy-Lax equations there is no coupling between different ℓ modes because each ℓ corresponds to a specific $k_{z\ell}$. Neither is there coupling between TE and TM waves because the via cylinders are assumed perfectly conducting.

The T matrix coefficients in equation (92) and (93) for perfect conducting cylinders are:

$$T_n^{(M)} = T_{-n}^{(M)} = -\frac{J_n'(k_{\rho\ell}a)}{H_n^{(2)\prime}(k_{\rho\ell}a)} \tag{94}$$

$$T_n^{(N)} = T_{-n}^{(N)} = -\frac{J_n(k_{\rho\ell}a)}{H_n^{(2)}(k_{\rho\ell}a)} \tag{95}$$

The incident field from the magnetic surface current source $\overline{M}_s$ onto cylinder q is. using translational addition theorem

$$-j\omega\varepsilon \int d\overline{\rho}' \bar{\bar{G}}_P(\overline{r}, \overline{r}') \cdot \overline{M}_s(\overline{\rho}') = -j\omega\varepsilon \int d\overline{\rho}' \bar{\bar{G}}_P(\overline{\rho} - \overline{\rho}_q, z, \overline{\rho}' - \overline{\rho}_q, z') \cdot \overline{M}_s(\overline{\rho}') \tag{96}$$

We calculate the incident field coefficients onto cylinder q:

$$a_{\ell n}^{TM(q)} = \frac{\eta j\omega\varepsilon}{2d} \frac{(-1)^{n+\ell}}{k_{\rho\ell}^2} f_\ell \int d\overline{\rho}' \overline{m}_{-n}(k_{\rho\ell}, k_{z\ell}, \overline{\rho}' - \overline{\rho}_q) e^{jn\phi'_{\overline{\rho'\rho_q}}} \cdot \overline{M}_s(\overline{\rho}') \tag{97}$$

$$a_{\ell n}^{TE(q)} = \frac{\eta\omega\varepsilon}{2d} \frac{(-1)^{n+\ell}}{k_{\rho\ell}^2} f_\ell \int d\overline{\rho}' \overline{n}_{-n}(k_{\rho\ell}, k_{z\ell}, \overline{\rho}' - \overline{\rho}_q) e^{jn\phi'_{\overline{\rho'\rho_q}}} \cdot \overline{M}_s(\overline{\rho}') \tag{98}$$

After the Foldy-Lax multiple scattering equations are solved. the surface currents on cylinder p are:

$$\begin{aligned} \overline{J}_s^{(p)} &= \sum_{m,\ell} w_{\ell m}^{TM(p)} \overline{J}_s^{TM}(k_{\rho\ell}, k_{z\ell}, z \pm d/2) \\ &\quad + \sum_{m,\ell} w_{\ell m}^{TE(p)} \overline{J}_s^{TE}(k_{\rho\ell}, k_{z\ell}, z \pm d/2) \end{aligned} \tag{99}$$

where the modal surface currents are:

$$\overline{J}_{sn}^{TE}(k_\rho, k_z, z) = -\frac{\frac{2j}{\eta\pi k_\rho a}e^{-jn\phi}}{H_n^{(2)\prime}(k_\rho a)}\left[-\widehat{z}\frac{nk_z}{ka}\cos(k_z z) + \widehat{\phi}\frac{k_\rho^2}{k}j\sin(k_z z)\right] \quad (100)$$

$$\overline{J}_{sn}^{TM}(k_\rho, k_z, z) = \widehat{z}\frac{\frac{2}{\eta\pi a}}{H_n^{(2)}(k_\rho a)}\{\cos k_z z\}\, e^{-jn\phi} \quad (101)$$

4.2.2 Excitation of Magnetic Frill Current

The excitation of magnetic frill currents is mentioned in the analysis of single via in chapter 3. Here we extend it to the general case with N cylinders with voltages $V_{1u}, V_{2u}, \ldots V_{Nu}$ and $V_{1b}, V_{2b}, \ldots V_{Nb}$ (Figure ??). Let there be magnetic frill currents at apertures of via j, $j = 1, 2, 3, \ldots, N$.

At $z' = d/2$:

$$\overline{M}_{su}(\overline{\rho}') = -\frac{V_{ju}}{|\overline{\rho}' - \overline{\rho}_j| \ln\frac{b}{a}}\widetilde{\phi}'_{\overline{\rho}\overline{\rho}_j} \quad \text{for } a \le |\overline{\rho}' - \overline{\rho}_j| \le b \quad (102)$$

At $z' = -d/2$:

$$\overline{M}_{sb}(\overline{\rho}') = -\frac{V_{jb}}{|\overline{\rho}' - \overline{\rho}_j| \ln\frac{b}{a}}\widetilde{\phi}'_{\overline{\rho}\overline{\rho}_j} \quad \text{for } a \le |\overline{\rho}' - \overline{\rho}_j| \le b \quad (103)$$

With upper sources at $z' = d/2$, the TE excitation is zero, the TM incident is:

$$\begin{aligned} & a_{\ell n}^{TM(q)} \\ = \; & \frac{jk}{2d}\frac{(-1)^{n+\ell}}{k_{\rho\ell}^2} f_\ell \frac{2\pi V_{qu}}{\ln\frac{b}{a}}\delta_{n0}\left[H_0^{(2)}(k_{\rho\ell}b) - H_0^{(2)}(k_{\rho\ell}a)\right] \\ & + \sum_{j\neq q}^{N}\frac{jk}{2d}\frac{(-1)^{n+\ell}}{k_{\rho\ell}^2} f_\ell H_n^{(2)}\left(k_{\rho\ell}|\overline{\rho}_q - \overline{\rho}_j|\right) e^{jn\phi_{\overline{\rho}_q\overline{\rho}_j}} \\ & \left[\frac{2\pi V_{ju}}{\ln\frac{b}{a}}\left[J_0(k_{\rho\ell}b) - J_0(k_{\rho\ell}a)\right]\right] \end{aligned} \quad (104)$$

We then solve Foldy-Lax equations for $w_{\ell n}^{TM(q)}$ and find I^{uu}, the currents on the cylinders

at $z = +d/2$ due to sources at $z' = d/2$:

$$I^{(p)uu} = 2\pi a \sum_{\ell} w_{\ell 0}^{TM(p)} k_{\rho\ell} \frac{\frac{2}{\pi k_{\rho\ell} a}}{H_0^{(2)}(k_{\rho\ell} a)} \frac{1}{\eta} (-1)^{\ell} \tag{105}$$

and I^{bu}, the currents on the cylinders at $z = -d/2$ due to sources at $z' = d/2$:

$$I^{(p)bu} = 2\pi a \sum_{\ell} w_{\ell 0}^{TM(p)} k_{\rho\ell} \frac{\frac{2}{\pi k_{\rho\ell} a}}{H_0^{(2)}(k_{\rho\ell} a)} \frac{1}{\eta} \tag{106}$$

Next we consider sources at the lower apertures of $z' = -d/2$, the Foldy-Lax equations are the same. Following similar procedure, we find I^{ub}, the currents on the cylinders at $z = +d/2$ due to sources at $z' = -d/2$; and I^{bb}, the currents on the cylinders at $z = -d/2$ due to sources at $z' = -d/2$.

The total currents are:

$$I^{(p)u} = I^{(p)uu} + I^{(p)ub} \tag{107}$$

$$I^{(p)b} = I^{(p)bu} + I^{(p)bb} \tag{108}$$

4.3 Matrix notation for interior problem

Using matrix notation for interior problem allows us write equations in matrix form, which helps in finding the admittance matrix of interior structure. It also helps the rearrangement of matrix equation later in the combination of exterior and interior problem, and the iterative solver for the entire matrix equation.

Suppose we have N vias, and we keep modes up to $\ell = L_{\max}$ and multipoles up to $n = \pm N_{\max}$. Then the dimension of vector $\overline{w}_{\ell}$ is $(2N_{\max} + 1) \times N$.

Using a combined index α for cylinder index $q = 1, 2, ...N$ and multipole index $n = -N_{\max}, -N_{\max} + 1, ...0, 1, ...N_{\max}$, we have $\alpha(q, n) = (2N_{\max} + 1) \times (q - 1) + n + N_{\max} + 1$. We define $M = N \times (2N_{\max} + 1)$ so $\alpha = 1, 2, ...M$.

Thus we have the excitation field $\overline{w}_\ell$ in vector form:

$$\overline{w}_\ell = \begin{bmatrix} w^{(1)}_{\ell(-N_{\max})} \\ w^{(1)}_{\ell(-N_{\max}+1)} \\ \cdots \\ w^{(1)}_{\ell(N_{\max})} \\ w^{(2)}_{\ell(-N_{\max})} \\ \cdots \\ w^{(2)}_{\ell(N_{\max})} \\ \cdots \\ w^{(N)}_{\ell(-N_{\max})} \\ \cdots \\ w^{(N)}_{\ell(N_{\max})} \end{bmatrix} \tag{109}$$

The Foldy-Lax matrix $\overline{\overline{F}}_\ell$ is of dimension $N(2N_{\max}+1) \times N(2N_{\max}+1) = M \times M$:

$$\left[\overline{\overline{F}}_\ell\right]_{qn,pm} = \delta_{nm}\delta_{qp} - (1-\delta_{pq}) H^{(2)}_{n-m}\left(k_{\rho\ell}\left|\overline{\rho}_p - \overline{\rho}_q\right|\right) e^{j(n-m)\phi_{\overline{\rho_p\rho_q}}} T^{(N)}_m \tag{110}$$

Define incident field matrix $\overline{\overline{E}}_\ell$ be of dimension $M \times N$ so that

$$\left[\overline{\overline{E}}_\ell\right]_{qn,j} = \left[\overline{a}_{\ell j}\right]_{qn} \tag{111}$$

where

$$\begin{aligned} &\left[\overline{a}_{\ell j}\right]_{qn} \\ &= \frac{jk}{2d}\frac{(-1)^\ell}{k^2_{\rho\ell}} f_\ell \frac{2\pi}{\ln\frac{b}{a}}\delta_{n0}\left[H^{(2)}_0(k_{\rho\ell}b) - H^{(2)}_0(k_{\rho\ell}a)\right] \quad .....if\ q = j \\ &= \frac{jk}{2d}\frac{(-1)^{n+\ell}}{k^2_{\rho\ell}} f_\ell H^{(2)}_n\left(k_{\rho\ell}\left|\overline{\rho}_q - \overline{\rho}_j\right|\right) e^{jn\phi_{\overline{\rho_q\rho_j}}}\left[\frac{2\pi}{\ln\frac{b}{a}}\left[J_0(k_{\rho\ell}b) - J_0(k_{\rho\ell}a)\right]\right] \quad .....if\ q \neq j \end{aligned} \tag{112}$$

For voltage sources at upper aperture $z' = d/2$, let voltage vector $\overline{V}^u$ of dimension N, with $\left[\overline{V}^u\right]_j = V_{ju}$.

Then in matrix form, the Foldy-Lax equation for upper sources is:

$$\overline{\overline{F}}_\ell \overline{w}_\ell^{(u)} = \overline{\overline{E}}_\ell \overline{V}^u \tag{113}$$

Solve equation (113), we have current on the pth cylinder at the upper aperture $\overline{I}^{uu}$, and current at the lower aperture $\overline{I}^{bu}$ given by

$$I^{(p)uu} = \sum_\ell B_\ell w_{\ell 0}^{TM(p)u} \tag{114}$$

$$I^{(p)bu} = \sum_\ell D_\ell w_{\ell 0}^{TM(p)u} \tag{115}$$

where

$$B_\ell = \frac{4(-1)^\ell}{\eta H_0^{(2)}(k_{\rho\ell} a)} \tag{116}$$

$$D_\ell = \frac{4}{\eta H_0^{(2)}(k_{\rho\ell} a)} \tag{117}$$

For voltage sources at lower aperture $z' = -d/2$. similarly we have Foldy-Lax equation for lower sources:

$$\overline{\overline{F}}_\ell \overline{w}_\ell^{(b)} = \overline{\overline{E}}_\ell \overline{V}^b$$

and currents on the pth cylinder at the upper aperture $\overline{I}^{ub}$. and at the lower aperture $\overline{I}^{bb}$:

$$I^{(p)ub} = \sum_\ell B_\ell w_{\ell 0}^{TM(p)b} \tag{118}$$

$$I^{(p)bb} = \sum_\ell D_\ell w_{\ell 0}^{TM(p)b} \tag{119}$$

The port current is the sum of upper and lower sources:

$$I^{(p)u} = I^{(p)uu} + I^{(p)ub} \tag{120}$$

$$I^{(p)b} = I^{(p)bu} + I^{(p)bb} \tag{121}$$

Write in the admittance matrix form:

$$\overline{I} = \begin{bmatrix} \overline{\overline{Y}}^{uu} & \overline{\overline{Y}}^{ub} \\ \overline{\overline{Y}}^{bu} & \overline{\overline{Y}}^{bb} \end{bmatrix} \begin{bmatrix} \overline{V}^{u} \\ \overline{V}^{b} \end{bmatrix} \tag{122}$$

4.4 Admittance matrix of the interior structure

If only considering the interior structure, we can already obtain the admittance matrix of the interior structure by now. In the previous section, we take into account the coupling terms, which are the lower order l modes, here we consider the higher order l modes. The definition of lower and higher order l modes depends on the actual geometry and the accuracy requirement of the simulation, usually $l > 1$ will be considered higher order modes. We know that the higher order l modes decays very fast and will not couple to other vias, so $w_{ln}^{TM(p)} = a_{ln}^{TM(p)}$. This $a_{ln}^{TM(p)}$ is generated by source at cylinder p and $n = 0$.

$$I^{(p)uu\_extra} = \sum_{l} B_{\ell} w_{l0}^{TM(p)u} = \sum_{l} B_{\ell} a_{l0}^{TM(p)u} \tag{123}$$

$$I^{(p)bu\_extra} = \sum_{l} D_{\ell} w_{l0}^{TM(p)u} = \sum_{l} D_{\ell} a_{l0}^{TM(p)u} \tag{124}$$

In matrix form:

$$\overline{I}^{uu\_extra} = \overline{\overline{Y}}^{uu\_extra}\,\overline{V}^{u} \tag{125}$$

$$\overline{I}^{bu\_extra} = \overline{\overline{Y}}^{bu\_extra}\,\overline{V}^{u} \tag{126}$$

Similarly, we have:

$$\overline{I}^{ub\_extra} = \overline{\overline{Y}}^{ub\_extra}\,\overline{V}^{b} \tag{127}$$

$$\overline{I}^{bb\_extra} = \overline{\overline{Y}}^{bb\_extra}\,\overline{V}^{b} \tag{128}$$

The total current is the sum of lower order mode currents and higher order currents:

$$\overline{I}^{total} = \overline{I} + \overline{I}^{extra} \tag{129}$$

and write in the admittance matrix form:

$$\begin{aligned} \overline{I}^{total} &= \overline{I} + \overline{I}^{extra} \\ &= \begin{bmatrix} \overline{\overline{Y}}^{uu} + \overline{\overline{Y}}^{uu\_extra} & \overline{\overline{Y}}^{ub} + \overline{\overline{Y}}^{ub\_extra} \\ \overline{\overline{Y}}^{bu} + \overline{\overline{Y}}^{bu\_extra} & \overline{\overline{Y}}^{bb} + \overline{\overline{Y}}^{bb\_extra} \end{bmatrix} \begin{bmatrix} \overline{V}^{u} \\ \overline{V}^{b} \end{bmatrix} \\ &= \overline{\overline{Y}}\,\overline{V} \end{aligned} \tag{130}$$

If the exterior problem is simplified as identical traces with characteristic admittance of Y_0, the scattering matrix of the entire structure is:

$$\overline{\overline{S}} = \left(\overline{\overline{Y}} + Y_0\overline{\overline{I}}\right)^{-1}\left(Y_0\overline{\overline{I}} - \overline{\overline{Y}}\right) \tag{131}$$

where $\overline{\overline{I}}$ is the unit diagonal matrix.

4.5 Formulation of exterior problem

In general, the exterior problem consists of large number of transmission lines that are bent to connect to the sections of vias that are outside the parallel plate waveguide. The exterior problem can be solved by the MOM approach. In the multi-via coupling problem, we consider two types of exterior problem.

4.5.1 Case A: Exterior problem with uncoupled transmission lines

In this case, there are N transmission lines/bent wires above the layered medium that are uncoupled and N transmission lines/wires below the layered medium that are also uncoupled. For simplicity, we shall assume that the transmission lines are identical. Using the notations in chapter 2, for the pth via, the exterior problem has

$$\begin{bmatrix} B_u^{(p)} \\ I_u^{(p)} \end{bmatrix} = \begin{bmatrix} \Gamma_{sc} & T_{ant} \\ I_{sc} & Y_{ant} \end{bmatrix} \begin{bmatrix} A_u^{(p)} \\ -V_u^{(p)} \end{bmatrix} \tag{132}$$

$$\begin{bmatrix} B_b^{(p)} \\ -I_b^{(p)} \end{bmatrix} = \begin{bmatrix} \Gamma_{sc} & T_{ant} \\ I_{sc} & Y_{ant} \end{bmatrix} \begin{bmatrix} A_b^{(p)} \\ V_b^{(p)} \end{bmatrix} \tag{133}$$

for upper port and bottom port respectively. This is solved in single via case in chapter 3.

4.5.2 Case B: Coupling among a small number of lines/wires in the exterior problem

We next consider the case where there is coupling among a small number of lines. Without loss of generality, in this chapter we consider the case of two coupled transmission lines that are bent into the two vertical via sections outside the parallel plate waveguide (figure 30). The method can be readily extended to coupling among a finite number of lines and two lines coupling is the most common case in differential signaling.

Let (1) and (2) be the two coupled lines/bent wires. Then we have:

$$\begin{bmatrix} B_u^{(1)} \\ B_u^{(2)} \\ I_u^{(1)} \\ I_u^{(2)} \end{bmatrix} = \begin{bmatrix} \Gamma_{sc11} & \Gamma_{sc12} & T_{ant11} & T_{ant12} \\ \Gamma_{sc21} & \Gamma_{sc22} & T_{ant21} & T_{ant22} \\ I_{sc11} & I_{sc12} & Y_{ant22} & Y_{ant22} \\ I_{sc21} & I_{sc22} & Y_{ant22} & Y_{ant22} \end{bmatrix} \begin{bmatrix} A_u^{(1)} \\ A_u^{(2)} \\ -V_u^{(1)} \\ -V_u^{(2)} \end{bmatrix} \tag{134}$$

$$\begin{bmatrix} B_b^{(1)} \\ B_b^{(2)} \\ -I_b^{(1)} \\ -I_b^{(2)} \end{bmatrix} = \begin{bmatrix} \Gamma_{sc11} & \Gamma_{sc12} & T_{ant11} & T_{ant12} \\ \Gamma_{sc21} & \Gamma_{sc22} & T_{ant21} & T_{ant22} \\ I_{sc11} & I_{sc12} & Y_{ant22} & Y_{ant22} \\ I_{sc21} & I_{sc22} & Y_{ant22} & Y_{ant22} \end{bmatrix} \begin{bmatrix} A_b^{(1)} \\ A_b^{(2)} \\ V_b^{(1)} \\ V_b^{(2)} \end{bmatrix} \tag{135}$$

Solve the exterior problem using MOM, and the matrix elements Γ_{sc}, T_{ant}, I_{sc} and Y_{ant} can be calculated using the matrix-penciled moment method [70][60]. Based on the equivalence principle and the image theorem, the two coupled transmission lines shown in the left of figure 30 can be treated as the new structure shown in the right of figure 30. We extend the approach in [60]. Let the two transmission lines be thin wire so that the current density on them can be represented by $I_1(s)$ and $I_2(s)$. The integral equation that the current has to satisfy is:

$$\begin{aligned} j\omega\epsilon\hat{s}\cdot\overline{E}^t(s) &= \int I_1(s')\left[\frac{\partial^2}{\partial s\partial s'} - k^2\hat{s}\cdot\hat{s}'\right]G(s,s')ds' \\ &\quad + \int I_2(s')\left[\frac{\partial^2}{\partial s\partial s'} - k^2\hat{s}\cdot\hat{s}'\right]G(s,s')ds' \end{aligned} \tag{136}$$

where s is the point on the two transmission lines and $\widehat{s}$ is the unit vector tangential to the transmission line at the point of s. $G(s,s') = \frac{e^{-jkr}}{4\pi r}$ is the Green's function of free space where $r = |\overline{s} - \overline{s}'|$.

The incident field $\overline{E}^i(s)$ on the wire is determined by the magnetic frill currents $\overline{M}_1(\overline{r}')$ and $\overline{M}_2(\overline{r}')$:

$$\overline{E}^i(s) = \nabla \times \left\{ \int G(s,\overline{r}') \cdot 2\overline{M}_1(\overline{r}')d\Omega' + \int G(s,\overline{r}') \cdot 2\overline{M}_2(\overline{r}')d\Omega' \right\} \tag{137}$$

Equation (136) can be solved using the method of moment [13]. Using the one dimensional rooftop basis function $f_n(s)$, current $I_1(s)$ and $I_2(s)$ can be expressed as

$$I_1(s) = \sum_{n=0}^{2N} c_n^1 f_n(s) \tag{138}$$

$$I_2(s) = \sum_{n=0}^{2N} c_n^2 f_n(s) \tag{139}$$

Because of the symmetry of this structure, the current coefficient c_n^1 at the nth subsection on wire 1 is the same as the current coefficient c_{2N-n}^1 at the $(2N-n)$th subsection. So are c_n^2 and c_{2N-n}^2, etc. Substituting the above equations into integral equation (136) and using Galerkin's method, we have:

$$\begin{aligned} & \sum_{n=1}^{N-1} (Z_{m,n}^{(i)(1)} + Z_{m,2N-n}^{(i)(1)}) c_n^1 + Z_{m,N}^{(i)(1)} c_N^1 \\ & \sum_{n=1}^{N-1} (Z_{m,n}^{(i)(2)} + Z_{m,2N-n}^{(i)(2)}) c_n^2 + Z_{m,N}^{(i)(2)} c_N^2 \\ = \; & V_m^{(i)} - (Z_{m,0}^{(i)(1)} + Z_{m,2N}^{(i)(1)}) c_0^1 - (Z_{m,0}^{(i)(2)} + Z_{m,2N}^{(i)(2)}) c_0^2 \end{aligned} \tag{140}$$

The index of $i = 1$ means the testing point is on wire 1 and $i = 2$ on wire 2.

The impedance matrix element is:

$$Z_{m,n}^{(i)(j)} = \int \int f_m(s^{(i)}) f_n(s'^{(j)}) \left[\frac{\partial^2}{\partial s^{(i)} \partial s'^{(j)}} - k^2 \widehat{s}^{(i)} \cdot \widehat{s}'^{(j)} \right] G(s^{(i)}, s'^{(j)}) ds'^{(j)} ds^{(i)} \tag{141}$$

and

$$V_m^{(i)} = j\omega\epsilon \int f_m(s^{(i)})\widehat{s}^{(i)} \cdot \overline{E}^t(s^{(i)})ds^{(i)} \tag{142}$$

Solving matrix equation (140) gives the current distribution on the two wires. Using the matrix pencil method [70], the amplitude A and B of the incident and reflected waves on the two wires can be extracted from the current distribution.

To obtain Γ_{sc}, I_{sc}, T_{ant} and Y_{ant}, first we let the voltage drop V between via and ground plane be zero and enforce a current source $c_0^1 = 1$ at the truncated end of the 1st transmission line. The amplitudes A_1, A_2, B_1 and B_2 are calculated as discussed above. Considering $V_u^{(1)} = V_u^{(2)} = 0$ and $\Gamma_{sc11} = \Gamma_{sc22}$, $\Gamma_{sc12} = \Gamma_{sc21}$ due to the symmetry of the two wire structure, Γ_{sc} and I_{sc} are calculated by:

$$\Gamma_{sc11} = \Gamma_{sc22} = \frac{A_1B_1 - A_2B_2}{A_1A_1 - A_2A_2} \tag{143}$$

$$\Gamma_{sc12} = \Gamma_{sc21} = \frac{A_1B_2 - A_2B_1}{A_1A_1 - A_2A_2} \tag{144}$$

$$I_{sc11} = I_{sc22} = \frac{A_1I_1 - A_2I_2}{A_1A_1 - A_2A_2} \tag{145}$$

$$I_{sc12} = I_{sc21} = \frac{A_1I_2 - A_2I_1}{A_1A_1 - A_2A_2} \tag{146}$$

After Γ_{sc} and I_{sc} are found, let $V_u^{(1)} = -1$, $V_u^{(2)} = 0$, $c_0^1 = c_0^2 = 0$. Following the same procedure, amplitudes A_1, A_2, B_1 and B_2 are obtained, and T_{ant} and Y_{ant} are calculated by:

$$T_{ant11} = T_{ant22} = B_1 - \Gamma_{sc11}A_1 - \Gamma_{sc12}A_2 \tag{147}$$

$$T_{ant12} = T_{ant21} = B_2 - \Gamma_{sc21}A_1 - \Gamma_{sc22}A_2 \tag{148}$$

$$Y_{ant11} = Y_{ant22} = I_1 - I_{sc11}A_1 - I_{sc12}A_2 \tag{149}$$

$$Y_{ant12} = Y_{ant21} = I_2 - I_{sc21}A_1 - I_{sc22}A_2 \tag{150}$$

Generalization to N lines/wires coupling in exterior problem The above illustrates the case for two coupled lines that are bent to connect to the vias outside the parallel plate waveguide. For N lines/bent wires in the exterior problem, we havethe following

general matrix expression:

$$\overline{B}^u = \overline{\overline{\Gamma}}_{sc}\overline{A}^u - \overline{\overline{T}}_{ant}\overline{V}^u \quad (151)$$

$$\overline{I}^u = \overline{\overline{I}}_{sc}\overline{A}^u - \overline{\overline{Y}}_{ant}\overline{V}^u \quad (152)$$

$$\overline{B}^b = \overline{\overline{\Gamma}}_{sc}\overline{A}^b + \overline{\overline{T}}_{ant}\overline{V}^b \quad (153)$$

$$-\overline{I}^b = \overline{\overline{I}}_{sc}\overline{A}^b + \overline{\overline{Y}}_{ant}\overline{V}^b \quad (154)$$

If we assume that coupling only exists among a small number of lines/wires where the rest are uncoupled (which is the most common case in real circuit application). Then $\overline{\overline{\Gamma}}_{sc}, \overline{\overline{T}}_{ant}, \overline{\overline{I}}_{sc}$ and $\overline{\overline{Y}}_{ant}$ are $\mathcal{N} \times \mathcal{N}$ sparse matrices in block form with no coupling among the blocks. For example, if only two lines are coupled, then we have a 2×2 block for these two lines and the rest of the $\mathcal{N} \times \mathcal{N}$ matrix are diagonal.

4.6 Combination of exterior and interior problem and iterative solution

Next we combine the exterior and interior problem. We consider two coupled transmission lines (bent) and the rest $\mathcal{N} - 2$ lines are uncoupled for the exterior problem. However, the $\mathcal{N}$ vias are coupled in the interior problem.

After the solution of interior and exterior problem, they are already in matrix form and can be readily combined by relating port voltages and currents without rearrangement. However, the resulting combined matrix equation has large condition number and unsuitable for iterative solver. The rearrangement of the matrix equation can result in a smaller matrix with much better condition number and is essential for iterative solver.

In the interior problem, there are strong coupling among vias because the TEM mode is propagating and decays only as square root of distance. For $\ell = 0$ mode, we include coupling of all vias. For small layer thickness, the higher order modes are quickly evanescent, so we assume that the higher order modes are coupled in the near field only. In the simulations, we consider higher order modes ($\ell \geq 1$) coupling for the several vias that have coupling in the corresponding exterior problem.

For $\ell = 0$ mode:

$$\overline{\overline{F}}_0 \overline{W}^{(0)u} = \overline{\overline{E}}_0 \overline{V}^u \tag{155}$$

$$\overline{\overline{F}}_0 \overline{W}^{(0)b} = \overline{\overline{E}}_0 \overline{V}^b \tag{156}$$

where $\overline{\overline{F}}_0$ and $\overline{\overline{E}}_0$ are dense $N \times N$ full matrices.

For $\ell \geq 1$ modes:

$$\overline{\overline{F}}_\ell \overline{W}^{(\ell)u} = \overline{\overline{E}}_\ell \overline{V}^u \tag{157}$$

$$\overline{\overline{F}}_\ell \overline{W}^{(\ell)b} = \overline{\overline{E}}_\ell \overline{V}^b \tag{158}$$

where $\overline{\overline{F}}_\ell$ and $\overline{\overline{E}}_\ell$ are given in equations (110) and (111). The elements in $\overline{\overline{F}}_\ell$ and $\overline{\overline{E}}_\ell$ are zero if the corresponding lines in the exterior problem are not coupled. Thus for higher order modes ($\ell \geq 1$), we have block sparse matrices of $\overline{\overline{F}}_\ell$ and $\overline{\overline{E}}_\ell$.

Let $\overline{\overline{P}}_\ell = \overline{\overline{F}}_\ell^{-1} \overline{\overline{E}}_\ell$, we have:

$$\overline{W}^{(\ell)u} = \overline{\overline{P}}_\ell \overline{V}^u \tag{159}$$

$$\overline{W}^{(\ell)b} = \overline{\overline{P}}_\ell \overline{V}^b \tag{160}$$

Note that taking inverse of block matrices $\overline{\overline{E}}_\ell$, $\overline{\overline{F}}_\ell$, $\overline{\overline{P}}_\ell$ ($\ell \geq 1$), $\overline{\overline{\Gamma}}_{sc}$, $\overline{\overline{T}}_{ant}$, $\overline{\overline{I}}_{sc}$ and $\overline{\overline{Y}}_{ant}$ are inexpensive.

From the interior problem we have:

$$\begin{aligned}
\overline{I}^u &= \overline{I}^{uu} + \overline{I}^{ub} \\
&= \sum_{\ell=0}^{\infty} B_\ell \overline{W}^{(\ell)u} + \sum_{\ell=0}^{\infty} D_\ell \overline{W}^{(\ell)b} \\
&= B_0 \overline{W}^{(0)u} + D_0 \overline{W}^{(0)b} + \sum_{\ell=1}^{\infty} B_\ell \overline{W}^{(\ell)u} + \sum_{\ell=1}^{\infty} D_\ell \overline{W}^{(\ell)b} \\
&= B_0 \overline{W}^{(0)u} + D_0 \overline{W}^{(0)b} + \overline{\overline{Y}}^{uu}_{extra} \overline{V}^u + \overline{\overline{Y}}^{ub}_{extra} \overline{V}^b
\end{aligned} \tag{161}$$

$$\overline{I}^b = D_0 \overline{W}^{(0)u} + B_0 \overline{W}^{(0)b} + \overline{\overline{Y}}^{bu}_{extra} \overline{V}^u + \overline{\overline{Y}}^{bb}_{extra} \overline{V}^b \tag{162}$$

where $\overline{\overline{Y}}^{uu}_{extra}, \overline{\overline{Y}}^{ub}_{extra}, \overline{\overline{Y}}^{bu}_{extra}$, and $\overline{\overline{Y}}^{bb}_{extra}$ are calculated from the block matrices:

$$\overline{\overline{Y}}^{uu}_{extra} = \overline{\overline{Y}}^{bb}_{extra} = \sum_{\ell=1}^{\infty} B_\ell \overline{\overline{P}}_\ell \tag{163}$$

$$\overline{\overline{Y}}^{ub}_{extra} = \overline{\overline{Y}}^{bu}_{extra} = \sum_{\ell=1}^{\infty} D_\ell \overline{\overline{P}}_\ell \tag{164}$$

Note that $\overline{\overline{Y}}^{uu}_{extra}$ and $\overline{\overline{Y}}^{ub}_{extra}$ are also $\mathcal{N} \times \mathcal{N}$ block matrices.

Since $B_0 = D_0$, we have:

$$\overline{I}^u - \overline{I}^b = (\overline{\overline{Y}}^{uu}_{extra} - \overline{\overline{Y}}^{ub}_{extra})(\overline{V}^u - \overline{V}^b) \tag{165}$$

From the exterior problem we have:

$$\overline{V}^u = \overline{\overline{T}}^{-1}_{ant}\overline{B}^u - \overline{\overline{T}}^{-1}_{ant}\overline{\overline{\Gamma}}_{sc}\overline{A}^u \tag{166}$$

$$\overline{V}^b = -\overline{\overline{T}}^{-1}_{ant}\overline{B}^b + \overline{\overline{T}}^{-1}_{ant}\overline{\overline{\Gamma}}_{sc}\overline{A}^b \tag{167}$$

$$\overline{I}^u = -\overline{\overline{Y}}_{ant}\overline{\overline{T}}^{-1}_{ant}\overline{B}^u + \left(\overline{\overline{I}}_{sc} + \overline{\overline{Y}}_{ant}\overline{\overline{T}}^{-1}_{ant}\overline{\overline{\Gamma}}_{sc}\right)\overline{A}^u \tag{168}$$

$$\overline{I}^b = \overline{\overline{Y}}_{ant}\overline{\overline{T}}^{-1}_{ant}\overline{B}^b - \left(\overline{\overline{I}}_{sc} + \overline{\overline{Y}}_{ant}\overline{\overline{T}}^{-1}_{ant}\overline{\overline{\Gamma}}_{sc}\right)\overline{A}^b \tag{169}$$

Subtract equations (166) and (168) with equations (167) and (169) and substitute into (165), we have:

$$-\overline{\overline{Y}}_{ant}\overline{\overline{T}}^{-1}_{ant}(\overline{B}^u + \overline{B}^b) + \left(\overline{\overline{I}}_{sc} + \overline{\overline{Y}}_{ant}\overline{\overline{T}}^{-1}_{ant}\overline{\overline{\Gamma}}_{sc}\right)(\overline{A}^u + \overline{A}^b) \tag{170}$$

$$= (\overline{\overline{Y}}^{uu}_{extra} - \overline{\overline{Y}}^{ub}_{extra})\left[\overline{\overline{T}}^{-1}_{ant}(\overline{B}^u + \overline{B}^b) - \overline{\overline{T}}^{-1}_{ant}\overline{\overline{\Gamma}}_{sc}(\overline{A}^u + \overline{A}^b)\right] \tag{171}$$

which gives:

$$(\overline{B}^u + \overline{B}^b) = \overline{\overline{\Gamma}}_{ratio}(\overline{A}^u + \overline{A}^b) \tag{172}$$

where

$$\begin{aligned}
&\bar{\bar{\Gamma}}_{ratio} \\
&= \bar{\bar{T}}_{ant}\left[\bar{\bar{Y}}_{ant} + (\bar{\bar{Y}}^{uu}_{extra} - \bar{\bar{Y}}^{ub}_{extra})\right]^{-1}\left[\bar{\bar{I}}_{sc} + (\bar{\bar{Y}}_{ant} + \bar{\bar{Y}}^{uu}_{extra} - \bar{\bar{Y}}^{ub}_{extra})\bar{\bar{T}}^{-1}_{ant}\bar{\bar{\Gamma}}_{sc}\right] \quad (173)
\end{aligned}$$

Note that the above are all block $N \times N$ matrices, so taking inverse does not require much CPU. Neither is much required for the memory.

Rewrite equation (167) using (172):

$$\begin{aligned}
\overline{V}^b &= -\bar{\bar{T}}^{-1}_{ant}\left[-\overline{B}^u + \bar{\bar{\Gamma}}_{ratio}(\overline{A}^u + \overline{A}^b)\right] + \bar{\bar{T}}^{-1}_{ant}\bar{\bar{\Gamma}}_{sc}\overline{A}^b \\
&= \bar{\bar{T}}^{-1}_{ant}\overline{B}^u - \bar{\bar{T}}^{-1}_{ant}\bar{\bar{\Gamma}}_{ratio}\overline{A}^u + \bar{\bar{T}}^{-1}_{ant}\left[\bar{\bar{\Gamma}}_{sc} - \bar{\bar{\Gamma}}_{ratio}\right]\overline{A}^b \qquad (174)
\end{aligned}$$

Multiply equation (161) by $\bar{\bar{F}}_0$, we have:

$$\bar{\bar{F}}_0\overline{I}^u = \left(B_0\bar{\bar{E}}_0 + \bar{\bar{F}}_0\bar{\bar{Y}}^{uu}_{extra}\right)\cdot\overline{V}^u + \left(D_0\bar{\bar{E}}_0 + \bar{\bar{F}}_0\bar{\bar{Y}}^{ub}_{extra}\right)\cdot\overline{V}^b \qquad (175)$$

Substitute $\overline{V}^u$ (from equation (166)), $\overline{V}^b$ (from equation (174)) and $\overline{I}^u$ (from equation (168)) into equation (175) we have:

$$\begin{aligned}
&\bar{\bar{F}}_0\left[-\bar{\bar{Y}}_{ant}\bar{\bar{T}}^{-1}_{ant}\overline{B}^u + \left(\bar{\bar{I}}_{sc} + \bar{\bar{Y}}_{ant}\bar{\bar{T}}^{-1}_{ant}\bar{\bar{\Gamma}}_{sc}\right)\overline{A}^u\right] \\
&= \left(B_0\bar{\bar{E}}_0 + \bar{\bar{F}}_0\bar{\bar{Y}}^{uu}_{extra}\right)\cdot\left[\bar{\bar{T}}^{-1}_{ant}\left(\overline{B}^u - \bar{\bar{\Gamma}}_{sc}\overline{A}^u\right)\right] \\
&\quad + \left(D_0\bar{\bar{E}}_0 + \bar{\bar{F}}_0\bar{\bar{Y}}^{ub}_{extra}\right)\cdot\left[\begin{array}{l}\bar{\bar{T}}^{-1}_{ant}\overline{B}^u - \bar{\bar{T}}^{-1}_{ant}\bar{\bar{\Gamma}}_{ratio}\overline{A}^u + \\ \bar{\bar{T}}^{-1}_{ant}\left[\bar{\bar{\Gamma}}_{sc} - \bar{\bar{\Gamma}}_{ratio}\right]\overline{A}^b\end{array}\right] \qquad (176)
\end{aligned}$$

Arrange equation (176) and we have a matrix equation for $\overline{B}^u$ in terms of $\overline{A}^u$ and $\overline{A}^b$:

$$\begin{aligned}
&\left[\bar{\bar{F}}_0\left(-\bar{\bar{Y}}_{ant}+\bar{\bar{Y}}^{uu}_{extra}+\bar{\bar{Y}}^{ub}_{extra}\right)+(B_0+D_0)\bar{\bar{\bar{E}}}_0\right]\bar{\bar{T}}^{-1}_{ant}\cdot\overline{B}^u \\
=&\left[\begin{array}{c}-\bar{\bar{F}}_0\left(\bar{\bar{I}}_{sc}+\bar{\bar{Y}}_{ant}\bar{\bar{T}}^{-1}_{ant}\bar{\bar{\Gamma}}_{sc}\right)-\left(B_0\bar{\bar{\bar{E}}}_0+\bar{\bar{F}}_0\bar{\bar{Y}}^{uu}_{extra}\right)\bar{\bar{\Gamma}}_{sc}\\ -\left(D_0\bar{\bar{\bar{E}}}_0+\bar{\bar{F}}_0\bar{\bar{Y}}^{ub}_{extra}\right)\bar{\bar{T}}^{-1}_{ant}\bar{\bar{\Gamma}}_{ratio}\end{array}\right]\cdot\overline{A}^u \\
&+\left(D_0\bar{\bar{\bar{E}}}_0+\bar{\bar{F}}_0\bar{\bar{Y}}^{ub}_{extra}\right)\bar{\bar{T}}^{-1}_{ant}\left[\bar{\bar{\Gamma}}_{sc}-\bar{\bar{\Gamma}}_{ratio}\right]\cdot\overline{A}^b
\end{aligned} \tag{177}$$

Note that only $\bar{\bar{\bar{E}}}_0$ and $\bar{\bar{F}}_0$ are dense full matrices in the above equation.

Equation (177) has only N unknowns and represents combined matrix equation incorporating both the exterior and interior problem. It is solved for $\overline{B}^u$ using iterative method and $\overline{B}^b$ is obtained from equation (172) after $\overline{B}^u$ is solved.

4.7 Results and Discussion

Because of the rearrangement of the coupling equations in a compact form (equation (177)), the final matrix equation only has N unknowns for the N via problem. The matrix equation is solved using the bi-conjugate gradient method and the CPU time for a problem of 2500 vias only takes less than 1 minutes (56 seconds) on a PC with AMD Athlon processor of 866 MHz and 512 Mb memory.

We first made a comparison with the result of paper [63]. Figure 31 shows the scattering parameters of two adjacent coupled vertical vias without surrounding vias. The purpose of this simulation for only two coupled vias is to validate the Foldy-Lax multiple scattering approach for via coupling. Comparison was made between the Foldy-Lax approach and the approach used in [63]. The simulation of exterior structure has been totally separated from the simulation of interior structure.

The scattering parameter of multi-via structure is defined as follows:

$$S_{ij}=\frac{B_i}{A_j}\Big|_{A_k=0 \text{ if } k\neq j} \tag{178}$$

where A_j is the incident wave at the jth port and B_i is the reflect wave at the ith port. The

boundary condition of $A_k = 0$ means that a matched load is connected at the kth port. A via with a matched load at both its lower and upper ports is called a terminated via.

In figure 31, for the sake of comparison, we use the same coaxial cable feed-in and the same parameters as used in paper [63], which are: via inner radius $a = 0.457mm$, via outer radius $b = 1.524mm$, separation of the two vias $s = 4mm$, layer thickness $h = 1.524mm$, layer relative dielectric constant of $\varepsilon_r = 2.2$. Results of the two approaches are in close agreement. The comparison was made for single layer due to the fact that the result can be easily extended to multi-layer structure using cascade of transfer matrices [63].

To illustrate the influence of large number of surrounding vias to the coupled vias, additional 2,498 randomly distributed vias are put around these two vias. The 2498 vias are terminated vias in this simulation. Figure 32 gives the geometry of these 2,498 randomly distributed vias and the two active signal vias that we are considering. Figure 33 shows the scattering parameters of two coupled active vias with and without considering the surrounding 2,498 idle vias. The result shows clearly that, due to the multiple scattering of large number of adjacent vias, the coupling from the surrounding vias could affect the original scattering parameters of the two vias, especially the coupling coefficient. Thus in densely packaged electronic circuits, where the number of vias could be large in certain region, this simulation technique will give accurate modelling of the coupling effect and the circuit behavior. The curve for coupling coefficient in figure 33 has random multiple ripples because of the random distribution and multiple scattering from other via cylinders.

4.8 Shorting Vias:

Another common type of via other than terminated via is the shorting via [71][72]. The two ends of shorting via is directly connected to the ground planes. Thus the voltages of upper and lower ports of the shorting via are zeros.

Shorting via has many applications in real circuit. For one example, the excited wave from active via aperture will propagate inside the parallel plate waveguide structure, hit the edge of reference plane and be bounced back. This will result in resonance effect, the whole double plate structure serve as a big resonance cavity with magnetic walls. Because of the relatively large dimension of the PCB, the resonance frequency could be quite low

and have multiples at higher frequency. By appropriately putting shoring vias between the two reference planes, we effectively put small perturbation to the resonance cavity and thus destroy the resonance or push the resonance frequency to a much higher level.

For another example, vertical vias always have return path problem because their special structure with the ground plane, waves sometimes need to travel far away from its source to find an appropriate return path. This long return path results in coupling noise, larger inductance and ground bounce problem. Differential signaling gives one solution by effectively using the other via as return path. For regular signaling vias, we may put shorting vias adjacent to the signal via and this will provide very good return path for the signal.

What's more, active vias will generate waves that propagates alongside the waveguide and create coupling noise problem, to shield the active vias from the rest of the PCB, it is often useful to put shorting vias around known as the guarding ring.

In all these applications we need to know how to put those shorting vias to get the best performance with minimum cost. This requires the simulation technique that deals with multi-via coupling. And obviously in this kind of applications, the surrounding vias (shorting vias in this case) cannot be negnected because they are actually the ones that have key effects on the performace.

4.8.1 Formulation

Let us consider a case with 2 active vias, N_T terminated idle vias, and N_S shorting vias. The total number of vias is $N = 2 + N_T + N_S$.

Let the shorting vias be labeled as $(N_T+3), (N_T+4), \ldots\ldots (2 + N_T + N_S)$, and we rewrite equation (175) as

$$\begin{aligned}
&(\overline{\overline{F}}_0^{(1)} + \overline{\overline{F}}_0^{(2)})\overline{I}^u \\
= \;& \left(B_0\overline{\overline{E}}_0 + \overline{\overline{F}}_0\overline{\overline{Y}}_{extra}^{uu}\right)^{(1)} \cdot \overline{V}^u + \left(D_0\overline{\overline{E}}_0 + \overline{\overline{F}}_0\overline{\overline{Y}}_{extra}^{ub}\right)^{(1)} \cdot \overline{V}^b \\
&+ \left(B_0\overline{\overline{E}}_0 + \overline{\overline{F}}_0\overline{\overline{Y}}_{extra}^{uu}\right)^{(2)} \cdot \overline{V}^u + \left(D_0\overline{\overline{E}}_0 + \overline{\overline{F}}_0\overline{\overline{Y}}_{extra}^{ub}\right)^{(2)} \cdot \overline{V}^b \qquad (179)
\end{aligned}$$

In the above matrix equation, matrix with superscript (1) has the same first $(N_T + 2)$ columns as its original matrix and the rest columns are 0; matrix with superscript (2) has

the same last N_S columns as its original matrix and the rest columns are 0.

$$\bar{\bar{F}}_0^{(1)} = \left[\bar{\bar{F}}_0(\text{first } (N_T+2) \text{ columns}) \quad \bar{\bar{0}} \right] \tag{180}$$

$$\bar{\bar{F}}_0^{(2)} = \left[\bar{\bar{0}} \quad \bar{\bar{F}}_0(\text{last } N_S \text{ columns}) \right] \tag{181}$$

Due to fact that the last N_S elements in the vectors $\overline{V}^b$ and $\overline{V}^u$ are 0, the last two terms on the right hand side of equation (179) will be zero. Also note that there is no exterior part for the shorting vias and thus there is no exterior problem and exterior parameter A and B for them. The unknown for the shorting vias is I.

Substitute $\overline{V}^u$, $\overline{V}^b$ and $\overline{I}^u$ into the above equation (179). We have:

$$\begin{aligned}
&\bar{\bar{F}}_0^{(1)} \left[-\bar{\bar{Y}}_{ant} \bar{\bar{T}}_{ant}^{-1} \overline{B}^u + \left(\bar{\bar{I}}_{sc} + \bar{\bar{Y}}_{ant} \bar{\bar{T}}_{ant}^{-1} \bar{\bar{\Gamma}}_{sc} \right) \overline{A}^u \right] + \bar{\bar{F}}_0^{(2)} \overline{I}^u \\
= &\left(B_0 \bar{\bar{E}}_0 + \bar{\bar{F}}_0 \bar{\bar{Y}}_{extra}^{uu} \right)^{(1)} \cdot \left[\bar{\bar{T}}_{ant}^{-1} \left(\overline{B}^u - \bar{\bar{\Gamma}}_{sc} \overline{A}^u \right) \right] \\
&+ \left(D_0 \bar{\bar{E}}_0 + \bar{\bar{F}}_0 \bar{\bar{Y}}_{extra}^{ub} \right)^{(1)} \cdot \begin{bmatrix} \bar{\bar{T}}_{ant}^{-1} \overline{B}^u - \bar{\bar{T}}_{ant}^{-1} \bar{\bar{\Gamma}}_{ratio} \overline{A}^u + \\ \bar{\bar{T}}_{ant}^{-1} \left[\bar{\bar{\Gamma}}_{sc} - \bar{\bar{\Gamma}}_{ratio} \right] \overline{A}^b \end{bmatrix}
\end{aligned} \tag{182}$$

Rearrange the above equation:

$$\begin{aligned}
&\left[\bar{\bar{F}}_0^{(1)} \left(-\bar{\bar{Y}}_{ant} + \bar{\bar{Y}}_{extra}^{uu} + \bar{\bar{Y}}_{extra}^{ub} \right) + (B_0 + D_0) \bar{\bar{E}}_0^{(1)} \right] \bar{\bar{T}}_{ant}^{-1} \cdot \overline{B}^u + \bar{\bar{F}}_0^{(2)} \overline{I}^u \\
= &\begin{bmatrix} -\bar{\bar{F}}_0^{(1)} \left(\bar{\bar{I}}_{sc} + \bar{\bar{Y}}_{ant} \bar{\bar{T}}_{ant}^{-1} \bar{\bar{\Gamma}}_{sc} \right) - \left(B_0 \bar{\bar{E}}_0^{(1)} + \bar{\bar{F}}_0^{(1)} \bar{\bar{Y}}_{extra}^{uu} \right) \bar{\bar{\Gamma}}_{sc} \\ - \left(D_0 \bar{\bar{E}}_0^{(1)} + \bar{\bar{F}}_0^{(1)} \bar{\bar{Y}}_{extra}^{ub} \right) \bar{\bar{T}}_{ant}^{-1} \bar{\bar{\Gamma}}_{ratio} \end{bmatrix} \cdot \overline{A}^u \\
&+ \left(D_0 \bar{\bar{E}}_0^{(1)} + \bar{\bar{F}}_0^{(1)} \bar{\bar{Y}}_{extra}^{ub} \right) \bar{\bar{T}}_{ant}^{-1} \left[\bar{\bar{\Gamma}}_{sc} - \bar{\bar{\Gamma}}_{ratio} \right] \cdot \overline{A}^b
\end{aligned} \tag{183}$$

Note that there are totally N unknowns in the above equation and the first (N_T+2) unknowns are elements of $\overline{B}^u$ and the last N_S unknowns are elements of $\overline{I}^u$.

4.9 Differential and common modes

Recently, differential signaling has drawn considerable attention because of its common noise depression and low radiation [73]-[75]. In differential signaling, two traces runs closely parallel to each other with signals of 180 degree phase shift (opposite polorization). At the receiver end, these two signals are subtracted to give the actual signal. In this subtraction process, common mode noises (which consists the large part of radiation and coupling noise) are mostly eliminated. Electromagnetic radiation from traces in differential signaling is also greatly reduced because of the strong cancellation of the two oppositely polorized signals on the two closely parallel traces. Also due to the two closely parallel traces, one automatically serves as the return path for the other, which helps a lot in the return current path problem especially in vertical via cases.

Here we study the characteristics of common and differential modes in differential signaling via pair using the technique we developed for multi-via coupling. Results are illustrated for power loss (most of it are due to radiation loss) for common and differential mode with and without adjacent terminated and shorting vias.

Consider two active vias 1 and 2, so that $N = 2$. This is a 4-port problem with four ports labeled as $1_u, 1_b, 2_u$ and 2_b. Vias are labeled as 1 and 2 and ports are further labeled as upper and bottom ports.

The scattering matrix for the differential pair is:

$$\begin{bmatrix} B^{1u} \\ B^{2u} \\ B^{1b} \\ B^{2b} \end{bmatrix} = \begin{bmatrix} S_{1u1u} & S_{1u2u} & S_{1u1b} & S_{1u2b} \\ S_{2u1u} & S_{2u2u} & S_{2u1b} & S_{2u2b} \\ S_{1b1u} & S_{1b2u} & S_{1b1b} & S_{1b2b} \\ S_{2b1u} & S_{2b2u} & S_{2b1b} & S_{2b2b} \end{bmatrix} \begin{bmatrix} A^{1u} \\ A^{2u} \\ A^{1b} \\ A^{2b} \end{bmatrix} \tag{184}$$

For differential mode, $A^{1u} = 1/2$, $A^{2u} = -1/2$, $A^{1b} = A^{2b} = 0$. The reflection and transmission coefficient is defined as:

$$R = B^{1u} - B^{2u} = (S_{1u1u} - S_{1u2u} - S_{2u1u} + S_{2u2u})/2 \tag{185}$$

$$T = B^{1b} - B^{2b} = (S_{1b1u} - S_{1b2u} - S_{2b1u} + S_{2b2u})/2 \tag{186}$$

For common mode, $A^{1u} = 1$, $A^{2u} = 1$, $A^{1b} = A^{2b} = 0$. The reflection and transmission coefficient is defined as:

$$R = B^{1u} = S_{1u1u} + S_{1u2u} \quad (187)$$

$$T = B^{1b} = S_{1b1u} + S_{1b2u} \quad (188)$$

In the numerical results, we consider two active vias in either common mode or differential mode. In figure 34, the transmission and reflection of two coupled active vias in both common and differential modes are shown. We plot the absolute value of $R = |S_{1u1u} + S_{1u2u}|$ and $T = |S_{1b1u} + S_{1b2u}|$ for the reflection and transmission of common mode. We also plot the absolute value of $|R| = |S_{1u1u} - S_{1u2u} - S_{2u1u} + S_{2u2u}|/2$ and $|T| = |S_{1b1u} - S_{1b2u} - S_{2b1u} + S_{2b2u}|/2$ for the reflection and transmission of differential mode. Magnitudes of reflection and transmission coefficient are plotted as function of frequency. For this case, we consider the effects of both interior and exterior coupling. Parameters are: via inner radius $a = 5mil$, via outer radius $b = 15mil$, separation of the two vias $s = 40mil$ and layer thickness $h = 90mil$. The material permittivity is $\varepsilon = 2.2\varepsilon_0$. It can be seen that most of the power in differential mode can pass through the via while the transmission in common mode is less than that in differential mode, especially in the high frequency end.

Because of the low transmission in common mode, shorting vias are put in the neighborhood of the active vias to reduce the power loss. In figure 35, transmission and reflection of four vias is plotted as a function of frequency. The geometry of the 4 vias is shown in figure 36. The 4 vias are put in a row, with two active vias in the middle and two shorting vias at both end. The separation of two active vias is $s1 = 40mil$ and the separation of active and shorting via is $s2 = 80mil$. Other parameters of vias are the same as in figure 34. It can be seen that transmission increases for both modes as compared with the case without shorting via (figure 34). To compare the losses with and without shorting via, the power loss is plotted in figure 37 for cases shown in figures 35 and 34. Here, power loss is defined as $1 - P_{trans} - P_{refl}$. The dashed and solid lines are for the case of two active vias only; the dashed-circle and solid-circle lines are for the case of 4 vias with 2 shorted. Figure 37 shows

that the shorting vias can reduce the power loss for both differential and common mode.

In figures 38 through 40, we show the capability of the proposed approach to handle the interactions among large number of vias. Figure 38 shows the power loss of two active vias surrounded with randomly distributed 1022 and 2498 idle vias, for the differential mode and common mode respectively. It can be seen that the increase of number of idle vias will not affect the loss of active vias very much and the loss in common mode is larger than that in the differential mode. The same cases are plotted in figure 39 and 40 with all the idle vias substituted by shorting vias. Comparing with figure 38, the power loss is greatly reduced for both common and differential mode because the shorting vias provide additional paths for the return currents.

4.10 Conclusion:

The approach presented in this chapter can be applied to the common discontinuity problem in high-speed circuit from very low frequency to very high frequency with accuracy and modest CPU and memory. It starts from the formulation of Green's function of cylindrical scatterer between parallel plate waveguide and relates the exciting, incident and scattered waves from each cylinder by Foldy-Lax equations. The interior problem is solved by giving out the admittance matrix and is combined with the exterior problem by relating the port voltages and currents. The system matrix of the interior and exterior problem is further combined to give a total matrix of system to be solved by iterative method.

For massively coupled vertical vias, compared with pure numerical method, simulation using Foldy Lax multiple scattering equations greatly improves the computational speed while reserves the accuracy because of its semi-analytical characteristics. On the other hand, compared with analytical approach which only takes into account of two vias coupling, Foldy Lax formulation improves the accuracy by considering the influence of multiple scattering from other adjacent vias. This is important especially for the calculation of coupling effect.

As shown in the numerical result, the coupling between two vias can be quite different when considering the influence of large number of adjacent vias. So in order to accurately consider the via coupling effect, the surrounding passive vias must be considered together with the active signal vias. The simulation technique can be used to solve the coupling

problem in multi-via structure which is quite common in high-speed circuit board.

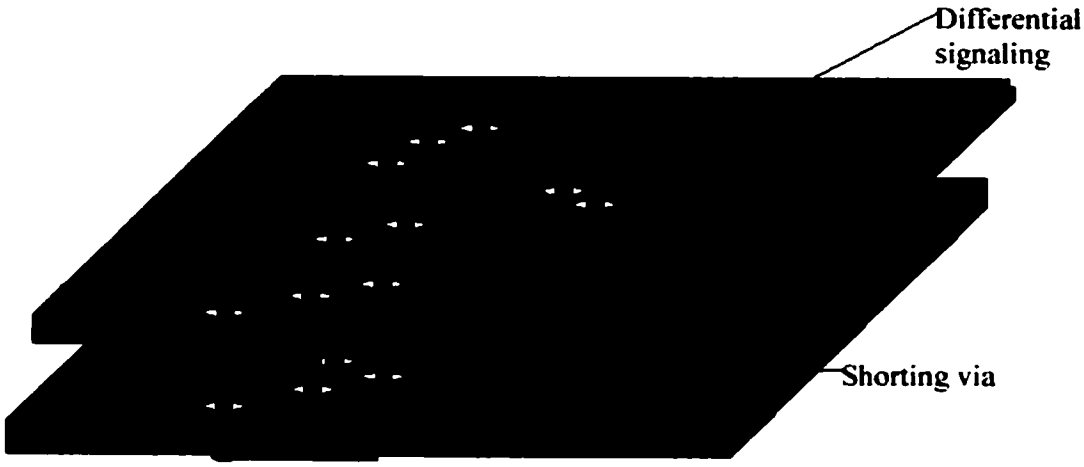

Figure 28: Typical multi-via structure

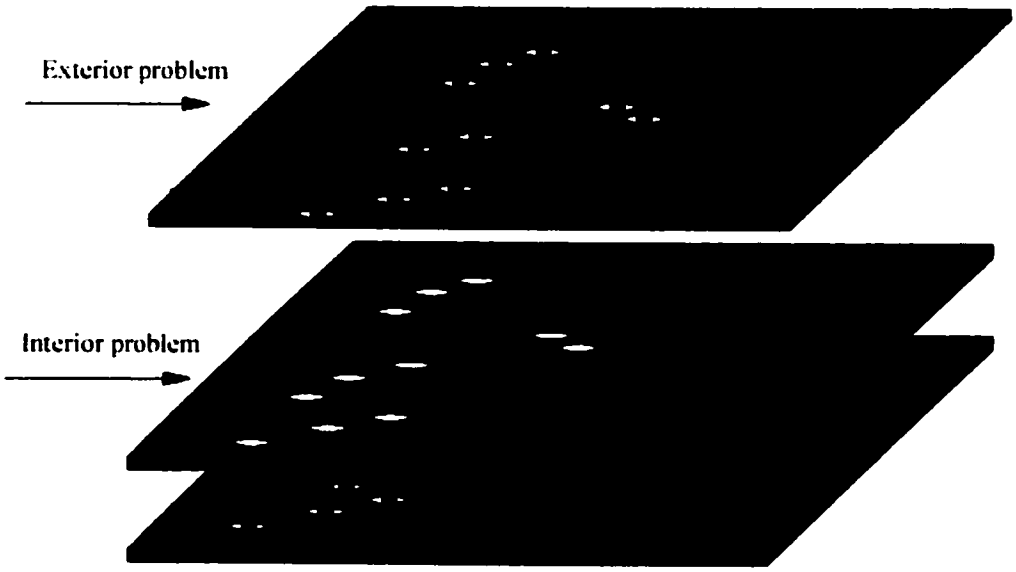

Figure 29: Decomposition of the multi-via structure

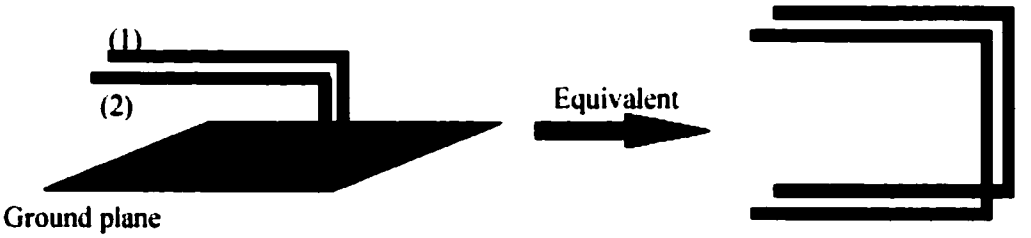

Figure 30: Coupled exterior problem

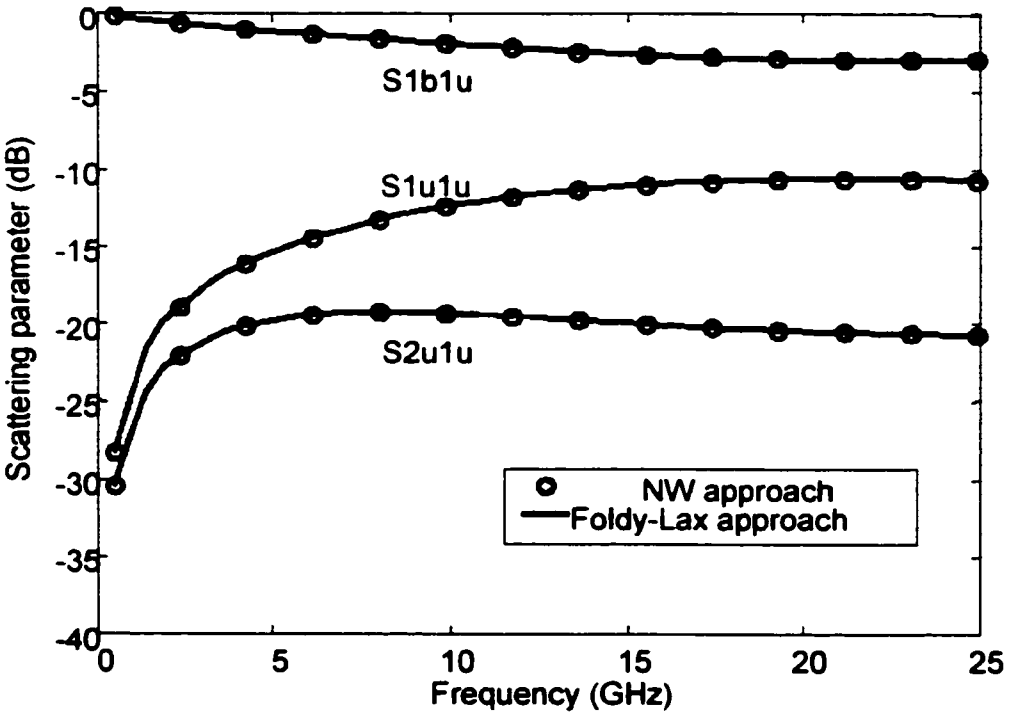

Figure 31: The scattering parameters of two coupled vertical vias. Comparison with existing literature.

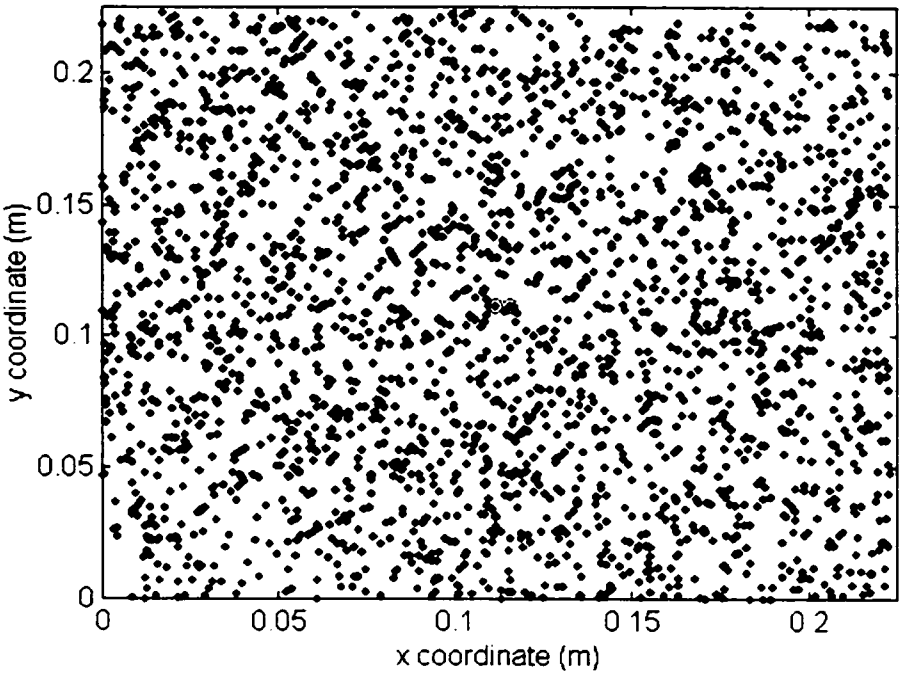

Figure 32: Distribution of 2500 vias

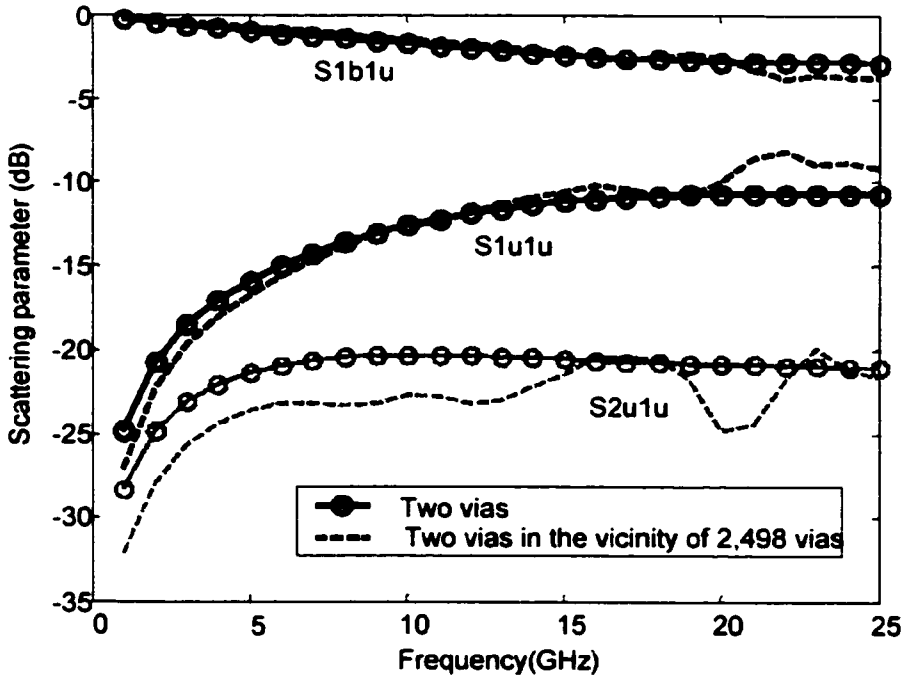

Figure 33: The scattering parameter of two coupled vertical vias in the vicinity of 2498 other vias. Comparison with two via coupling

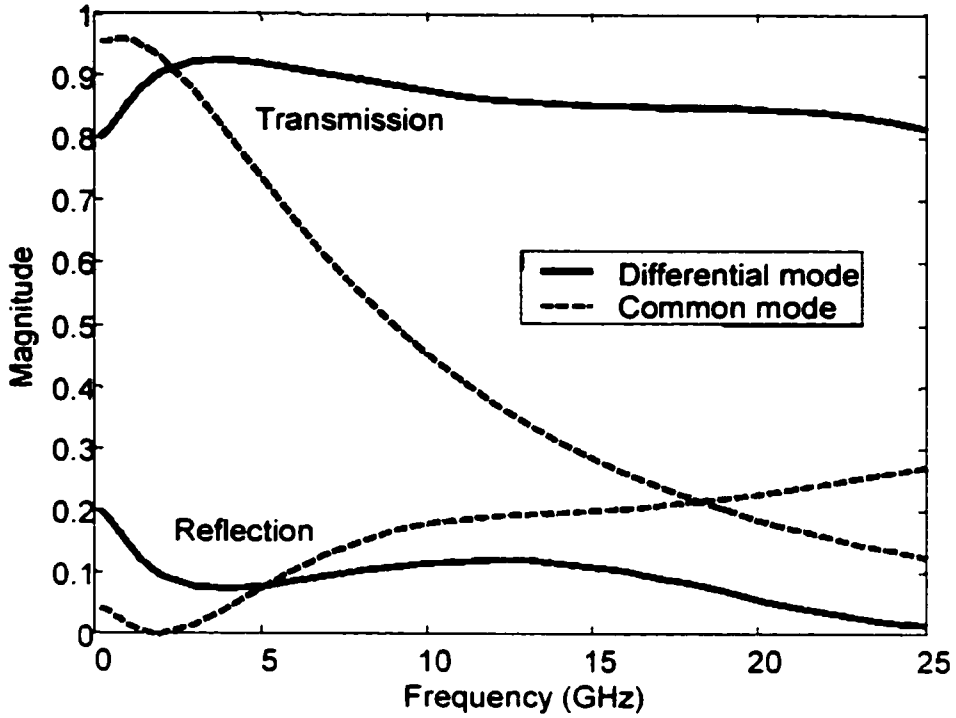

Figure 34: Transmission and reflection of two vias in differential signaling

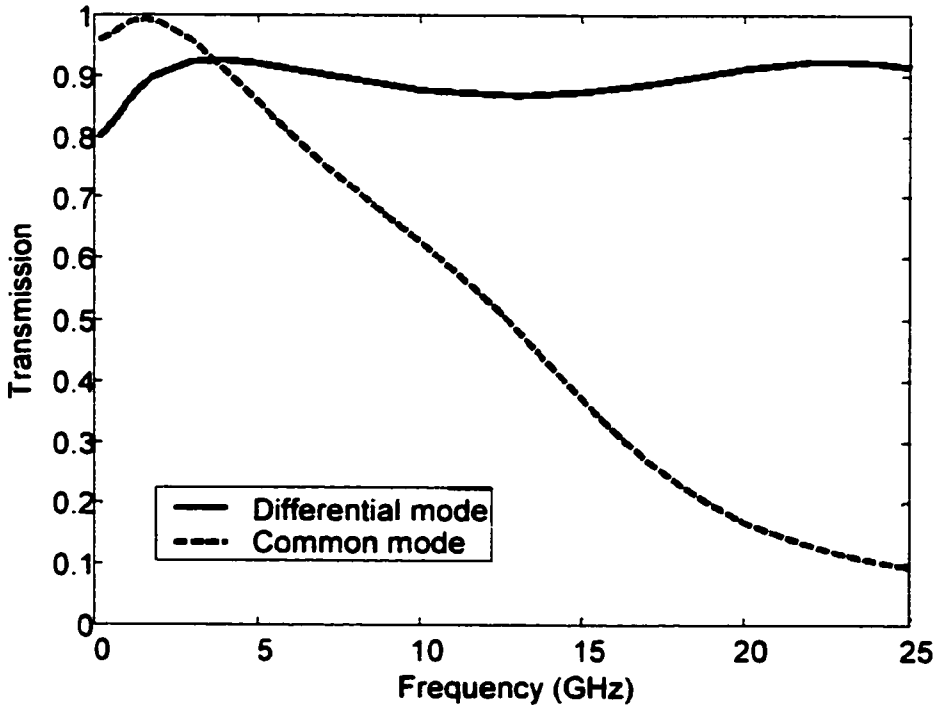

Figure 35: Transmission of 4 vias with 2 shorting vias

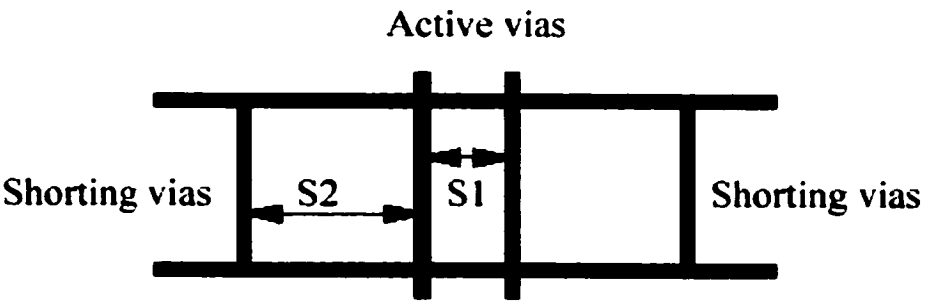

Figure 36: Geometry of 4 vias with 2 shorting vias

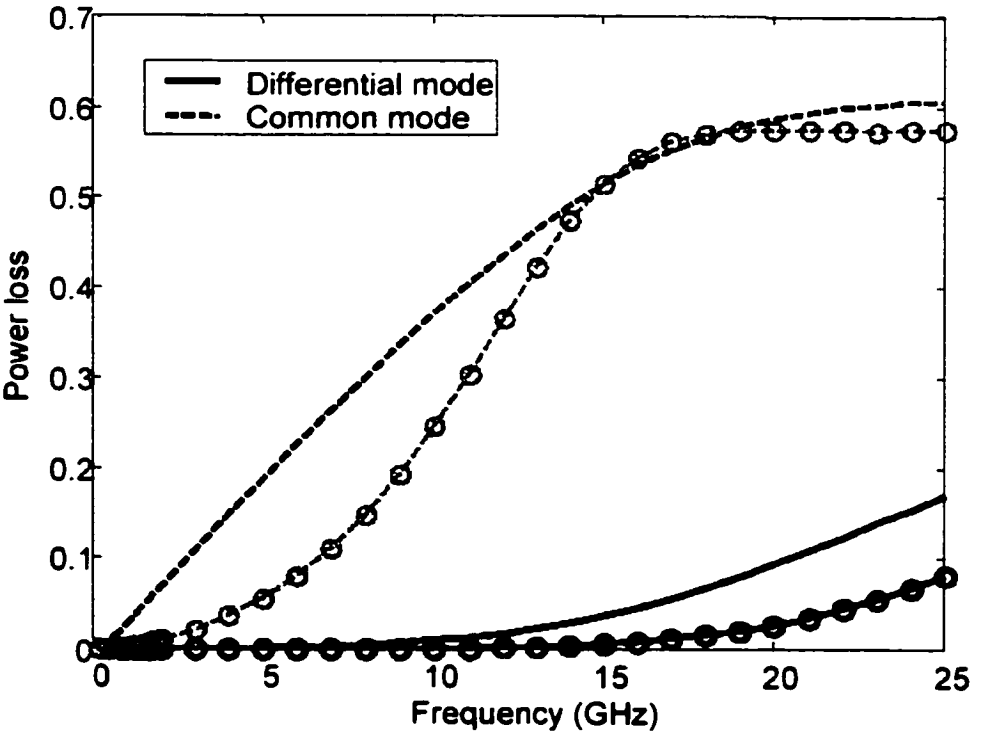

Figure 37. Loss comparison with (circled lines) and without shorting vias

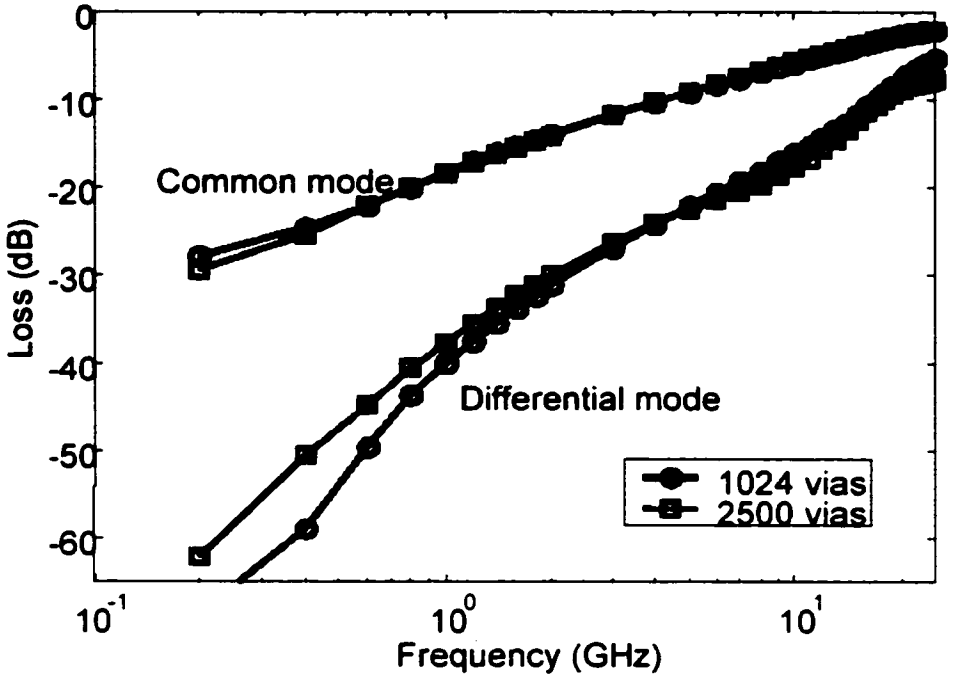

Figure 38: Loss comparison between different number of vias (differential and common mode)

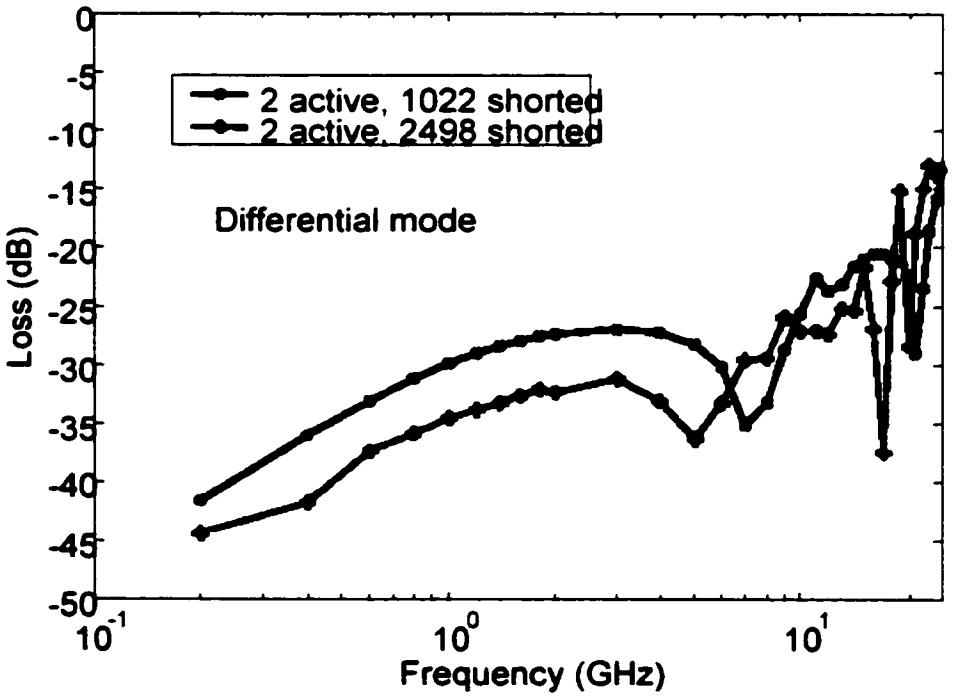

Figure 39: Loss comparison between different number of shorting vias

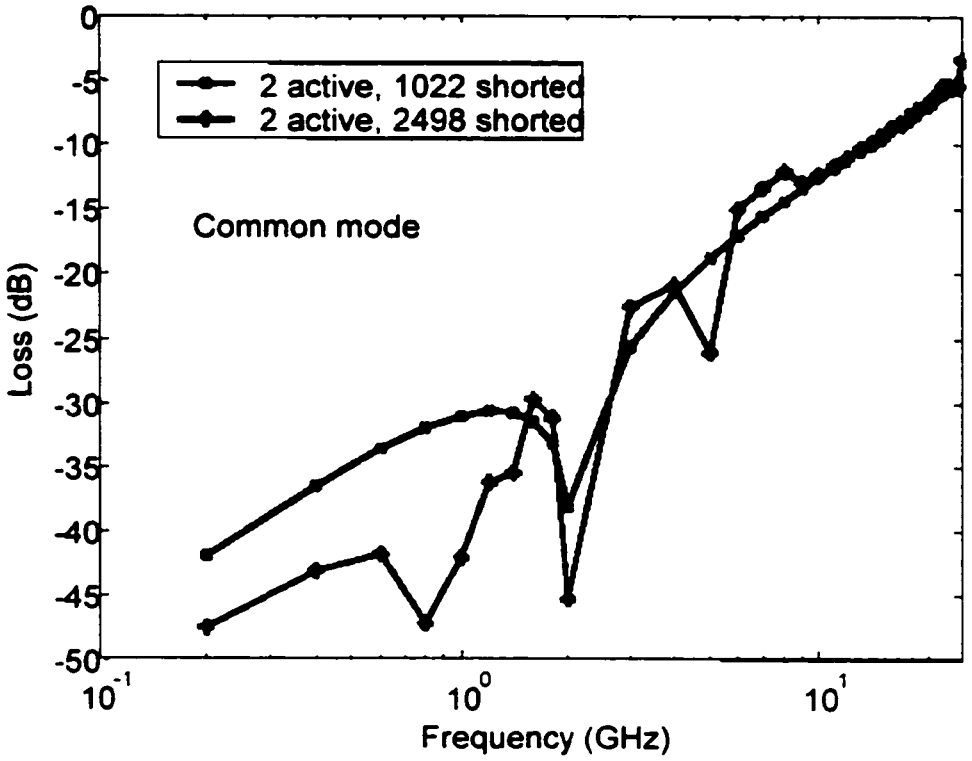

Figure 40: Loss comparison between different number of shorting vias

5 More rigorous approach for the exterior structure in via discontinuity

In the previous chapters, we deal the exterior structure of via using two kind of appproximations. One is to assume that all the exterior traces are characterized as a transmission line with known characteristic impedance Z_0, the other is to use thin wire approximation which approximate the exterior traces as thin wire over ground plane (figure 41).

For the first kind of approximation, although very convenient, it failes to take into account the effect of pad and corner discontinuity, the only discontinuity effect it considers is the impedance mismatch of the trace and the interior structure of the via.

For the second kind of approximation, although it takes into account the effect of corner and the vertical section, it approximates the microstrip structure into a wire over ground plane and use thin wire antenna formulation for the exterior structure. This is not appropriate in some applications, eg. when the substrate thickness is very thin, the height of the wire above the ground plane h and the wire radius a does not satisfy the thin wire approximation $h >> a$, the thin wire simulation gives significant errors. At low frequency range when $\lambda >> h$, thin wire simulation also renders considerable errors. And again, thin wire approximation fails to take into account the effect of via pad. We know this kind of geometry and frequency range (thin substrate, wide trace and low frequency) happens in real application a lot, which requires more accurate and rigorous modeling of the exterior structure.

In this chapter, we formulate the exterior structure of the via more elaborately, including the effect of the pad and the vertical section. The microstrip structure is also taken care of by using the spatial domain layered-medium Green's function. Electric field integral equation [76]-[79] is set up on the metal strip using fast evaluation of spatial domain layered-medium Green's function which gives accurate modeling of the exterior structure and the effect of the via pad size. The simulation result can be combined with interior structure to give a fast and accurate modeling of massively coupled via structure for the entire electronic package.

5.1 Formulation

The exterior structure is again decomposed into short circuit problem and wire antenna problem (notice the only different formulation in this two problems is that wire antenna problem has the excitation source at the aperture while short circuit problem has the excitation at one end of the strip). But in this chapter, we no longer use thin wire approximation, but use the actual layout of the exterior structure with microstrip, circular pad and the vertical section of via bent into the ground plane (figure 41).

5.1.1 Electric field integral equations

The electric field integral equation (EFIE) is established on the surface of the traces (either microstrip or stripline). The source is the electric current on the metal strip (both horizontal and vertical section) for the short circuit problem, and the magnetic current source at the via aperture for the wire antenna problem.

The electric field can be expressed as:

$$\vec{E} = \int_s dr' \overline{\overline{G}}_{EJ} \vec{J}_s(\vec{r}') \tag{189}$$

$$\vec{E} = \int_s dr' \overline{\overline{G}}_{EM} \vec{M}_s(\vec{r}') \tag{190}$$

for electric current source and magnetic current source respectively. Here $\overline{\overline{G}}_{EJ}$ is the electric field layer-medium Green's function of electric current source and $\overline{\overline{G}}_{EM}$ is the electric field layer-medium Green's function of magnetic current source. In the setup of matrix equation, $\overline{\overline{G}}_{EJ}$ is used in the evaluation of impedance matrix elements in both short circuit and wire antenna problem, while $\overline{\overline{G}}_{EM}$ is used in the evaluation of right hand side for matrix equation in the wire antenna problem.

The electric field integral equation is:

$$\vec{E}_{inc} = \int_s dr' \overline{\overline{G}}_{EJ} \vec{J}_s(\vec{r}') \tag{191}$$

where $\vec{E}_{inc}$ is the incident electric field on the exterior structure, it depends on the excitation

scheme in short circuit problem and in wire antenna problem.

$$\vec{E}_{inc} = \int_a dr' \overline{\overline{G}}_{EM} \vec{M}_s(\vec{r}') \tag{192}$$

where the integral is taken on the via aperture.

Free space case Layer-medium case will be elaborated later with the derivation of layer-medium Green's function. First let's look at the free space case, the electric field can be expressed as:

$$\vec{E} = -j\omega\vec{A} + \frac{1}{j\omega\varepsilon\mu}\overline{\nabla}(\overline{\nabla}\cdot\vec{A}) \tag{193}$$

where the vector potential

$$\vec{A} = \mu \int_s da' \vec{J}_s(\vec{r}')g(\vec{r}, \vec{r}') \tag{194}$$

$g(r, r') = \frac{e^{-jk|r-r'|}}{4\pi|r-r'|}$ is the scalar Green's function for free space.

The final integral equation can be written as:

$$\vec{E}_{inc} = -\frac{1}{j\omega\varepsilon}\int_s da' \left\{ \vec{J}_s(\vec{r}')\nabla_s \cdot \nabla'_s g(\vec{r}, \vec{r}') - k^2 \vec{J}_s(\vec{r}')g(\vec{r}, \vec{r}') \right\} \tag{195}$$

5.1.2 Choice of basis function

Basically the choice for basis function could be 2D rooftop function, a mix of rectangular rooftop function and triangle rooftop function and RWG function. Recently there is also literature about generalized polygonal basis function [80], but basically it is based on rectangular and triangular rooftop basis function. Among these choices, 2D rooftop basis function has been widely used in the solution of integral equation for planar structure [81]-[84], it has the advantage of simple mesh of the structure and less number of unknowns. For non-rectangular structure, special form of linear "rooftop" basis functions is used to approximate the current distribution by Mosig in [85], but it is also on a set of rectangular cells. 2D rooftop function obviously are most appropriate when the structure under investigation can be naturally divided into rectangular cells, but it would not be as efficient when

cells of reasonable size (about 20 cells per operating wavelength) cannot be fittd into the boundaries of a structure.

Mixture of rectangular and triangle rooftop basis function were introduced in [86]-[89]. This kind of basis function uses a combination of rectangular and triangular cells in a self-consistent manner in order to take into account the regularity in shape over the major portion on the planar structure, while still preserving the flexibility to model junctions of arbitrary shape locally. The self-consistency is actually derived from the observation that in order to avoid the unphysical occurence of a δ function charge density in the numerical process, only the normal component of the current density, but not the current density itself, is required to be continuous across a cell boundary.

Pure triangular basis function (RWG basis function) is also widely used in the MoM solution [90]-[92], it naturally has the self-consistency of normal current density across cell boundary without the tricky setup in the mixture of rectangular and triangular cells. Besides, it also has the flexibility in handling arbitrary shape of discontinuity. In our formulation of exterior structure, we use RWG basis function for its flexibility in handling the shape of pad. Rectangular and triangular mixture is not tried here because of the more complexity in formulation and programming, while the save in unknown numbers is very limited (because the microstrip where the rectangular basis can be used is short in our problem).

5.1.3 Matrix equation

A RWG basis function is composed of two triangles sharing the same side (figure 42). The mathematical expression of RWG basis function f_n is:

$$f_n(\vec{r}) = \begin{cases} \frac{l_n}{2A_n^+}\vec{\rho}_n^+ \text{ if } \vec{r} \text{ is in } T_n^+ \\ \frac{l_n}{2A_n^-}\vec{\rho}_n^- \text{ if } \vec{r} \text{ is in } T_n^- \\ 0 \text{ elsewhere} \end{cases} \tag{196}$$

here l_n is the length of the common side and $\vec{\rho}_n^+ = \vec{r} - \vec{r}_n^+$, $\vec{\rho}_n^- = \vec{r}_n^- - \vec{r}$. A_n^+ and A_n^- are the area of the two triangles respectively. The weighting in equation (196) makes that the normal current density at the common side is continuous across the edge, and hence no

unphysical δ charge density arises on the edge.

Let's consider free space case first, the layer medium case is similar with free space Green's function replaced with layer-medium Green's function. The unknown surface current in equation (195) is represented by RWG basis function, the mesh of the exterior structure is shown in figure 43. Usually the height of the vertical section h is small, and one rectangular cell (two triangular cell) will be enough. The circular pad is approximated by a polygon, the number of sides of the polygon depends on what kind of accuracy we are looking for. The vertical cylindrical section is also approximated by polygon structure, it can be either hexagon (6 side) or rectangle (4 side) or even just a strip (1 side). Usually rectangle will be enough for the vertical via section.

Use Galerkin's testing and perform transfer of derivatives in integral equation (195), we have:

$$\begin{aligned} & \int_s da \overline{J}_s(\overline{r}) \cdot \overline{E}_{inc} \\ = & -\frac{1}{j\varpi\varepsilon} \int_s \int_s dada' \left\{ \begin{array}{c} \nabla_s \cdot \overline{J}_s(\overline{r}) g(\overline{r}, \overline{r}') \nabla'_s \cdot \overline{J}_s(\overline{r}') \\ -k^2 \overline{J}_s(\overline{r}) \cdot \overline{J}_s(\overline{r}') g(\overline{r}, \overline{r}') \end{array} \right\} \end{aligned} \tag{197}$$

Using RWG function $f(\overline{r})$ as basis and testing function, we have the following matrix equation:

$$\overline{\overline{Z}} \cdot \overline{J} = \overline{b} \tag{198}$$

where the impedance matrix element

$$\begin{aligned} & Z_{mn} \\ = & -\frac{1}{j\varpi\varepsilon} \int_s \int_s dada' \{ \nabla_s \cdot \overline{f}_m(\overline{r}) g(\overline{r}, \overline{r}') \nabla'_s \cdot \overline{f}_n(\overline{r}') - k^2 \overline{f}_m(\overline{r}) \cdot \overline{f}_n(\overline{r}') g(\overline{r}, \overline{r}') \} \\ = & Z_{mn\_div} + Z_{mn\_wave} \end{aligned} \tag{199}$$

The element of right hand side vector

$$b_m = \int_s da \overline{f}_m(\overline{r}) \cdot \overline{E}_{inc} \tag{200}$$

and it depends on different excitation scheme.

For a proper δ gap source excitation:

$$\overline{b} = \begin{bmatrix} 1 \\ 0 \\ \cdots \\ 0 \end{bmatrix} \tag{201}$$

where the 1 happens at the cell where the δ electric field source is.

For an end current excitation:

$$\overline{b} = \left[\overline{\overline{Z}}\right]_m \tag{202}$$

which is the mth column of the impedance matrix, if the excitation current is at the mth cell. Normally δ gap source excitation is much straight-forward. We will discuss this later in the excitation scheme section.

5.1.4 Vertical current

Vertical current elements here are also represented by RWG basis function (figure 43). For all other kind of basis function, notice the current and charge relation $\nabla \cdot \overrightarrow{J}_s = -j\omega q_s$, it is necessary that the normal current density across the common edge of the two kind of basis function is continuous so there is no δ charge density on the edge. By using the same RWG function for vertical current, this is automatically taken care of. In this arrangement, current can flow both vertically and horizontally on the via.

For a full RWG basis function, the charge distribution will be + in one triangle and − in the other. For a half RWG basis function, there will be dirac charge distribution δ on the edge.

So for the vertical-horizontal junction in the exterior structure, we simply add one more RWG function with one triangle on the horizontal section and the other on the vertical section, as in figure ??. This RWG basis function shares the same edge with a horizontal RWG function, but this doesn't matter at all, since all the normal current density at the internal edges are continuous and there is no singular charge distribution.

5.1.5 Evaluation of impedance matrix element

The evaluation of impedance matrix element falls into 3 categories: self- and overlap-patch, near field interaction and non-near field interaction.

For non-near field interaction, which is for cell separation more than 1/10 wavelength, we use centroid approximation where

$$Z_{mn} = \vec{f}_m(\vec{r}_m) \cdot \overline{\overline{G}}(\vec{r}_m, \vec{r}_n) \cdot \vec{f}_n(\vec{r}_n) \cdot A_m A_n \tag{203}$$

here $\vec{r}_m$ and $\vec{r}_n$ are the centroid of two triangles, A_m and A_n are the area of two triangles.

For near field interaction, which is for cell separation less than 1/10 wavelength but not overlap, we use seven point rule gaussian integration which is analytically accurate to any cubic functions. Seven points are sampled inside the triangle (figure 45), each with a certain weight, and the final result is given as the sum of interaction from all the sample points with certain weight.

$$Z_{mn} = \sum_{i=1}^{7} w_i f_m(\vec{r}_i) \sum_{j=1}^{7} \overline{\overline{G}}(\vec{r}_i, \vec{r}_j) w_j f_n(\vec{r}_j) \cdot A_m A_n \tag{204}$$

The relative sampling coordinates are:

$$\vec{r}_i = \begin{bmatrix} 0.3333 & 0.3333 \\ 0.0597 & 0.4701 \\ 0.4701 & 0.0597 \\ 0.4701 & 0.4701 \\ 0.7974 & 0.1013 \\ 0.1013 & 0.7974 \\ 0.1013 & 0.1013 \end{bmatrix} \tag{205}$$

The corresponding weighting vector is:

$$\vec{w} = \begin{bmatrix} 0.225 & 0.1324 & 0.1324 & 0.1324 & 0.1259 & 0.1259 & 0.1259 \end{bmatrix} \tag{206}$$

For self- and overlap-patch, numerical integration cannot be performed because of the singularity, thus for such interaction, we use analytical integration. There has been literatures where impedance matrix element of MoM matrix is analytically integrated for two rectangular patch interaction [93] and two polygon patch interaction [???]. Here in this chapter, we perform analytical integration for point to triangle interaction, and then perform seven point gaussian integration in the other triangle. Due to the vertical section in the exterior structure, analytical 3D point to triangle interaction will be performed.

$$Z_{mn} = \sum_{i=1}^{7} w_i f_m(\vec{r}_i) \cdot I_i \cdot A_m \tag{207}$$

where

$$I_i = \int_{T_n} \overline{\overline{G}}(\vec{r}_i, \vec{r}') f_n(\vec{r}') \tag{208}$$

is the analytical point to triangle interaction.

Analytical 3D point to triangle interaction For 3D point to triangle interaction, the point and triangle may not be at the same plane. There are two kinds of interactions as in equation (199). One is the divergence part interaction Z_{mn_div}, which has a constant charge distribution on the triangular patches, the other is the vector part interaction Z_{mn_wave}, which has a linear current distribution on the triangular patch.

Uniform Source Distribution Refer to [94], the analytical integration with a uniform source distribution in triangle is:

$$\begin{aligned} &\int_S \frac{ds'}{R} \\ = &\sum_i \hat{P}_i^0 \cdot \hat{u}_i \\ &\left[P_i^0 \ln \frac{R_i^+ + l_i^+}{R_i^- + l_i^-} - |d| \times \left(\tan^{-1} \frac{P_i^0 l_i^+}{(R_i^0)^2 + |d| R_i^+} - \tan^{-1} \frac{P_i^0 l_i^-}{(R_i^0)^2 + |d| R_i^-} \right) \right] \end{aligned} \tag{209}$$

where all the definition of symbols can be found in [94]. Need to notice that, if the projection of the point lies on one edge or its extension of the triangle, then the contribution from that edge will be 0.

Linear source distribution Also refer to [94], the analytical integration with a linear source distribution in triangle is:

$$\begin{aligned} & \int_S \frac{\rho' - \rho}{R} ds' \\ = \; & \frac{1}{2} \sum_i \widehat{u}_i \left[(R_i^0)^2 \ln \frac{R_i^+ + l_i^+}{R_i^- + l_i^-} + R_i^+ l_i^+ - R_i^- l_i^- \right] \end{aligned} \tag{210}$$

where all the definition of symbols can also be found in [94]. Here $\rho' - \rho$ is not in the original 3D coordinate, but the projection onto the triangle plane.

Full wave interaction Notice that the interaction in equation (209) and (210) are for integrand of $1/r$. For full wave case we have integrand of e^{-jkr}/r. Separate the integrand into static term and wave term:

$$\frac{e^{-jkr}}{r} = \frac{1}{r} + \frac{e^{-jkr} - 1}{r} \tag{211}$$

where the second term in the right hand side can be approximated by a taylor expansion and is not singular, thus can be integrated by seven point rule.

$$\frac{e^{-jkr} - 1}{r} = -jk - \frac{k^2}{2} r - j \frac{k^3}{6} r^2 + \frac{k^4}{24} r^3 + j \frac{k^5}{120} r^4 \tag{212}$$

Notice that the approximation is good when $kr << 1$, which is satisfied for self- and overlap-patch interaction.

5.1.6 Excitation scheme

There are generally four kind of excitation scheme, each used in a different context.

Plane wave incident (Figure 46) Plane wave incident has been used in formulating scattering problems [95][96]. The equivalent circuit of this excitation scheme is shown in the below of figure 46 and as we can see that it is not suitable for our exterior problem, because the voltage sources everywhere make it impossible to extract out the travelling waves due to the discontinuity.

Port extension. (Figure 47) The scheme of port extension is used in [97][98]. Tangential electrical field is placed on the port extension part as the excitation source (figure 47). Currents are then induced on the metal surface and solved by the MoM approach derived previously.

By putting tangential electric field at the extension port, it is like adding voltage source at one end of the strip (figure 47). This does not eliminate the open end discontinuity at the excitation end, but since in our exterior formulation we are only interested in the current reflection pattern on the trace, the current reflected by this open end will serve as another incident wave, together with many other reflected and excited waves, thus this open end discontinuity at the source part will not affect the reflect pattern caused by the discontinuity at the other end of the trace.

This scheme is much similar to δ gap excitation which we will mention later, sometimes people take them as the same. But this scheme is better than δ gap excitation in the cases where the physical current density at excitation end will be zero (eg. short circuit termination with strip length of multiples of half wavelength). Also this scheme allows point-matching testing in the MoM solution while δ gap excitation only supports Galerking's testing.

Impression of current source (figure 48) This scheme is used in [60][61] and also our formulation of exterior structure in chapter 3 and 4. It excites the whole structure by putting a mathematical current source at one end (away from the discontinuity). Because of the extraction technique, as long as the excitation is away from the discontinuity, it can take any mathematical form. In [60][61], it is a half rooftop. It can also be a full rooftop, a half RWG, or a full RWG for the convenience of the calculation of the right hand side of matrix equation. For an excitation on a full basis function, the right hand side of the matrix equation takes the form of one column of impedance matrix, depending on where the excitation cell is, of course normally we put excitation away from the discontinuity, which is at the other end. The strange shape of excitation current doesn't matter because this discontinuity effect at the excitation will vanish quickly away from the end, as long as it has some distance from the real discontinuity, we have no trouble extracting out the travelling

waves.

δ gap source (figure 49) The scheme of delta-gap source is used in [99]-[102]. This scheme impresses δ electric field in an infinitesmal small gap (figure 49), which makes it look like a constant voltage from circuit point of view (middle of figure 49). After introducing the δ gap source, doing Galerkin's testing on this cell introduces a non-zero right hand side in the matrix equation (because of the electric field at the gap), people usually just put a "1" in the right hand side.

Because of its simplicity, we use δ gap source excitation in our exterior formulation. This scheme can be applied very conveniently with RWG basis function. As illustrated in figure 49, the normal electric field across the internal edge of one RWG basis function will make its right hand side non-zero, while this edge will not affect other basis function because the electric field is normal to this edge, while current at other basis function are tangential to this edge.

5.1.7 Extraction of exterior parameters

The exterior paramters Γ_{sc}, I_{sc}, Y_{ant} and T_{ant} are obtained following the same process in chapter 3 and 4. Using the formulation in this chapter, we obtain a more accurate current distribution on the traces. From the current distribution, matrix-penciled method is applied to extract out the travelling wave components on the traces and gives those exterior parameters. Worth to mention is that in the matrix-penciled method, sampling points should be taken some distance away from either end of the trace so that the higher order modes excited by the discontinuity at either end will not have much influence on the extraction.

5.2 Layer-medium structure

The formulation for layer-medium structure is similar to that of free space, except the Green's function. We only illustrate the different part in layer-medium case while the unmentioned are supposed to be the same as free space case.

5.2.1 Layer-medium Green's function

Our exterior structure has three layers, region 0 is the air region above the dielectric substrate, region 1 is the dielectric substrate above ground plane with relative dielectric constant of ε_{r1}, region 2 is the ground plane or reference plane. For our exterior formulation, we need the following layer-medium Green's functions. (figure 50)

1) $\overline{\overline{G}}^{EJ}_{00xx}$, $\overline{\overline{G}}^{EJ}_{00xy}$, $\overline{\overline{G}}^{EJ}_{00yx}$ and $\overline{\overline{G}}^{EJ}_{00yy}$ for electric current interaction on horizontal traces in region 0, where

$$G_{00xx} = W_{00\rho}(\rho)\cos^2\phi - W_{00\phi}(\rho)\sin^2\phi \tag{213}$$

$$G_{00yy} = -W_{00\phi}(\rho)\cos^2\phi + W_{00\rho}(\rho)\sin^2\phi \tag{214}$$

$$G_{00xy} = G_{00yx} = \sin\phi\cos\phi\left[W_{00\rho}(\rho) + W_{00\phi}(\rho)\right] \tag{215}$$

2) $\overline{\overline{G}}^{EJ}_{11xx}$, $\overline{\overline{G}}^{EJ}_{11xy}$, $\overline{\overline{G}}^{EJ}_{11yx}$, $\overline{\overline{G}}^{EJ}_{11yy}$, $\overline{\overline{G}}^{EJ}_{11zx}$and $\overline{\overline{G}}^{EJ}_{11zy}$ for electric current interaction between horizontal traces and vertical section of via in region 1, where

$$G_{11xx} = W_{11\rho}(\rho)\cos^2\phi - W_{11\phi}(\rho)\sin^2\phi \tag{216}$$

$$G_{11yy} = -W_{11\phi}(\rho)\cos^2\phi + W_{11\rho}(\rho)\sin^2\phi \tag{217}$$

$$G_{11xy} = G_{11yx} = \sin\phi\cos\phi\left[W_{11\rho}(\rho) + W_{11\phi}(\rho)\right] \tag{218}$$

$$G_{11zx} = W_{11z}(\rho)\cos\phi \tag{219}$$

$$G_{11zy} = W_{11z}(\rho)\sin\phi \tag{220}$$

3) $\overline{\overline{G}}^{EM}_{11xx}$, $\overline{\overline{G}}^{EM}_{11xy}$, $\overline{\overline{G}}^{EM}_{11yx}$, $\overline{\overline{G}}^{EM}_{11yy}$, $\overline{\overline{G}}^{EM}_{11zx}$and $\overline{\overline{G}}^{EM}_{11zy}$ for magnetic current induced electric field on horizontal traces and on vertical section of via in region 1, where

$$G^{EM}_{11xx} = W^{EM}_{11\rho}(\rho)\cos^2\phi - W^{EM}_{11\phi}(\rho)\sin^2\phi \tag{221}$$

$$G^{EM}_{11yy} = -W^{EM}_{11\phi}(\rho)\cos^2\phi + W^{EM}_{11\rho}(\rho)\sin^2\phi \tag{222}$$

$$G^{EM}_{11xy} = G^{EM}_{11yx} = \sin\phi\cos\phi\left[W^{EM}_{11\rho}(\rho) + W^{EM}_{11\phi}(\rho)\right] \tag{223}$$

$$G^{EM}_{11zx} = W^{EM}_{11z}(\rho)\cos\phi \tag{224}$$

$$G^{EM}_{11zy} = W^{EM}_{11z}(\rho)\sin\phi \tag{225}$$

In chapter 6, we show how the layered-medium Green's function can be expressed in the form of $W_\rho(\rho)$, $W_\phi(\rho)$ and $W_z(\rho)$, which has only ρ dependence.

5.2.2 Evaluation of impedance matrix element

The evaluation of impedance matrix element again falls into 3 categories: self- and overlap-patch, near field interaction and non-near field interaction. For near field and non-near field interaction, we use seven point rule integration and centroid approximation respectively.

For self- and overlap-patch, due to the singularity in the Green's function, we cannot perform numerical integration, but need analytical integration. Because the layer-medium Green's function mentioned above is actually evaluated numerically, they cannot be used directly in the analytical integration in the self- and overlap-patch interaction. To perform analytical integration, we need analytical formula for layer-medium Green's function for self- and overlap-patch.

We express the layer-medium Green's function using mixed potential G_a and G_v, notice that for self- and overlap-patch, the distance from the field point to source point is much less than the wavelength, we can ignore the field created by G_a, and only consider the effect of G_v. Due to the same reason, we use electrostatic approximation in the expression of G_v and obtain the quasi-static analytical formula for G_v which is used in the self- and overlap-patch interaction.

The following gives the derivation for G_{v00} while others are listed in the appendix.

$$\vec{E} = -j\omega G_A \hat{x} - \hat{x}\frac{j}{\omega}\frac{\partial^2 G_V}{\partial x^2} - \hat{y}\frac{j}{\omega}\frac{\partial^2}{\partial x \partial y} G_V \tag{226}$$

$$\frac{\partial}{\partial x} G_V = G_V'(\rho)\cos\phi \tag{227}$$

So:

$$\begin{aligned} \vec{E} \;=\; & -j\omega G_A \hat{x} - \hat{x}\frac{j}{\omega}\left[\frac{d^2 G_V(\rho)}{d\rho^2}\cos^2\phi + \frac{dG_V(\rho)}{d\rho}\sin^2\phi\right] \\ & -\hat{y}\frac{j}{\omega}\left[\frac{d^2 G_V(\rho)}{d\rho^2}\cos\phi\sin\phi - \frac{dG_V(\rho)}{d\rho}\frac{1}{\rho}\cos\phi\sin\phi\right] \end{aligned} \tag{228}$$

which gives:

$$\frac{d^2G_V(\rho)}{d\rho^2} - \frac{dG_V(\rho)}{d\rho}\frac{1}{\rho} = \omega^2\mu\left[W_\rho(\rho) + W_\phi(\rho)\right] \tag{229}$$

Since:

$$-\frac{d^2}{d\rho^2}\frac{J_0(k_\rho\rho)}{k_\rho^2} + \frac{1}{\rho}\frac{d}{d\rho}\frac{J_0(k_\rho\rho)}{k_\rho^2} = \left[J_1'(k_\rho\rho) - \frac{J_1(k_\rho\rho)}{k_\rho\rho}\right] \tag{230}$$

We have:

$$G_{V00}(\rho) = -\frac{j}{4\pi\varepsilon}\int_0^\infty dk_\rho \frac{1}{k_z}\left[k_\rho + \frac{k^2R^{TE} + k_z^2R^{TM}}{k_\rho}\right]J_0(k_\rho\rho) \tag{231}$$

At electrostatics:

$$k = 0 \tag{232}$$

$$k_1 = 0 \tag{233}$$

$$k_z = -jk_\rho \tag{234}$$

$$k_{1z} = -jk_\rho \tag{235}$$

$$R^{TE} = 0 \tag{236}$$

$$R_{01}^{TM} = \frac{\varepsilon_1 - \varepsilon}{\varepsilon_1 + \varepsilon} \tag{237}$$

$$R_{TM} = -\sum_{n=0}^{\infty}\left(R_{10}^{TM}\right)^{n+1}\exp(-2k_\rho dn) + \sum_{n=0}^{\infty}\left(R_{10}^{TM}\right)^{n}\exp(-2k_\rho d(n+1)) \tag{238}$$

thus:

$$\begin{aligned} G_{V00}(\rho) &= -\frac{j}{4\pi\varepsilon}\int_0^\infty dk_\rho \frac{1}{-jk_\rho}\left[k_\rho + \frac{-k_\rho^2R^{TM}}{k_\rho}\right]J_0(k_\rho\rho) \\ &= \frac{1}{4\pi\varepsilon}\int_0^\infty dk_\rho(1 - R^{TM})J_0(k_\rho\rho) \end{aligned} \tag{239}$$

According to integral identity:

$$\int_0^\infty dk_\rho J_0(k_\rho\rho) = \frac{1}{\rho} \tag{240}$$

$$\int_0^\infty dk_\rho J_0(k_\rho\rho)e^{-k_\rho z} = \frac{1}{\sqrt{\rho^2+z^2}} \tag{241}$$

we have the analytical form of $G_{V00}(\rho)$:

$$\begin{aligned}
G_{V00}(\rho) &= \frac{1}{4\pi\varepsilon}\int_0^\infty dk_\rho(1-R^{TM})J_0(k_\rho\rho) \\
&= \frac{1}{4\pi\varepsilon\rho} - \frac{1}{4\pi\varepsilon}\int_0^\infty dk_\rho R^{TM}J_0(k_\rho\rho) \\
&= \frac{1}{4\pi\varepsilon\rho} - \frac{1}{4\pi\varepsilon}\int_0^\infty dk_\rho \left\{ \begin{array}{l} -\sum_{n=0}^\infty \left(R_{10}^{TM}\right)^{n+1}\exp(-2k_\rho dn) \\ +\sum_{n=0}^\infty \left(R_{10}^{TM}\right)^{n}\exp(-2k_\rho d(n+1)) \end{array} \right\} J_0(k_\rho\rho) \\
&= \frac{1}{4\pi\varepsilon\rho} + \frac{1}{4\pi\varepsilon}\sum_{n=0}^\infty \left(R_{10}^{TM}\right)^{n+1}\frac{1}{\sqrt{\rho^2+(2nd)^2}} \\
&\quad -\frac{1}{4\pi\varepsilon}\sum_{n=0}^\infty \left(R_{10}^{TM}\right)^{n}\frac{1}{\sqrt{\rho^2+(2(n+1)d)^2}} \\
&= (1+R_{10}^{TM})\frac{1}{4\pi\varepsilon\rho} + \frac{1}{4\pi\varepsilon}\sum_{n=1}^\infty \left(R_{10}^{TM}\right)^{n+1}\frac{1}{\sqrt{\rho^2+(2nd)^2}} \\
&\quad -\frac{1}{4\pi\varepsilon}\sum_{n=0}^\infty \left(R_{10}^{TM}\right)^{n}\frac{1}{\sqrt{\rho^2+(2(n+1)d)^2}}
\end{aligned} \tag{242}$$

The first part can be integrated analytically, the rest are not singular, thus can be integrated numerically.

5.3 Result and Discussion

Figure 51 shows the scattering parameters and loss of a through-hole via with the exterior formulation derived in this chapter. The parameters are: strip width $w = 10mil$, layer thickness $h = 20mil$, via inner radius $a = 5mil$, via outer radius $b = 12mil$ and pad radius $r = 15mil$. For such dimensions, because strip width w is comparable to layer thickness h, thin wire approximation will not give reasonable result, while the exterior formulation in this chapter gives reasonable result. Figure 51 shows that the loss and reflection in dB versus frequency in decade is linear. The reason we use a through-hole via here is that it is

actually composed of two exterior structure, thus it can best reflect the improvement in the formulation without the influence by the interior structure. As introduced in chapter 3 and 4, exterior problem is solved separately with interior problem, it has no difficult to combine the exterior parameter extracted here with the interior results obtained previously.

One of the important parameters in the exterior structure is the pad radius. The via pad introduces parasitic capacitance in the circuit and pad size directly influence this parasitic capacitance. Figure 52 shows the result of reflection and loss of a through-hole via with different pad radius. We can see that although the loss remains almost unchanged with the pad radius, reflection changes linearly with the pad radius.

5.4 Conclusion

In this chapter, the exterior structure of via is formulated using more rigorous approach than that in chapter 3 and 4. Compared with traces with known characteristic impedance which failes to take into account the corner and pad effect, and compared with thin wire approximation, which is improper for some layout dimensions and also failes to consider the pad effect, this formulation considers the actual layout of the exterior structure thus gives a more reliable simulation result. Simulation results are given for reflection characteristic under different pad radius.

Also in this chapter, the fast evaluation of spatial domain layered-medium Green's function has been widely used in the formulation. Combined with our formulation of interior structure of multi-via coupling, this approach gives fast and accurate modelling of the entire multi-via structure on PCB and electronic packaging, which can find application in EDA simulation softwares.

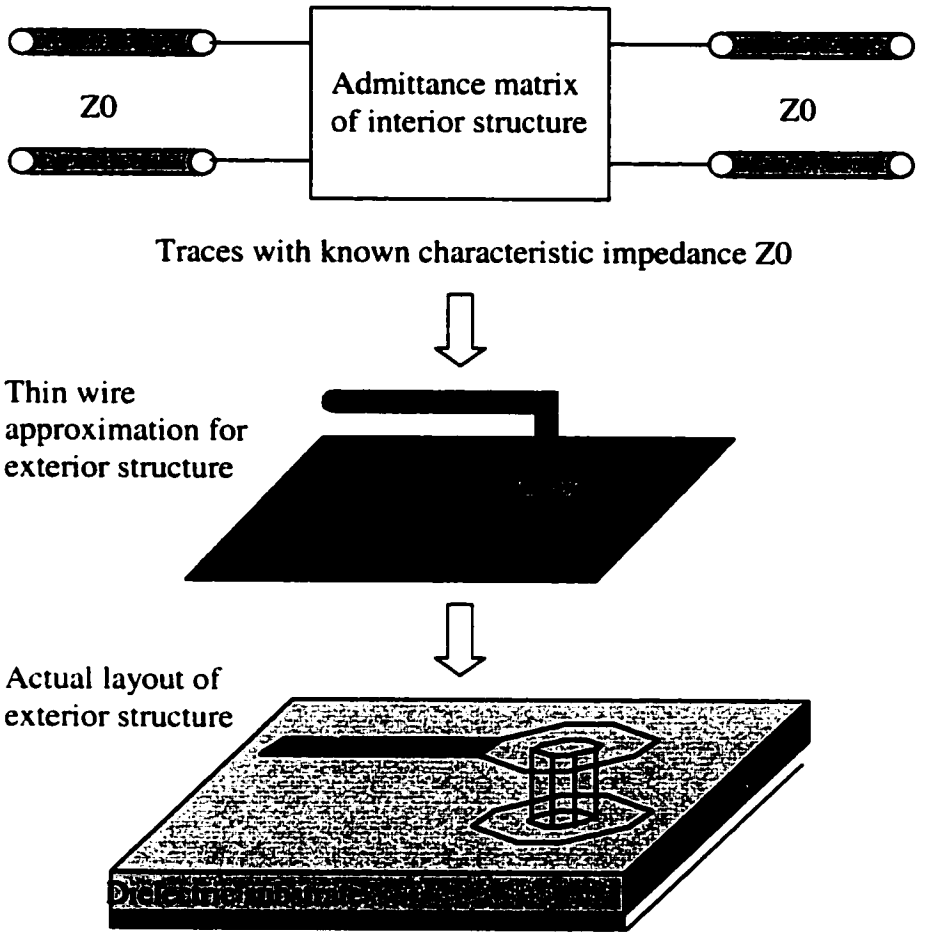

Figure 41: Three kind of exterior formulation

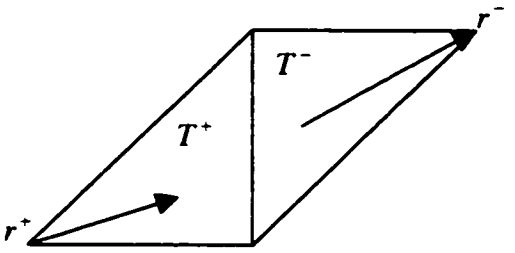

Figure 42: RWG basis function

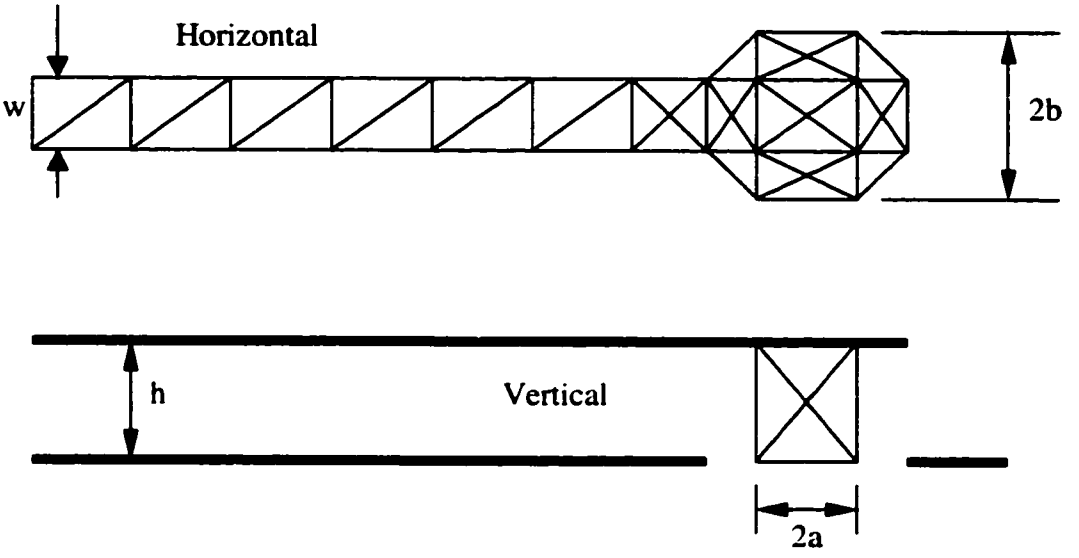

Figure 43: RWG mesh of the exterior structure

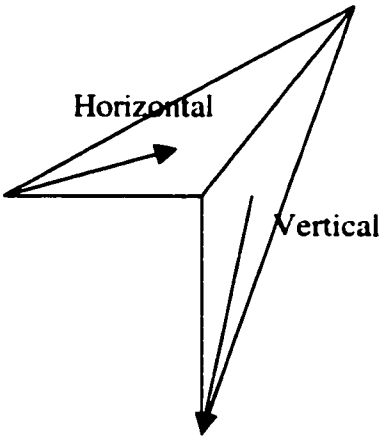

Figure 44: RWG basis for horizontal-vertical junction

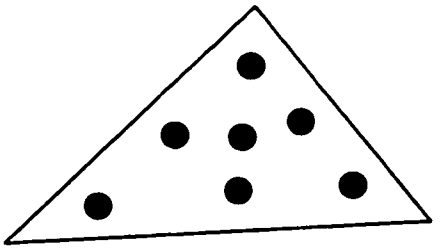

Figure 45: 7 sampling points inside triangle

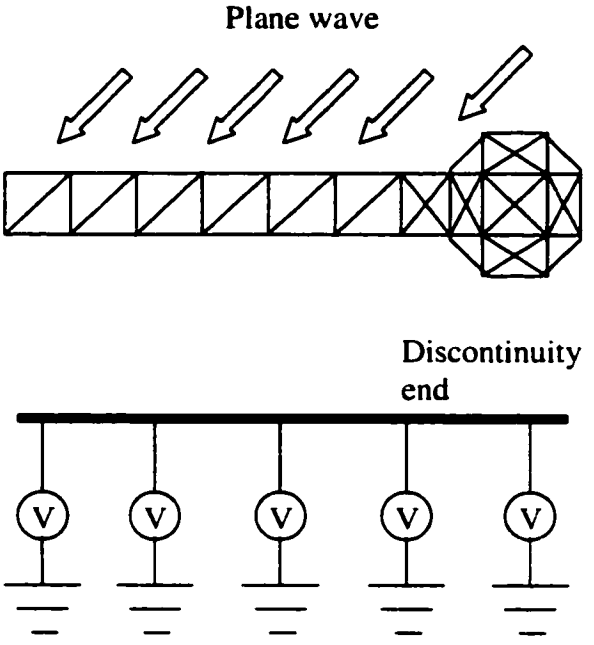

Fig 46: Plane wave excitation and its circuit equivalent

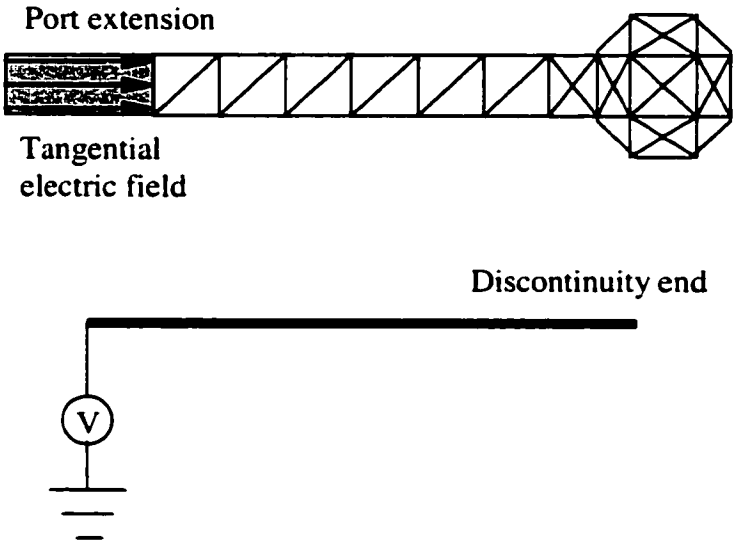

Fig 47: Port extension excitation and its circuit equivalent

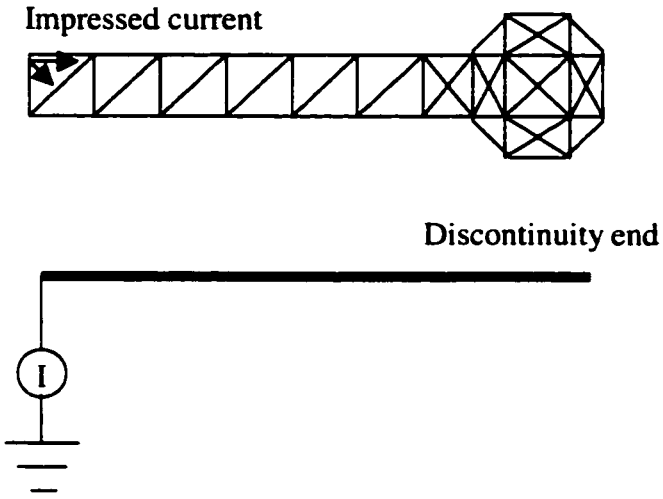

Fig 48: Impressed current excitation and its circuit equivalent

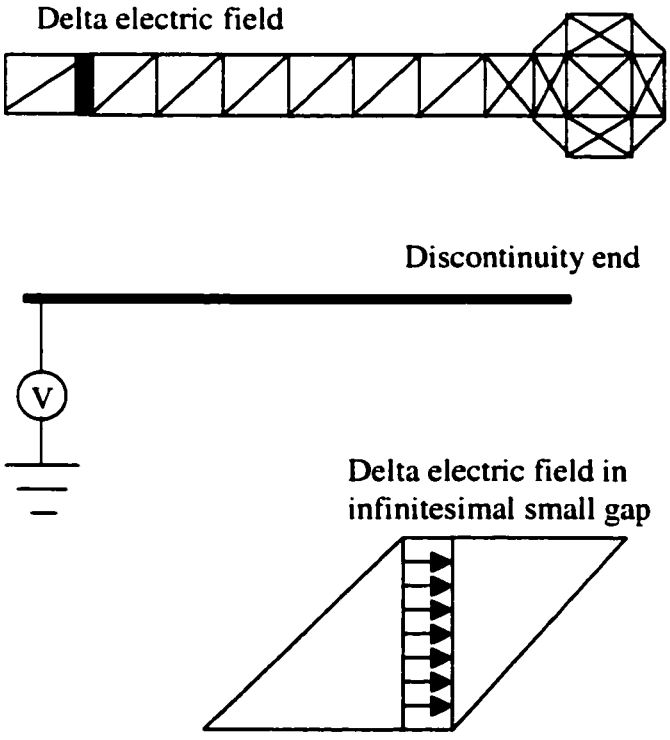

Fig 49: Delta gap excitation and its circuit equivalent

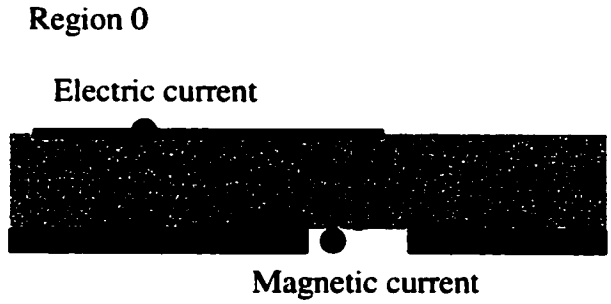

Fig 50: Layered-medium structure

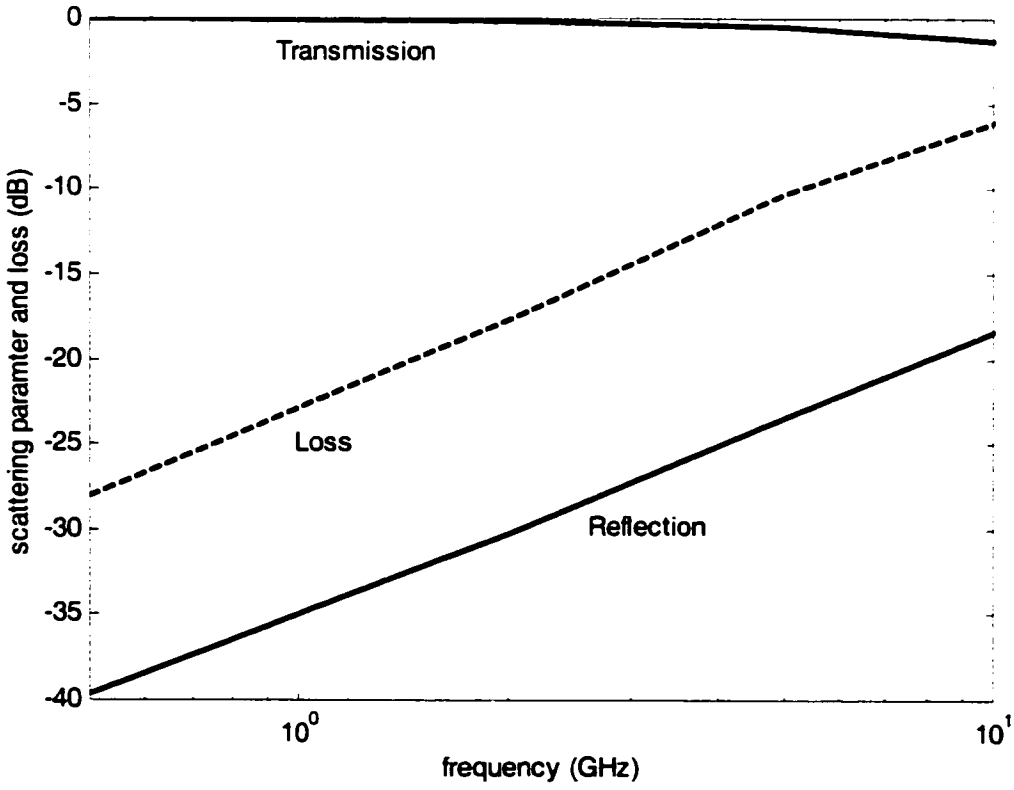

Fig 51: Scattering parameter and loss of a through-hole via

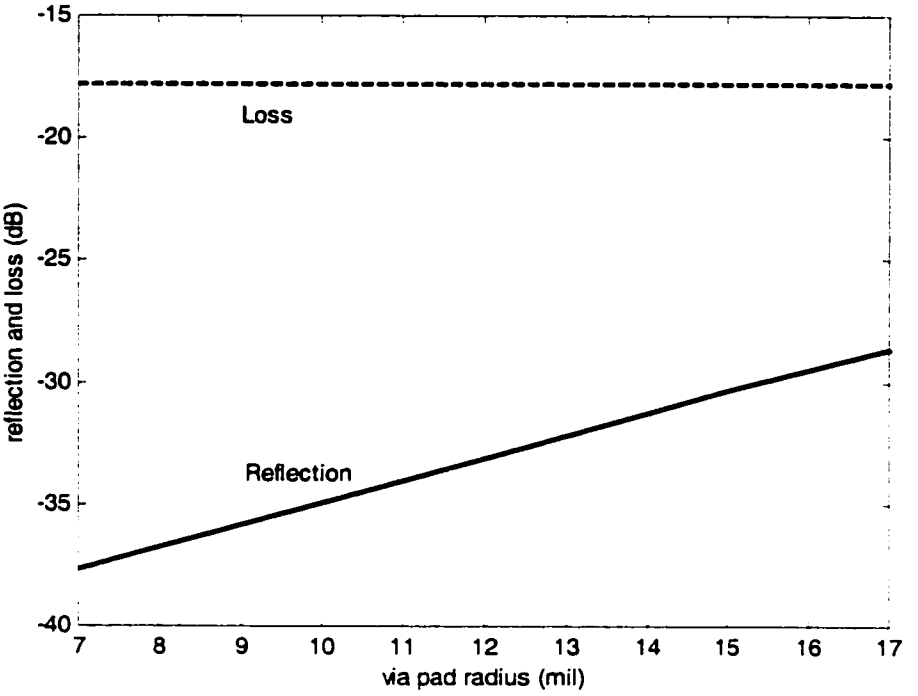

Fig 52: Reflection and loss vs. via pad radius (2 GHz)

6 Layer-medium Green's function

Let's consider the layer-medium Green's function in chapter 5. In figure 50, region 0 has a dielectric constant of ε. region 1 ε_1 and region 2 is perfect conductor. The boundaries are at $z = 0$ and $z = -d$. G_{ij} is the layer-medium Green's function with source in region j and field in region i.

6.1 Dyadic Green's function in region 0 with horizontal source at $z' = 0$

This is for the source and field on the microstrip line. The field in region 0 is:

$$\bar{\bar{G}}_{00} = \bar{\bar{G}}_p + \bar{\bar{G}}_R \tag{243}$$

where

$$\begin{aligned} \bar{\bar{G}}_p &= -\frac{j}{8\pi^2}\int_{-\infty}^{\infty} dk_x \int_{-\infty}^{\infty} dk_y e^{-jk_x(x-x')-jk_y(y-y')-jk_z|z-z'|} \cdot \\ &\quad \frac{1}{k_z}\begin{cases} \widehat{e}(k_z)\widehat{e}(k_z) + \widehat{h}(k_z)\widehat{h}(k_z) \\ \widehat{e}(k_z)\widehat{e}(k_z) + \widehat{h}(-k_z)\widehat{h}(-k_z) \end{cases} \end{aligned} \tag{244}$$

$$\begin{aligned} \bar{\bar{G}}_R &= -\frac{j}{8\pi^2}\int_{-\infty}^{\infty} dk_x \int_{-\infty}^{\infty} dk_y e^{-jk_x(x-x')-jk_y(y-y')-jk_z z-jk_z z'} \\ &\quad \frac{1}{k_z}\left[R_{TE}\widehat{e}(k_z)\widehat{e}(-k_z) + R^{TM}\widehat{h}(k_z)\widehat{h}(-k_z)\right] \end{aligned} \tag{245}$$

for upward going wave and match with $\bar{\bar{G}}_p$ in prime coordinate for $z < z'$.

The field in region 1 is:

$$\bar{\bar{G}}_{10} = \bar{\bar{G}}_{10TE} + \bar{\bar{G}}_{10TM} \tag{246}$$

$$\begin{aligned} G_{10TE} &= -\frac{j}{8\pi^2}\int_{-\infty}^{\infty} dk_x \int_{-\infty}^{\infty} dk_y e^{-jk_x(x-x')-jk_y(y-y')} e^{-jk_z z'} \cdot \\ &\quad \frac{1}{k_z}\{A_1\widehat{e}_1(k_{1z})e^{-jk_{1z}z} + B_1 e^{jk_{1z}z}\widehat{e}_1(-k_{1z})\}\widehat{e}(-k_z) \end{aligned} \tag{247}$$

Note r coordinate has to obey wave equation in region 1. r' coordinate matches to the

source.

$$G_{10TM} = -\frac{j}{8\pi^2}\int_{-\infty}^{\infty} dk_x \int_{-\infty}^{\infty} dk_y e^{-jk_x(x-x')-jk_y(y-y')} e^{-jk_z z'} \cdot \frac{1}{k_z}\{C_1 \widehat{h}_1(k_{1z}) e^{-jk_{1z}z} + D_1 e^{jk_{1z}z}\widehat{h}_1(-k_{1z})\}\widehat{h}(-k_z) \quad (248)$$

$$\widehat{e}(\pm k_z) = \widehat{e}_1(\pm k_{1z}) = \frac{1}{k_\rho}(\widehat{x}k_y - \widehat{y}k_x) \quad (249)$$

$$\widehat{h}(k_z) = -\frac{k_z}{kk_\rho}(\widehat{x}k_x + \widehat{y}k_y) + \frac{k_\rho}{k}\widehat{z} \quad (250)$$

$$\widehat{h}(-k_z) = \frac{k_z}{kk_\rho}(\widehat{x}k_x + \widehat{y}k_y) + \frac{k_\rho}{k}\widehat{z} \quad (251)$$

$$\widehat{h}_1(k_{1z}) = -\frac{k_{1z}}{k_1 k_\rho}(\widehat{x}k_x + \widehat{y}k_y) + \frac{k_\rho}{k_1}\widehat{z} \quad (252)$$

$$\widehat{h}_1(-k_{1z}) = \frac{k_{1z}}{k_1 k_\rho}(\widehat{x}k_x + \widehat{y}k_y) + \frac{k_\rho}{k_1}\widehat{z} \quad (253)$$

Match boundary conditon:

$$\widehat{z} \times \overline{\overline{G}}_{10} = 0 \text{ at } z = -d \quad (254)$$

$$\widehat{z} \times \overline{\overline{G}}_{10} = \widehat{z} \times \overline{\overline{G}}_{00} \text{ at } z = 0 \quad (255)$$

$$\widehat{z} \times \nabla \times \overline{\overline{G}}_{10} = \widehat{z} \times \nabla \times \overline{\overline{G}}_{00} \text{ at } z = 0 \quad (256)$$

gives the following equations:

$$A_1 e^{jk_{1z}d} + B_1 e^{-jk_{1z}d} = 0 \quad (257)$$

$$C_1 e^{jk_{1z}d} - D_1 e^{-jk_{1z}d} = 0 \quad (258)$$

$$A_1 + B_1 = R_{TE} + 1 \quad (259)$$

$$\frac{k_{1z}}{k_1}(-C_1 + D_1) = \frac{k_z}{k}(-R_{TM} + 1) \quad (260)$$

$$k_1(C_1 + D_1) = k\,(R_{TM} + 1) \quad (261)$$

$$k_{1z}(-A_1 + B_1) = k_z(-R_{TE} + 1) \quad (262)$$

Solving the above 6 equations and we have:

$$R_{TE} = \frac{R_{01}^{TE} - \exp(-2jk_{1z}d)}{1 - R_{01}^{TE}\exp(-2jk_{1z}d)} \tag{263}$$

$$R_{01}^{TE} = \frac{k_z - k_{1z}}{k_z + k_{1z}} \tag{264}$$

$$\begin{aligned} B_1 &= \frac{1}{1-\exp(-2jk_{1z}d)} \frac{1-\exp(-2jk_{1z}d) + R_{01}^{TE}\left[1-\exp(-2jk_{1z}d)\right]}{1 - R_{01}^{TE}\exp(-2jk_{1z}d)} \\ &= \frac{1 + R_{01}^{TE}}{1 - R_{01}^{TE}\exp(-2jk_{1z}d)} \end{aligned} \tag{265}$$

$$A_1 = -\exp(-2jk_{1z}d)B_1 = -\exp(-2jk_{1z}d)\frac{1 + R_{01}^{TE}}{1 - R_{01}^{TE}\exp(-2jk_{1z}d)} \tag{266}$$

$$R_{TM} = \frac{R_{01}^{TM} + \exp(-2jk_{1z}d)}{1 + R_{01}^{TM}\exp(-2jk_{1z}d)} \tag{267}$$

$$R_{01}^{TM} = \frac{k_1^2 k_z - k^2 k_{1z}}{k_1^2 k_z + k^2 k_{1z}} \tag{268}$$

$$D_1 = \frac{k}{k_1}\frac{(1 + R_{TM})}{1 + \exp(-2jk_{1z}d)} = \frac{k}{k_1}\frac{1 + R_{01}^{TM}}{1 + R_{01}^{TM}\exp(-2jk_{1z}d)} \tag{269}$$

$$C_1 = \exp(-2jk_{1z}d)D_1 = \exp(-2jk_{1z}d)\frac{k}{k_1}\frac{1 + R_{01}^{TM}}{1 + R_{01}^{TM}\exp(-2jk_{1z}d)} \tag{270}$$

6.1.1 Electric field Green's function

Apply the transverse vector to both side of $\overline{\overline{G}}_{00}$, we have:

$$\begin{aligned} G_{xx} &= -\frac{j}{8\pi^2}\int_{-\infty}^{\infty} dk_x \int_{-\infty}^{\infty} dk_y e^{-jk_x(x-x')-jk_y(y-y')} \\ &\quad \frac{1}{k_z}\left(\frac{k_y^2}{k_\rho^2}(1+R^{TE}) + \frac{k_x^2 k_z^2}{k_\rho^2 k^2}(1-R^{TM})\right) \qquad (271) \\ G_{xy} &= G_{yx} \\ &= -\frac{j}{8\pi^2}\int_{-\infty}^{\infty} dk_x \int_{-\infty}^{\infty} dk_y e^{-jk_x(x-x')-jk_y(y-y')} \\ &\quad \frac{1}{k_z}\left(-\frac{k_x k_y}{k_\rho^2}(1+R^{TE}) + \frac{k_x k_y k_z^2}{k_\rho^2 k^2}(1-R^{TM})\right) \qquad (272) \\ G_{yy} &= -\frac{j}{8\pi^2}\int_{-\infty}^{\infty} dk_x \int_{-\infty}^{\infty} dk_y e^{-jk_x(x-x')-jk_y(y-y')} \\ &\quad \frac{1}{k_z}\left(\frac{k_x^2}{k_\rho^2}(1+R^{TE}) + \frac{k_y^2 k_z^2}{k_\rho^2 k^2}(1-R^{TM})\right) \qquad (273) \end{aligned}$$

6.1.2 Reduction to Single Integral

We next make a transformation to polar coordinates in the spectral domain and the space domain.

$$\begin{aligned} k_x &= k_\rho \cos\phi_k \qquad (274) \\ k_y &= k_\rho \sin\phi_k \qquad (275) \\ x-x' &= \rho\cos\phi \qquad (276) \\ y-y' &= \rho\sin\phi \qquad (277) \end{aligned}$$

Then

$$k_x(x-x') + k_y(y-y') = k_\rho\rho\cos(\phi_k - \phi) \qquad (278)$$

Note that R^{TE} and R^{TM} are functions of k_ρ but not of ϕ_k. We use the following integral identity

$$(-j)^n J_n(w) = \frac{1}{2\pi}\int_0^{2\pi} d\phi_k e^{-jw\cos\phi_k} e^{-jn\phi_k} \qquad (279)$$

thus

$$\frac{1}{2\pi}\int_0^{2\pi} d\phi_k e^{-jk_\rho\rho\cos\phi_k}\sin^2\phi_k = \frac{1}{2}\left[J_0(w)+J_2(w)\right] = \frac{J_1(w)}{w} \quad (280)$$

$$\frac{1}{2\pi}\int_0^{2\pi} d\phi_k e^{-jk_\rho\rho\cos\phi_k}\cos^2\phi_k = \frac{1}{2}\left[J_0(w)-J_2(w)\right] = J_1'(w) \quad (281)$$

$$\int_0^{2\pi} d\phi_k e^{-jk_\rho\rho\cos\phi_k}\cos\phi_k\sin\phi_k = 0 \quad (282)$$

Define

$$W_\rho(\rho) = -\frac{j}{4\pi}\int_0^\infty dk_\rho\frac{k_\rho}{k_z}\left[\frac{J_1(k_\rho\rho)}{k_\rho\rho}(1+R^{TE})+\frac{k_z^2}{k^2}J_1'(k_\rho\rho)(1-R^{TM})\right] \quad (283)$$

$$W_\phi(\rho) = \frac{j}{4\pi}\int_0^\infty dk_\rho\frac{k_\rho}{k_z}\left[J_1'(k_\rho\rho)(1+R^{TE})+\frac{k_z^2}{k^2}\left(\frac{J_1(k_\rho\rho)}{k_\rho\rho}\right)(1-R^{TM})\right] \quad (284)$$

We have:

$$G_{xx} = W_\rho(\rho)\cos^2\phi - W_\phi(\rho)\sin^2\phi \quad (285)$$

$$G_{yy} = -W_\phi(\rho)\cos^2\phi + W_\rho(\rho)\sin^2\phi \quad (286)$$

$$G_{xy} = G_{yx} = \sin\phi\cos\phi\left[W_\rho(\rho)+W_\phi(\rho)\right] \quad (287)$$

6.1.3 Electrostatics Extraction

The sommerfeld integration in $W_\rho(\rho)$ and $W_\phi(\rho)$ does not converge. thus we need to extract out and do analytical integration on the asympotic term. and do numerical integration on the rest part which converges. Using electrostatics approximation. for large k_ρ. we have:

$$k \simeq 0 \quad (288)$$

$$k_1 \simeq 0 \quad (289)$$

$$k_z \simeq -jk_\rho \quad (290)$$

$$k_{1z} \simeq -jk_\rho \quad (291)$$

$$R_{01}^{TE} \simeq 0 \quad (292)$$

$$R_{TE} = \frac{R_{01}^{TE}-\exp(-2jk_{1z}d)}{1-R_{01}^{TE}\exp(-2jk_{1z}d)} = -\exp(-2k_\rho d) \quad (293)$$

$$R_{01}^{TM} = \frac{\varepsilon_1 - \varepsilon}{\varepsilon_1 + \varepsilon} = -R_{10}^{TM} \tag{294}$$

$$\begin{aligned} R_{TM} &= \frac{R_{01}^{TM} + \exp(-2jk_{1z}d)}{1 + R_{01}^{TM}\exp(-2jk_{1z}d)} \\ &= \left[R_{01}^{TM} + \exp(-2jk_{1z}d)\right] \sum_{n=0}^{\infty} \left(R_{10}^{TM}\right)^n \exp(-2jk_{1z}dn) \\ &= -\sum_{n=0}^{\infty} \left(R_{10}^{TM}\right)^{n+1} \exp(-2k_\rho dn) + \sum_{n=0}^{\infty} \left(R_{10}^{TM}\right)^n \exp(-2k_\rho d(n+1)) \end{aligned} \tag{295}$$

$$W_\rho(\rho) = -\frac{j}{4\pi} \int_0^\infty dk_\rho \frac{k_\rho}{k_z} \left[\frac{J_1(k_\rho\rho)}{k_\rho\rho}(1 + R^{TE}) + \frac{k_z^2}{k^2} J_1'(k_\rho\rho)(1 - R^{TM})\right] \tag{296}$$

$$W_\varphi(\rho) = \frac{j}{4\pi} \int_0^\infty dk_\rho \frac{k_\rho}{k_z} \left[J_1'(k_\rho\rho)(1 + R^{TE}) + \frac{k_z^2}{k^2} \left(\frac{J_1(k_\rho\rho)}{k_\rho\rho}\right)(1 - R^{TM})\right] \tag{297}$$

$$\begin{aligned} W_\rho(\rho) &= \frac{1}{4\pi} \int_0^\infty dk_\rho \frac{J_1(k_\rho\rho)}{k_\rho\rho}(1 - \exp(-2k_\rho d))\exp(-k_\rho z) \\ &\quad -\frac{1}{4\pi} \int_0^\infty dk_\rho \frac{k_\rho^2}{k^2} J_1'(k_\rho\rho)\exp(-k_\rho z) \\ &\quad \begin{bmatrix} 1 + \sum_{n=0}^{\infty} \left(R_{10}^{TM}\right)^{n+1} \exp(-2k_\rho dn) \\ -\sum_{n=0}^{\infty} \left(R_{10}^{TM}\right)^n \exp(-2k_\rho d(n+1)) \end{bmatrix} \end{aligned} \tag{298}$$

$$\begin{aligned} W_\varphi(\rho) &= -\frac{1}{4\pi} \int_0^\infty dk_\rho J_1'(k_\rho\rho)(1 - \exp(-2k_\rho d))\exp(-k_\rho z) \\ &\quad +\frac{1}{4\pi} \int_0^\infty dk_\rho \frac{k_\rho^2}{k^2} \left(\frac{J_1(k_\rho\rho)}{k_\rho\rho}\right)\exp(-k_\rho z) \\ &\quad \begin{bmatrix} 1 + \sum_{n=0}^{\infty} \left(R_{10}^{TM}\right)^{n+1} \exp(-2k_\rho dn) \\ -\sum_{n=0}^{\infty} \left(R_{10}^{TM}\right)^n \exp(-2k_\rho d(n+1)) \end{bmatrix} \end{aligned} \tag{299}$$

Using integral identities in [103], it is not difficult to find that the analytical term of

$W_\rho(\rho)$ and $W_\phi(\rho)$:

$$\begin{aligned} & W_{\rho\_ana}(\rho) \\ = & \frac{1}{4\pi\rho}\left[\frac{r-z}{\rho}-\frac{r_1-z_1}{\rho}\right] \\ & -\frac{1}{4\pi k^2}\left\{\begin{array}{c} -\frac{2}{r^3}+\frac{3z^2}{r^5}+\sum_{n=0}^{\infty}\left(R_{10}^{TM}\right)^{n+1}\left(-\frac{2}{r_n^3}+\frac{3z_n^2}{r_n^5}\right) \\ -\sum_{n=0}^{\infty}\left(R_{10}^{TM}\right)^{n}\left(-\frac{2}{r_{n+1}^3}+\frac{3z_{n+1}^2}{r_{n+1}^5}\right) \end{array}\right\} \end{aligned} \tag{300}$$

$$\begin{aligned} & W_{\phi\_ana}(\rho) \\ = & -\frac{1}{4\pi}\left[\frac{z(r-z)}{\rho^2 r}-\frac{z_1(r_1-z_1)}{\rho^2 r_1}\right] \\ & +\frac{1}{4\pi k^2}\left[\frac{1}{r^3}+\sum_{n=0}^{\infty}\left(R_{10}^{TM}\right)^{n+1}\frac{1}{r_n^3}-\sum_{n=0}^{\infty}\left(R_{10}^{TM}\right)^{n}\frac{1}{r_{n+1}^3}\right] \end{aligned} \tag{301}$$

where:

$$z_n = z+2nd \tag{302}$$

$$r_n = \sqrt{\rho^2+(z+2nd)^2} \tag{303}$$

6.1.4 G_{V00} for the near field using electrostatic approximation

For near field interaction, we write electric field in terms of the gradient of a potential, and compute the matrix element by parts so that the derivataive of the basis function is taken.

$$\begin{aligned} & \frac{d^2G_{V00}(\rho)}{d\rho^2}-\frac{dG_{V00}(\rho)}{d\rho}\frac{1}{\rho} \\ = & \omega^2\mu\left[W_{\rho 00}(\rho)+W_{\phi 00}(\rho)\right] \\ = & \frac{j\omega^2\mu}{4\pi}\int_0^\infty dk_\rho k_\rho\frac{1}{k_z}\left[(1+R^{TE})-\frac{k_z^2}{k^2}(1-R^{TM})\right]\left[J_1'(k_\rho\rho)-\frac{J_1(k_\rho\rho)}{k_\rho\rho}\right] \end{aligned} \tag{304}$$

$$G_{V00}(\rho) = -\frac{j}{4\pi\varepsilon}\int_0^\infty dk_\rho\frac{1}{k_z}\left[k_\rho+\frac{k^2R^{TE}+k_z^2R^{TM}}{k_\rho}\right]J_0(k_\rho\rho) \tag{305}$$

Using electrostatics approximation and integral identities [103]:

$$\begin{aligned} & G_{V00}(\rho) \\ = & -\frac{j}{4\pi\varepsilon}\int_0^\infty dk_\rho \frac{1}{-jk_\rho}\left[k_\rho + \frac{-k_\rho^2 R^{TM}}{k_\rho}\right] J_0(k_\rho\rho) \\ = & \frac{1}{4\pi\varepsilon}\int_0^\infty dk_\rho (1-R^{TM}) J_0(k_\rho\rho) \\ = & (1+R_{10}^{TM})\frac{1}{4\pi\varepsilon\rho} + \frac{1}{4\pi\varepsilon}\sum_{n=1}^{\infty}\left(R_{10}^{TM}\right)^{n+1}\frac{1}{\sqrt{\rho^2+(2nd)^2}} \\ & -\frac{1}{4\pi\varepsilon}\sum_{n=0}^{\infty}\left(R_{10}^{TM}\right)^{n}\frac{1}{\sqrt{\rho^2+(2(n+1)d)^2}} \end{aligned} \tag{306}$$

The first part of the above expression can be integrated analytically: the rest are not singular, thus can be integrated numerically.

6.2 Dyadic Green's function in region 1 with source in region 1

This is for the vertical current source in region 1 (figure 50).

$$\begin{aligned} \bar{\bar{G}}_{11p} = & -\frac{j}{8\pi^2}\int_{-\infty}^{\infty} dk_x \int_{-\infty}^{\infty} dk_y e^{-jk_x(x-x')-jk_y(y-y')-jk_{1z}|z-z'|} \cdot \\ & \frac{1}{k_{1z}}\begin{cases} \widehat{e}(k_{1z})\widehat{e}(k_{1z}) + \widehat{h}(k_{1z})\widehat{h}(k_{1z}) & for \quad z > z' \\ \widehat{e}(-k_{1z})\widehat{e}(-k_{1z}) + \widehat{h}(-k_{1z})\widehat{h}(-k_{1z}) & for \quad z < z' \end{cases} \end{aligned} \tag{307}$$

6.2.1 TE mode

$$\bar{\bar{G}}_{11TE} = \bar{\bar{G}}_{11pTE} + \bar{\bar{G}}_{11RTE} \tag{308}$$

The reflection field in region 1 are for both $z > z'$ and $z < z'$:

$$\begin{aligned} \bar{\bar{G}}_{11RTE} = & -\frac{j}{8\pi^2}\int_{-\infty}^{\infty} dk_x \int_{-\infty}^{\infty} dk_y e^{-jk_x(x-x')-jk_y(y-y')} \cdot \\ & \frac{1}{k_{1z}}\begin{bmatrix} A_1 \exp(-jk_{1z}(z))\widehat{e}(k_{1z}) \\ +B_1 \exp(jk_{1z}(z))\widehat{e}(-k_{1z}) \end{bmatrix} \exp(-jk_{1z}z')\widehat{e}(-k_{1z}) \end{aligned} \tag{309}$$

The transmitted field in region 0 are for $z > z'$:

$$\begin{aligned}\bar{\bar{G}}_{01TE} &= -\frac{j}{8\pi^2}\int_{-\infty}^{\infty} dk_x \int_{-\infty}^{\infty} dk_y e^{-jk_x(x-x')-jk_y(y-y')} \cdot \\ &\quad \frac{1}{k_{1z}}\left[T_{TE}\exp(-jk_z z)\widehat{e}(k_z)\right]\exp(-jk_{1z}z')\widehat{e}(-k_{1z}) \end{aligned} \tag{310}$$

Thus for $z < z'$, we have the total field:

$$\begin{aligned}&\bar{\bar{G}}_{11TE} \\ &= -\frac{j}{8\pi^2}\int_{-\infty}^{\infty} dk_x \int_{-\infty}^{\infty} dk_y e^{-jk_x(x-x')-jk_y(y-y')} \cdot \frac{1}{k_{1z}} \\ &\quad \begin{bmatrix} \exp(jk_{1z}z)\widehat{e}(-k_{1z}) \\ +A_1\exp(-jk_{1z}z)\widehat{e}(k_{1z}) \\ +B_1\exp(jk_{1z}(z))\widehat{e}(-k_{1z}) \end{bmatrix} \exp(-jk_{1z}z')\widehat{e}(-k_{1z}) \end{aligned} \tag{311}$$

Match boundary conditoin $\hat{z} \times \bar{\bar{G}}_{11TE} = 0$ at $z = -d$ gives:

$$\exp(-jk_{1z}d) + A_1\exp(jk_{1z}d) + B_1\exp(-jk_{1z}d) = 0 \tag{312}$$

For $z > z'$, match boundary condition

$$\hat{z} \times \bar{\bar{G}}_{11TE} = \hat{z} \times \bar{\bar{G}}_{01TE} \text{ at } z = 0 \tag{313}$$

$$\hat{z} \times \nabla \times \bar{\bar{G}}_{11TE} = \hat{z} \times \nabla \times \bar{\bar{G}}_{01TE} \text{ at } z = 0 \tag{314}$$

gives:

$$\exp(2jk_{1z}z') + A_1 + B_1 = T_{TE} \tag{315}$$

$$-\exp(2jk_{1z}z') - A_1 + B_1 = -\frac{k_z}{k_{1z}}T_{TE} \tag{316}$$

solve equations (312), (315) and (316) we have:

$$A_1 = -\frac{R_{10}^{TE}\exp(2jk_{1z}z')\exp(-2jk_{1z}d)}{\left[1+R_{10}^{TE}\exp(-2jk_{1z}d)\right]} - \frac{\exp(-2jk_{1z}d)}{\left[1+R_{10}^{TE}\exp(-2jk_{1z}d)\right]} \tag{317}$$

$$\begin{aligned} B_1 &= R_{10}^{TE}\exp(2jk_{1z}z') + R_{10}^{TE}A_1 \\ &= \frac{R_{10}^{TE}\exp(2jk_{1z}z')}{\left[1+R_{10}^{TE}\exp(-2jk_{1z}d)\right]} - R_{10}^{TE}\frac{\exp(-2jk_{1z}d)}{\left[1+R_{10}^{TE}\exp(-2jk_{1z}d)\right]} \end{aligned} \tag{318}$$

6.2.2 TM mode

$$\bar{\bar{G}}_{11TM} = \bar{\bar{G}}_{11pTM} + \bar{\bar{G}}_{11RTM} \tag{319}$$

$$\begin{aligned} \bar{\bar{G}}_{11pTM} &= -\frac{j}{8\pi^2}\int_{-\infty}^{\infty}dk_x\int_{-\infty}^{\infty}dk_y e^{-jk_x(x-x')-jk_y(y-y')-jk_z|z-z'|}\cdot \\ &\quad \frac{1}{k_{1z}}\begin{cases} \widehat{h}(k_{1z})\widehat{h}(k_{1z}) & for \quad z>z' \\ \widehat{h}(-k_{1z})\widehat{h}(-k_{1z}) & for \quad z<z' \end{cases} \\ &= -\frac{j}{8\pi^2}\int_{-\infty}^{\infty}dk_x\int_{-\infty}^{\infty}dk_y e^{-jk_x(x-x')-jk_y(y-y')-jk_z|z-z'|}\cdot \\ &\quad \frac{1}{k_{1z}}\begin{cases} \widehat{h}(k_{1z})\widehat{h}(k_{1z})\cdot\left(\bar{\bar{I}}_t+\widehat{z}\widehat{z}\right) & for\ z>z' \\ \widehat{h}(-k_{1z})\widehat{h}(-k_{1z})\cdot\left(\bar{\bar{I}}_t+\widehat{z}\widehat{z}\right) & for\ z<z' \end{cases} \end{aligned} \tag{320}$$

The reflection field in region 1 is:

$$\begin{aligned} \bar{\bar{G}}_{11RTM} &= -\frac{j}{8\pi^2}\int_{-\infty}^{\infty}dk_x\int_{-\infty}^{\infty}dk_y e^{-jk_x(x-x')-jk_y(y-y')}\cdot\frac{1}{k_{1z}} \\ &\quad \begin{bmatrix} C_{1t}\exp(-jk_{1z}(z))\widehat{h}(k_{1z}) \\ +D_{1t}\exp(jk_{1z}(z))\widehat{h}(-k_{1z}) \end{bmatrix}\exp(-jk_{1z}z')\widehat{h}(-k_{1z})\cdot\bar{\bar{I}}_t \\ &\quad -\frac{j}{8\pi^2}\int_{-\infty}^{\infty}dk_x\int_{-\infty}^{\infty}dk_y e^{-jk_x(x-x')-jk_y(y-y')}\cdot\frac{1}{k_{1z}} \\ &\quad \begin{bmatrix} C_{1z}\exp(-jk_{1z}(z))\widehat{h}(k_{1z}) \\ +D_{1z}\exp(jk_{1z}(z))\widehat{h}(-k_{1z}) \end{bmatrix}\exp(-jk_{1z}z')\widehat{h}(-k_{1z})\cdot\widehat{z}\widehat{z} \end{aligned} \tag{321}$$

For $z < z'$, the total field in region 1 is:

$$\begin{aligned}
\bar{\bar{G}}_{11TM} &= -\frac{j}{8\pi^2}\int_{-\infty}^{\infty} dk_x \int_{-\infty}^{\infty} dk_y e^{-jk_x(x-x')-jk_y(y-y')} \cdot \frac{1}{k_{1z}} \\
&\quad \begin{bmatrix} \widehat{h}(-k_{1z})\exp(jk_{1z}(z)) \\ +C_{1t}\exp(-jk_{1z}(z))\widehat{h}(k_{1z}) \\ +D_{1t}\exp(jk_{1z}(z))\widehat{h}(-k_{1z}) \end{bmatrix} \exp(-jk_{1z}z')\widehat{h}(-k_{1z}) \cdot \bar{\bar{I}}_t \\
&\quad -\frac{j}{8\pi^2}\int_{-\infty}^{\infty} dk_x \int_{-\infty}^{\infty} dk_y e^{-jk_x(x-x')-jk_y(y-y')} \cdot \frac{1}{k_{1z}} \\
&\quad \begin{bmatrix} \widehat{h}(-k_{1z})\exp(jk_{1z}(z)) \\ +C_{1z}\exp(-jk_{1z}(z))\widehat{h}(k_{1z}) \\ +D_{1z}\exp(jk_{1z}(z))\widehat{h}(-k_{1z}) \end{bmatrix} \exp(-jk_{1z}z')\widehat{h}(-k_{1z}) \cdot \widehat{z}\widehat{z}
\end{aligned} \tag{322}$$

Match boundary condition $\widehat{z} \times \bar{\bar{G}}_{11TM} = 0$ at $z = -d$ gives:

$$0 = -\exp(-jk_{1z}d) + C_{1t}\exp(jk_{1z}d) - D_{1t}\exp(-jk_{1z}d) \tag{323}$$

$$0 = -\exp(-jk_{1z}d) + C_{1z}\exp(jk_{1z}d) - D_{1z}\exp(-jk_{1z}d) \tag{324}$$

The transmitted field in region 0 is:

$$\begin{aligned}
\bar{\bar{G}}_{01TM} &= -\frac{j}{8\pi^2}\int_{-\infty}^{\infty} dk_x \int_{-\infty}^{\infty} dk_y e^{-jk_x(x-x')-jk_y(y-y')} \cdot \\
&\quad \frac{1}{k_{1z}}\left[T_t^{TM}\exp(-jk_z(z))\widehat{h}(k_z)\right]\exp(-jk_{1z}z')\widehat{h}(-k_{1z}) \cdot \bar{\bar{I}}_t \\
&\quad -\frac{j}{8\pi^2}\int_{-\infty}^{\infty} dk_x \int_{-\infty}^{\infty} dk_y e^{-jk_x(x-x')-jk_y(y-y')} \cdot \\
&\quad \frac{1}{k_{1z}}\left[T_z^{TM}\exp(-jk_z(z))\widehat{h}(k_z)\right]\exp(-jk_{1z}z')\widehat{h}(-k_{1z}) \cdot \widehat{z}\widehat{z}
\end{aligned} \tag{325}$$

For $z > z'$, the total field in region 1 is:

$$\begin{aligned}
\bar{\bar{G}}_{11TM} &= -\frac{j}{8\pi^2}\int_{-\infty}^{\infty}dk_x\int_{-\infty}^{\infty}dk_y e^{-jk_x(x-x')-jk_y(y-y')}\cdot\frac{1}{k_{1z}} \\
&\quad \begin{bmatrix} -\widehat{h}(k_{1z})\exp(-jk_{1z}z+2jk_{1z}z') \\ +C_{1t}\exp(-jk_{1z}(z))\widehat{h}(k_{1z}) \\ +D_{1t}\exp(jk_{1z}(z))\widehat{h}(-k_{1z}) \end{bmatrix}\exp(-jk_{1z}z')\widehat{h}(-k_{1z})\cdot\bar{\bar{I}}_t \\
&\quad -\frac{j}{8\pi^2}\int_{-\infty}^{\infty}dk_x\int_{-\infty}^{\infty}dk_y e^{-jk_x(x-x')-jk_y(y-y')}\cdot\frac{1}{k_{1z}} \\
&\quad \begin{bmatrix} \widehat{h}(k_{1z})\exp(-jk_{1z}z+2jk_{1z}z') \\ +C_{1z}\exp(-jk_{1z}(z))\widehat{h}(k_{1z}) \\ +D_{1z}\exp(jk_{1z}(z))\widehat{h}(-k_{1z}) \end{bmatrix}\exp(-jk_{1z}z')\widehat{h}(-k_{1z})\cdot\widehat{z}\widehat{z} \qquad (326)
\end{aligned}$$

Note that there is a minus sign introduced.

Match boundary condition

$$\widehat{z}\times\bar{\bar{G}}_{TM}\text{ at }z = 0 \qquad (327)$$

$$\widehat{z}\times\nabla\times\bar{\bar{G}}_{TM}\text{ at }z = 0 \qquad (328)$$

gives:

$$\left[-\exp(2jk_{1z}z')+C_{1t}-D_{1t}\right]\frac{k_{1z}}{k_1} = T_t^{TM}\frac{k_z}{k} \qquad (329)$$

$$\left[\exp(2jk_{1z}z')+C_{1z}-D_{1z}\right]\frac{k_{1z}}{k_1} = T_z^{TM}\frac{k_z}{k} \qquad (330)$$

$$\left[-\exp(2jk_{1z}z')+C_{1t}+D_{1t}\right]k_1 = T_t^{TM}k \qquad (331)$$

$$\left[\exp(2jk_{1z}z')+C_{1z}+D_{1z}\right]k_1 = T_z^{TM}k \qquad (332)$$

Solve equation (323)(324) and (329)-(332) and we have:

$$
\begin{aligned}
C_{1t} &= \frac{\exp(2jk_{1z}z')(1-\frac{k^2k_{1z}}{k_1^2k_z})+1+\frac{k^2k_{1z}}{k_1^2k_z}}{(1-\frac{k^2k_{1z}}{k_1^2k_z})+\exp(2jk_{1z}d)(1+\frac{k^2k_{1z}}{k_1^2k_z})} \\
&= \frac{\exp(2jk_{1z}z')R_{01}^{TM}+1}{R_{01}^{TM}+\exp(2jk_{1z}d)} \\
&= \frac{\exp(2jk_{1z}z')R_{01}^{TM}+1}{1+\exp(-2jk_{1z}d)R_{01}^{TM}}\exp(-2jk_{1z}d) \qquad (333)
\end{aligned}
$$

$$
\begin{aligned}
D_{1t} &= C_{1t}\exp(2jk_{1z}d)-1 \\
&= \frac{R_{01}^{TM}(\exp(2jk_{1z}z')-\exp(-2jk_{1z}d))}{1+\exp(-2jk_{1z}d)R_{01}^{TM}} \qquad (334)
\end{aligned}
$$

$$
\begin{aligned}
C_{1z} &= \frac{\exp(2jk_{1z}z')(-1+\frac{k^2k_{1z}}{k_1^2k_z})+1+\frac{k^2k_{1z}}{k_1^2k_z}}{(1-\frac{k^2k_{1z}}{k_1^2k_z})+\exp(2jk_{1z}d)(1+\frac{k^2k_{1z}}{k_1^2k_z})} \\
&= \frac{-\exp(2jk_{1z}z')R_{01}^{TM}+1}{R_{01}^{TM}+\exp(2jk_{1z}d)} \\
&= \frac{-\exp(2jk_{1z}z')R_{01}^{TM}+1}{1+\exp(-2jk_{1z}d)R_{01}^{TM}}\exp(-2jk_{1z}d) \qquad (335)
\end{aligned}
$$

$$
\begin{aligned}
D_{1z} &= C_{1z}\exp(2jk_{1z}d)-1 \\
&= -\frac{R_{01}^{TM}(\exp(2jk_{1z}z')+\exp(-2jk_{1z}d))}{1+\exp(-2jk_{1z}d)R_{01}^{TM}} \qquad (336)
\end{aligned}
$$

6.2.3 Reduction to single integral

Use the reduction to single integral technique in the previous section. we have for TE waves:

$$
\begin{aligned}
&\bar{\bar{G}}_{11TE} \\
&= -\frac{j}{8\pi^2}\int_{-\infty}^{\infty}dk_x\int_{-\infty}^{\infty}dk_y e^{-jk_x(x-x')-jk_y(y-y')}\cdot \\
&\quad \frac{1}{k_{1z}}\begin{bmatrix} \exp(-jk_{1z}|z-z'|)\widehat{e}(-k_{1z})\widehat{e}(-k_{1z}) \\ +A_1\exp(-jk_{1z}(z+z'))\widehat{e}(k_{1z})\widehat{e}(-k_{1z}) \\ +B_1\exp(jk_{1z}(z-z'))\widehat{e}(-k_{1z})\widehat{e}(-k_{1z}) \end{bmatrix} \qquad (337)
\end{aligned}
$$

then

$$
\begin{aligned}
& G_{11TExx} \\
= & -\frac{j}{4\pi}\int_0^\infty dk_\rho k_\rho \frac{1}{k_{1z}} \begin{bmatrix} \exp(-jk_{1z}|z-z'|) \\ +A_1\exp(-jk_{1z}(z+z')) \\ +B_1\exp(jk_{1z}(z-z')) \end{bmatrix} \\
& \left[\frac{J_1(k_\rho\rho)}{k_\rho\rho}\cos^2\phi + J_1'(k_\rho\rho)\sin^2\phi\right] \qquad (338)
\end{aligned}
$$

$$
\begin{aligned}
& G_{11TExy} \\
= & \; G_{11TEyx} \\
= & \frac{j}{4\pi}\int_0^\infty dk_\rho k_\rho \frac{1}{k_{1z}} \begin{bmatrix} \exp(-jk_{1z}|z-z'|) \\ +A_1\exp(-jk_{1z}(z+z')) \\ +B_1\exp(jk_{1z}(z-z')) \end{bmatrix} \\
& \left[J_1'(k_\rho\rho) - \frac{J_1(k_\rho\rho)}{k_\rho\rho}\right]\sin\phi\cos\phi \qquad (339)
\end{aligned}
$$

$$
\begin{aligned}
& G_{11TEyy} \\
= & -\frac{j}{4\pi}\int_0^\infty dk_\rho k_\rho \begin{bmatrix} \exp(-jk_{1z}|z-z'|) \\ +A_1\exp(-jk_{1z}(z+z')) \\ +B_1\exp(jk_{1z}(z-z')) \end{bmatrix} \\
& \left[\frac{J_1(k_\rho\rho)}{k_\rho\rho}\sin^2\phi + J_1'(k_\rho\rho)\cos^2\phi\right] \qquad (340)
\end{aligned}
$$

For TM waves, it is more complicated.

For $z > z'$

$$
\begin{aligned}
\bar{\bar{G}}_{11TM} &= -\frac{j}{8\pi^2}\int_{-\infty}^{\infty} dk_x \int_{-\infty}^{\infty} dk_y e^{-jk_x(x-x')-jk_y(y-y')} \cdot \frac{1}{k_{1z}} \\
&\quad \begin{bmatrix} -\widehat{h}(k_{1z})\exp(-jk_{1z}(z-z'))\widehat{h}(-k_{1z}) \\ +C_{1t}\exp(-jk_{1z}(z+z'))\widehat{h}(k_{1z})\widehat{h}(-k_{1z}) \\ +D_{1t}\exp(jk_{1z}(z-z'))\widehat{h}(-k_{1z})\widehat{h}(-k_{1z}) \end{bmatrix} \cdot \bar{\bar{I}}_t \\
&\quad -\frac{j}{8\pi^2}\int_{-\infty}^{\infty} dk_x \int_{-\infty}^{\infty} dk_y e^{-jk_x(x-x')-jk_y(y-y')} \cdot \frac{1}{k_{1z}} \\
&\quad \begin{bmatrix} \widehat{h}(k_{1z})\exp(-jk_{1z}(z-z')) \\ +C_{1z}\widehat{h}(k_{1z})\exp(-jk_{1z}(z+z')) \\ +D_{1z}\exp(jk_{1z}(z-z'))\widehat{h}(-k_{1z}) \end{bmatrix} \frac{k_\rho}{k_1}\widehat{z}
\end{aligned} \tag{341}
$$

thus

$$
\begin{aligned}
G_{11TMxx} &= -\frac{j}{4\pi}\int_0^{\infty} dk_\rho k_\rho \frac{1}{k_{1z}} \begin{bmatrix} \exp(-jk_{1z}(z-z')) \\ -C_{1t}\exp(-jk_{1z}(z+z')) \\ +D_{1t}\exp(jk_{1z}(z-z')) \end{bmatrix} \\
&\quad \frac{k_{1z}^2}{k_1^2}\left[\frac{J_1(k_\rho\rho)}{k_\rho\rho}\sin^2\phi + J_1'(k_\rho\rho)\cos^2\phi\right]
\end{aligned} \tag{342}
$$

$$
\begin{aligned}
G_{11TMxy} &= G_{11TMyx} \\
&= -\frac{j}{4\pi}\int_0^{\infty} dk_\rho k_\rho \frac{1}{k_{1z}} \begin{bmatrix} \exp(-jk_{1z}(z-z')) \\ -C_{1t}\exp(-jk_{1z}(z+z')) \\ +D_{1t}\exp(jk_{1z}(z-z')) \end{bmatrix} \\
&\quad \frac{k_{1z}^2}{k_1^2}\sin\phi\cos\phi\left[J_1'(k_\rho\rho) - \frac{J_1(k_\rho\rho)}{k_\rho\rho}\right]
\end{aligned} \tag{343}
$$

$$G_{11TMyy} = -\frac{j}{4\pi}\int_0^\infty dk_\rho k_\rho \frac{1}{k_{1z}} \begin{bmatrix} \exp(-jk_{1z}(z-z')) \\ -C_{1t}\exp(-jk_{1z}(z+z')) \\ +D_{1t}\exp(jk_{1z}(z-z')) \end{bmatrix} \frac{k_{1z}^2}{k_1^2}\left[\frac{J_1(k_\rho\rho)}{k_\rho\rho}\cos^2\phi + J_1'(k_\rho\rho)\sin^2\phi\right] \tag{344}$$

$$G_{11TMzx} = -\frac{j}{4\pi}\int_0^\infty dk_\rho k_\rho \frac{1}{k_{1z}} \begin{bmatrix} -\exp(-jk_{1z}(z-z')) \\ +C_{1t}\exp(-jk_{1z}(z+z')) \\ +D_{1t}\exp(jk_{1z}(z-z')) \end{bmatrix} \frac{k_{1z}}{k_1^2}k_\rho\left[-jJ_1(k_\rho\rho)\cos\phi\right] \tag{345}$$

$$G_{11TMzy} = -\frac{j}{4\pi}\int_0^\infty dk_\rho k_\rho \frac{1}{k_{1z}} \begin{bmatrix} -\exp(-jk_{1z}(z-z')) \\ +C_{1t}\exp(-jk_{1z}(z+z')) \\ +D_{1t}\exp(jk_{1z}(z-z')) \end{bmatrix} \frac{k_{1z}}{k_1^2}k_\rho\left[-jJ_1(k_\rho\rho)\sin\phi\right] \tag{346}$$

$$G_{11TMxz} = -\frac{j}{4\pi}\int_0^\infty dk_\rho k_\rho \frac{1}{k_{1z}} \begin{bmatrix} -\exp(-jk_{1z}(z-z')) \\ -C_{1z}\exp(-jk_{1z}(z+z')) \\ +D_{1z}\exp(jk_{1z}(z-z')) \end{bmatrix} \frac{k_{1z}}{k_1^2}k_\rho\left[-jJ_1(k_\rho\rho)\cos\phi\right] \tag{347}$$

$$G_{11TMyz} = -\frac{j}{4\pi}\int_0^\infty dk_\rho k_\rho \frac{1}{k_{1z}} \begin{bmatrix} -\exp(-jk_{1z}(z-z')) \\ -C_{1z}\exp(-jk_{1z}(z+z')) \\ +D_{1z}\exp(jk_{1z}(z-z')) \end{bmatrix} \frac{k_{1z}}{k_1^2}k_\rho\left[-jJ_1(k_\rho\rho)\sin\phi\right] \tag{348}$$

$$G_{11TMzz} = -\frac{j}{4\pi}\int_0^\infty dk_\rho k_\rho \frac{1}{k_{1z}} \begin{bmatrix} \exp(-jk_{1z}(z-z')) \\ +C_{1z}\exp(-jk_{1z}(z+z')) \\ +D_{1z}\exp(jk_{1z}(z-z')) \end{bmatrix} \frac{k_\rho^2}{k_1^2} J_0(k_\rho\rho) \tag{349}$$

For $z < z'$

$$\begin{aligned} \overline{\overline{G}}_{11TM} &= -\frac{j}{8\pi^2}\int_{-\infty}^\infty dk_x \int_{-\infty}^\infty dk_y e^{-jk_x(x-x')-jk_y(y-y')} \cdot \frac{1}{k_{1z}} \\ &\quad \begin{bmatrix} \widehat{h}(-k_{1z})\exp(jk_{1z}(z-z'))\widehat{h}(-k_{1z}) \\ +C_{1t}\exp(-jk_{1z}(z+z'))\widehat{h}(k_{1z})\widehat{h}(-k_{1z}) \\ +D_{1t}\exp(jk_{1z}(z-z'))\widehat{h}(-k_{1z})\widehat{h}(-k_{1z}) \end{bmatrix} \cdot \overline{\overline{I}}_t \\ &\quad -\frac{j}{8\pi^2}\int_{-\infty}^\infty dk_x \int_{-\infty}^\infty dk_y e^{-jk_x(x-x')-jk_y(y-y')} \cdot \\ &\quad \frac{1}{k_{1z}} \begin{bmatrix} \widehat{h}(-k_{1z})\exp(jk_{1z}(z-z')) \\ +C_{1z}\exp(-jk_{1z}(z+z'))\widehat{h}(k_{1z}) \\ +D_{1z}\exp(jk_{1z}(z-z'))\widehat{h}(-k_{1z}) \end{bmatrix} \frac{k_\rho}{k_1}\widehat{z} \end{aligned} \tag{350}$$

thus:

$$\begin{aligned} G_{11TMxx} &= -\frac{j}{4\pi}\int_0^\infty dk_\rho k_\rho \frac{1}{k_{1z}} \begin{bmatrix} \exp(jk_{1z}(z-z')) \\ -C_{1t}\exp(-jk_{1z}(z+z')) \\ +D_{1t}\exp(jk_{1z}(z-z')) \end{bmatrix} \\ &\quad \frac{k_{1z}^2}{k_1^2}\left[\frac{J_1(k_\rho\rho)}{k_\rho\rho}\sin^2\phi + J_1'(k_\rho\rho)\cos^2\phi\right] \end{aligned} \tag{351}$$

$$\begin{aligned} G_{11TMyy} &= G_{11TMyx} \\ &= -\frac{j}{4\pi}\int_0^\infty dk_\rho k_\rho \frac{1}{k_{1z}} \begin{bmatrix} \exp(jk_{1z}(z-z')) \\ -C_{1t}\exp(-jk_{1z}(z+z')) \\ +D_{1t}\exp(jk_{1z}(z-z')) \end{bmatrix} \\ &\quad \frac{k_{1z}^2}{k_1^2}\sin\phi\cos\phi\left[J_1'(k_\rho\rho) - \frac{J_1(k_\rho\rho)}{k_\rho\rho}\right] \end{aligned} \tag{352}$$

$$G_{11TMyy} = -\frac{j}{4\pi}\int_0^\infty dk_\rho k_\rho \frac{1}{k_{1z}} \begin{bmatrix} \exp(jk_{1z}(z-z')) \\ -C_{1t}\exp(-jk_{1z}(z+z')) \\ +D_{1t}\exp(jk_{1z}(z-z')) \end{bmatrix} \frac{k_{1z}^2}{k_1^2}\left[\frac{J_1(k_\rho\rho)}{k_\rho\rho}\cos^2\phi + J_1'(k_\rho\rho)\sin^2\phi\right] \tag{353}$$

$$G_{11TMzx} = -\frac{j}{4\pi}\int_0^\infty dk_\rho k_\rho \frac{1}{k_{1z}} \begin{bmatrix} \exp(jk_{1z}(z-z')) \\ +C_{1t}\exp(-jk_{1z}(z+z')) \\ +D_{1t}\exp(jk_{1z}(z-z')) \end{bmatrix} \frac{k_{1z}}{k_1^2}k_\rho\left[-jJ_1(k_\rho\rho)\cos\phi\right] \tag{354}$$

$$G_{11TMzy} = -\frac{j}{4\pi}\int_0^\infty dk_\rho k_\rho \frac{1}{k_{1z}} \begin{bmatrix} \exp(jk_{1z}(z-z')) \\ +C_{1t}\exp(-jk_{1z}(z+z')) \\ +D_{1t}\exp(jk_{1z}(z-z')) \end{bmatrix} \frac{k_{1z}}{k_1^2}k_\rho\left[-jJ_1(k_\rho\rho)\sin\phi\right] \tag{355}$$

$$G_{11TMxz} = -\frac{j}{4\pi}\int_0^\infty dk_\rho k_\rho \frac{1}{k_{1z}} \begin{bmatrix} \exp(jk_{1z}(z-z')) \\ -C_{1z}\exp(-jk_{1z}(z+z')) \\ +D_{1z}\exp(jk_{1z}(z-z')) \end{bmatrix} \frac{k_{1z}}{k_1^2}k_\rho\left[-jJ_1(k_\rho\rho)\cos\phi\right] \tag{356}$$

$$G_{11TMyz} = -\frac{j}{4\pi}\int_0^\infty dk_\rho k_\rho \frac{1}{k_{1z}} \begin{bmatrix} \exp(jk_{1z}(z-z')) \\ -C_{1z}\exp(-jk_{1z}(z+z')) \\ +D_{1z}\exp(jk_{1z}(z-z')) \end{bmatrix} \frac{k_{1z}}{k_1^2}k_\rho\left[-jJ_1(k_\rho\rho)\sin\phi\right] \tag{357}$$

$$G_{11TMzz} = -\frac{j}{4\pi}\int_0^\infty dk_\rho k_\rho \frac{1}{k_{1z}} \begin{bmatrix} \exp(jk_{1z}(z-z')) \\ +C_{1z}\exp(-jk_{1z}(z+z')) \\ +D_{1z}\exp(jk_{1z}(z-z')) \end{bmatrix} \frac{k_\rho^2}{k_1^2} J_0(k_\rho\rho) \tag{358}$$

6.3 Magnetic dyadic Green's function in region 1 with source in region 1

This is for the magnetic field generated by the magnetic current sheet at the via aperture (figure 50). The magnetic current source sheet $\overline{M}_s$ flows in the horizontal plane at $z' = -d$. Let $\overline{\overline{I}}_t = \widehat{x}\widehat{x} + \widehat{y}\widehat{y}$ be the transverse dyad. Then the dyadic Green's function for the magnetic field is such that:

$$\overline{H}_1 = -j\omega\varepsilon_1 \iint dx'dy' \overline{\overline{G}}_{11}^{HM}(\overline{r},\overline{r}') \cdot \overline{M}_s(\overline{r}') \tag{359}$$

The primary Green's function is:

$$\begin{aligned} & \overline{\overline{G}}_{11P}^{HM}(\overline{r},\overline{r}') \cdot \overline{\overline{I}}_t \\ = \; & -\frac{j}{8\pi^2}\int_{-\infty}^{\infty} dk_x \int_{-\infty}^{\infty} dk_y e^{-jk_x(x-x')-jk_y(y-y')-jk_{1z}|z-z'|} \cdot \\ & \frac{1}{k_{1z}} \begin{cases} \widehat{e}(k_{1z})\widehat{e}(k_{1z}) \cdot \overline{\overline{I}}_t + \widehat{h}(k_{1z})\widehat{h}(k_{1z}) \cdot \overline{\overline{I}}_t & for \;\; z > z' \\ \widehat{e}(-k_{1z})\widehat{e}(-k_{1z}) \cdot \overline{\overline{I}}_t + \widehat{h}(-k_{1z})\widehat{h}(-k_{1z}) \cdot \overline{\overline{I}}_t & for \;\; z < z' \end{cases} \end{aligned} \tag{360}$$

The response Green's function is:

$$\begin{aligned} & \overline{\overline{G}}_{11R}^{HM}(\overline{r},\overline{r}') \cdot \overline{\overline{I}}_t \\ = \; & -\frac{j}{8\pi^2}\int_{-\infty}^{\infty} dk_x \int_{-\infty}^{\infty} dk_y e^{-jk_x(x-x')-jk_y(y-y')} \cdot \\ & \frac{1}{k_{1z}} \left[\widehat{e}(k_{1z})A_1 e^{-jk_{1z}(z-z')} + \widehat{e}(-k_{1z})B_1 e^{jk_{1z}(z-z')}\right] \widehat{e}(-k_{1z}) \cdot \overline{\overline{I}}_t \\ & -\frac{j}{8\pi^2}\int_{-\infty}^{\infty} dk_x \int_{-\infty}^{\infty} dk_y e^{-jk_x(x-x')-jk_y(y-y')} \cdot \\ & \frac{1}{k_{1z}} \left[\widehat{h}(k_{1z})C_1 e^{-jk_{1z}(z-z')} + \widehat{h}(-k_{1z})D_1 e^{jk_{1z}(z-z')}\right] \widehat{h}(-k_{1z}) \cdot \overline{\overline{I}}_t \end{aligned} \tag{361}$$

The boundary condition is that the tangential electric field is equal to zero at $z = -d$:

$$\widehat{z} \times \nabla \times \overline{\overline{G}}(\overline{r},\overline{r}') \cdot \overline{\overline{I}}_t = 0 \text{ at } z = -d \tag{362}$$

which gives:

$$-e^{-jk_{1z}(z+d)} + A_1 e^{jk_{1z}(z'+d)} - B_1 e^{-jk_{1z}(z'+d)} = 0 \quad (363)$$

$$e^{-jk_{1z}(z+d)} + C_1 e^{jk_{1z}(z'+d)} + D_1 e^{-jk_{1z}(z'+d)} = 0 \quad (364)$$

The transmitted field in region 0 is:

$$\begin{aligned} & \overline{\overline{G}}_{01}^{HM}(\bar{r},\bar{r}') \cdot \overline{\overline{I}}_t \\ = & -\frac{j}{8\pi^2}\int_{-\infty}^{\infty} dk_x \int_{-\infty}^{\infty} dk_y e^{-jk_x(x-x')-jk_y(y-y')} \cdot \\ & \frac{1}{k_{1z}}\left[\widehat{e}(k_z)T^{TM}e^{-jk_{1z}z}\right] e^{jk_{1z}z'}\widehat{e}(-k_{1z}) \cdot \overline{\overline{I}}_t \\ & -\frac{j}{8\pi^2}\int_{-\infty}^{\infty} dk_x \int_{-\infty}^{\infty} dk_y e^{-jk_x(x-x')-jk_y(y-y')} \cdot \\ & \frac{1}{k_{1z}}\left[\widehat{h}(k_z)T^{TE}e^{-jk_{1z}z}\right] e^{jk_{1z}z'}\widehat{h}(-k_{1z}) \cdot \overline{\overline{I}}_t \end{aligned} \quad (365)$$

$$\begin{aligned} & \nabla \times \overline{\overline{G}}_{01}^{HM}(\bar{r},\bar{r}') \cdot \overline{\overline{I}}_t \\ = & -\frac{k}{8\pi^2}\int_{-\infty}^{\infty} dk_x \int_{-\infty}^{\infty} dk_y e^{-jk_x(x-x')-jk_y(y-y')} \cdot \\ & \frac{1}{k_{1z}}\left[-\widehat{h}(k_z)T^{TM}e^{-jk_{1z}z}\right] e^{jk_{1z}z'}\widehat{e}(-k_{1z}) \cdot \overline{\overline{I}}_t \\ & -\frac{k}{8\pi^2}\int_{-\infty}^{\infty} dk_x \int_{-\infty}^{\infty} dk_y e^{-jk_x(x-x')-jk_y(y-y')} \cdot \\ & \frac{1}{k_{1z}}\left[\widehat{e}(k_z)T^{TE}e^{-jk_{1z}z}\right] e^{jk_{1z}z'}\widehat{h}(-k_{1z}) \cdot \overline{\overline{I}}_t \end{aligned} \quad (366)$$

Matching fields at $z = 0$ gives:

$$e^{jk_{1z}z'} + A_1 e^{jk_{1z}(z')} + B_1 e^{-jk_{1z}z'} = T^{TM}e^{jk_{1z}z'} \quad (367)$$

$$e^{jk_{1z}z'} - C_1 e^{jk_{1z}z'} + D_1 e^{-jk_{1z}z'} = -T^{TE}e^{jk_{1z}z'}\frac{k_z k_1}{k k_{1z}} \quad (368)$$

$$e^{jk_{1z}(z')} + A_1 e^{jk_{1z}(z')} - B_1 e^{-jk_{1z}(z')} = T^{TM}e^{jk_{1z}z'}\frac{k_z}{k_{1z}}\frac{\varepsilon_1}{\varepsilon} \quad (369)$$

$$-e^{jk_{1z}(z')} + C_1 e^{jk_{1z}(z')} + D_1 e^{-jk_{1z}(z')} = \frac{k_1}{k}T^{TE}e^{jk_{1z}z'} \quad (370)$$

Solving equations (363)(364) and the above 4 equations gives that for $z' = -d$:

$$B_1 = \frac{2R_{10}^{TM}e^{-2jk_{1z}d}}{1+R_{01}^{TM}e^{-2jk_{1z}d}} \tag{371}$$

$$A_1 = (1+B_1) = \frac{1-R_{01}^{TM}e^{-2jk_{1z}d}}{1+R_{01}^{TM}e^{-2jk_{1z}d}} \tag{372}$$

$$D_1 = -\frac{2e^{-2jk_{1z}d}R_{10}^{TE}}{\left(1+e^{-2jk_{1z}d}R_{10}^{TE}\right)} \tag{373}$$

$$C_1 = -(1+D_1) = -\frac{1-e^{-2jk_{1z}d}R_{10}^{TE}}{1+e^{-2jk_{1z}d}R_{10}^{TE}} \tag{374}$$

References

[1] W.D. Becker, P.H. Harms and R. Mittra, "Time-Domain Electromagnetic Analysis of Interconnects in a Computer Chip Package", *IEEE Trans. on MTT*, Vol. 40, No. 12, 1992, p2155-2163

[2] B. Chen, D.G. Fang and B.H. Zhou, "Modified Berenger PML Absorbing Boundary Condition for FD-TD Meshes", *IEEE Microwave and Guided Wave Letters*, Vol. 5, No. 11, 1995

[3] W.C. Chew and W.H. Weedon, "A 3D Perfectly Matched Medium from Modified Maxwell's Equations with Stretched Coordinates", *Microwave and Optical Technology Letters*, Vol. 7, No. 13, 1994, p599-604

[4] B. Archambeault, C. Brench and O. M. Ramahi, "Emi Emc Computational Modeling Handbook", Kluwer Academic Publishers, 1998

[5] G.W. Pan; X. Zhu; Gilbert, B.K., "Analysis of transient behavior of vertical interconnects in stacked circuit board layers using quasi-static techniques", *IEEE Trans. Advanced Packaging*, Vol. 18, Aug. 1995, pp521-531

[6] Morsey, J.; Coperich, K.; Okhmatovski, V.; Cangellaris, A.C.; Ruehli, A., "A new broadband transmission line model for accurate simulation of dispersive interconnects", *Electronics Packaging Technology Conference, 2000. (EPTC 2000) 2000*, pp345-351

[7] Specks, J.W., "Efficient three-dimensional LCR extraction and modeling of VLSI packages", *Circuits and Systems, 1993., Proceedings of the 36th Midwest Symposium on . 1993*, pp1166-1169

[8] Arora, N.D.; Raol, K.V.; Schumann, R.; Richardson, L.M., "Modeling and extraction of interconnect capacitances for multilayer VLSI circuits", *IEEE Trans. Computer-Aided Design of Integrated Circuits and Systems*, Vol. 15, Jan. 1996, pp58-67

[9] Sun, W.; Wei-Ming Dai, W.; Wei Hong, "Fast parameter extraction of general interconnects using geometry independent measured equation of invariance", *IEEE Trans. Microwave Theory and Techniques*, Vol. 45, May 1997, pp827-836

[10] Y. Cao, Z.F. Li, J.F. Mao, J.F. Mao, "A PEEC with a new capacitance model for circuit simulation of interconnects and packaging structures", *IEEE Trans. Microwave Theory and Techniques*, Vol. 48, Feb. 2000, pp281-287

[11] Brambilla, A.; Maffezzoni, P., "Statistical method for the analysis of interconnects delay in submicrometer layouts", *IEEE Trans. Computer-Aided Design of Integrated Circuits and Systems*, Vol. 20, Aug. 2001, pp957-966

[12] Husain, A., "Models for interconnect capacitance extraction", *International Symposium on Quality Electronic Design*, 2001, pp167-172

[13] R.F. Harrington, "Field computation by moment methods", The Macmillan Company, New York

[14] Carin, L., "Efficient computation of high-frequency two-dimensional effects in multiconductor printed interconnects", *IEEE Trans. Microwave Theory and Techniques*, Vol. 40, Jan. 1992, pp155-158

[15] Li, L.L.; Zhang, Q.J.; Nakhla, M., "A moment method for statistical analysis of high speed VLSI interconnects", *Proceedings of the IEEE. Custom Integrated Circuits Conference*, 1994, pp305-308

[16] M.J. Tsai; C.L. Chen; Alexopoulos, N.G.; T.S. Horng, "Multiple arbitrary shape via-hole and air-bridge transitions in multilayered structures", *IEEE Trans. Microwave Theory and Techniques*, Vol. 44, Dec. 1996, pp2504-2511

[17] Hildebrand, L.T.; Joubert, J., "Full-wave analysis of a new microstrip-to-waveguide interconnect configuration", *IEEE Trans. Microwave Theory and Techniques*, Vol. 48, Jan. 2000, pp1-7

[18] S.Q. Li; Y.X. Yu; K.F. Chan; C.H. Chan; L. Tsang, "A sparse-matrix/canonical grid method for analyzing densely packed interconnects", *IEEE Antennas and Propagation Society International Symposium*, 2000., Vol. 1, 2000, pp128-131

[19] Hayes, T.F.; Barrett, J.J., "Modeling of multiconductor systems for packaging and interconnecting high-speed digital IC's", *IEEE Trans. Computer-Aided Design of Integrated Circuits and Systems*, Vol. 11, April 1992, pp424-431

[20] J.G. Yook; Dib, N.I.; Ratehi, L.P.B., "Characterization of high frequency interconnects using finite difference time domain and finite element methods", *IEEE Trans. Microwave Theory and Techniques*, Vol. 42, Sept. 1994, pp1727-1736

[21] Polycarpou, A.C.; Tirkas, P.A.; Balanis, C.A., "The finite-element method for modeling circuits and interconnects for electronic packaging", *IEEE Trans. Microwave Theory and Techniques*, Vol. 45, Oct. 1997, pp1868-1874

[22] Y. Zhao; Y.Y. Wang, "A new finite-element solution for parameter extraction of multilayer and multiconductor interconnects", *IEEE Microwave and Guided Wave Letters*, Vol. 7, June 1997, pp156-158

[23] J. Tan; G. Pan, "Finite element modeling of 3D interconnection structures", *1998 International Conference on Microwave and Millimeter Wave Technology Proceedings, ICMMT '98.*, 1998, pp957-960

[24] Kyung S.O.; Kuznetsov, D.; Schutt-Aine, J.E., "Capacitance computations in a multilayered dielectric medium using closed-form spatial Green's functions", *IEEE Trans. Microwave Theory and Techniques*, Vol. 42, Aug. 1994, pp1443-1453

[25] G.W. Pan; X. Zhu; Gilbert, B.K., "Analysis of transient behavior of vertical interconnects in stacked circuit board layers using quasi-static techniques", *IEEE Trans. Components, Packaging, and Manufacturing Technology, Part B: Advanced Packaging*, Vol. 18, Aug. 1995, pp521-531

[26] Alimenti, F.; Goebel, U.; Sorrentino, R., "Quasi static analysis of microstrip bondwire interconnects", *IEEE Microwave Symposium Digest, IEEE MTT-S International*, vol. 2, 1995, pp679-682

[27] Alimenti, F.; Mezzanotte, P.; Roselli, L.; Sorrentino, R., "Modeling and characterization of the bonding-wire interconnection", *IEEE Trans. Microwave Theory and Techniques*, Vol. 49, Jan. 2001, pp142-150

[28] M.F. Cátedra, et al., "The CG-FFT method: application of signal processing techniques to electromagnetics"

[29] German, F.J.; Johnson, R.W., "Full wave three-dimensional simulation of Maxwell's equations for the electrical characterization of high-speed interconnects", *IEEE Trans. Components, Hybrids, and Manufacturing Technology*, Vol. 13, June 1990, pp341-346

[30] Alexopoulos, N.G.; S.C. Wu, "Frequency-independent equivalent circuit model for microstrip open-end and gap discontinuities", *IEEE Trans. Microwave Theory and Techniques*, Vol. 42, July 1994, pp1268-1272

[31] Bernardi, P.; Cicchetti, R.; Faraone, A., "A full-wave characterization of an interconnecting line printed on a dielectric slab backed by a gridded ground plane", *IEEE Trans. Electromagnetic Compatibility*, Vol. 38, Aug. 1996, pp237-243

[32] Pinello, W.; Ruehli, A.; Cangellaris, A., "Analysis of interconnect and package structures using PEEC models with radiated emissions", *IEEE 1997 International Symposium on Electromagnetic Compatibility*, 1997, pp353-358

[33] Drissi, M.; Elkandoussi, M.; Kergonou, G.; Zak, T.; Xavier, C., "A full-wave characterization of PCB having various ground plane shapes", *2001 International Symposium on Electromagnetic Compatibility*, 2001, pp1213-1216

[34] L. Tsang, "Near-field radiation from microstrip lines", *Microwave and Optical Technology Letters*, vol. 19, pp. 176-184, Oct. 1998.

[35] L. Tsang, J. Cha and J.R. Thomas, "Electric fields of spatial Green's functions of microstrip structures and applications to the calculations of impedance matrix elements", *Microwave and Optical Technology Letters*, vol. 20, pp. 90-97, Jan. 1999.

[36] Zhu, N.Y.; Landstorfer, F.M., "Application of MFIE to three-dimensional conducting waveguide transitions of arbitrary shape", *Electronics Letters*, Vol. 26, Jan. 1990, pp143-145

[37] W. Sun, C.A. Balanis, "MFIE analysis and design of ridged waveguides", *IEEE Transactions on MTT*, Vol. 41, Nov. 1993, pp. 1965 -1971

[38] D.M. Pozar, "Input impedance and mutual coupling of rectangular microstrip antennas", *IEEE Trans. Antennas and Propagation*, vol. AP-30, pp. 1191-1196, Nov. 1982.

[39] McLean, J.; Itoh, T., "Full wave modeling of electrically wide microstrip open end discontinuities via a deterministic spectral domain method", *IEEE MTT-S International Microwave Symposium Digest*, 1990, pp1155-1158

[40] Sabry, R.; Chaudhuri, S.K., "Analysis of suspended substrate stripline discontinuities using full-wave spectral domain approach", *IEEE Antennas and Propagation Society International Symposium*, 1992. AP-S. 1992 Digest., pp2288-2291

[41] Shively, D., "Scattering from perfectly conducting and resistive strips on a grounded dielectric slab", *IEEE Trans. Antennas and Propagation*, Vol. 42, April 1994, pp552-556

[42] Li, K., "General full-wave Green's functions in spectral domain for arbitrarily multilayered dielectric media", *IEEE MTT-S International Microwave Symposium Digest*, Vol. 3, 1997, pp1571-1574

[43] M. Kahrizi, T.K. Sarkar and Z.A. Maricevic, "Analysis of a wide radiating slot in the ground plane of a microstrip line", *IEEE Trans. Microwave Theory Tech.*, vol. 41, pp. 29-37, Jan. 1993.

[44] Dural, G.; Aksun, M.I., "Closed-form Green's functions for general sources and stratified media", *IEEE Trans. Microwave Theory and Techniques*, Vol. 43, July 1995, pp1545-1552

[45] R.C. Hsieh; J.T. Kuo, "Fast full-wave analysis of planar microstrip circuit elements in stratified media", *IEEE Trans. Microwave Theory and Techniques*, Vol. 46, Sept. 1998, pp1291-1297

[46] F. Ling; D. Jiao; J.M. Jin, "Efficient electromagnetic modeling of microstrip structures in multilayer media", *IEEE Trans. Microwave Theory and Techniques*, Vol. 47, Sept. 1999, pp1810-1818

[47] L. Tsang, J.H. Cha, C.C. Huang and C.H. Chan, "Surface Electric Fields of Multilayered Medium Green's Functions and Calculation of Impedance Matrix Elements of Microstrip Structure", *IEE Proc. Microwaves, Antennas and Propagation*, Vol. 147, June 2000, pp179-186

[48] L. Tsang, C.C. Huang and C.H. Chan, "Surface electric fields and impedance matrix elements of stratified media", *IEEE Trans. Antennas and Propagation*, Vol. 48, Oct. 2000, pp1533-1543

[49] S.M. Rao, D.R. Wilton and A.W. Glisson, "Electromagnetic scattering by surfaces of arbitrary shape", *IEEE Trans. Antennas and Propagation*, vol. AP-30, pp. 409-418, May, 1982.

[50] D.M. Pozar, "A reciprocity method of analysis for printed slot and slot-coupled microstrip antennas", *IEEE Trans. Antennas and Propagation*, vol. AP-34, pp1439-1446, Dec. 1986.

[51] Cina, J.L.; Carin, L., "Mode conversion and leaky-wave excitation at open-end coupled-microstrip discontinuities", *IEEE Trans. Microwave Theory and Techniques*, Vol. 43, Sept. 1995, pp2066-2072

[52] A. Djordjevic and T. K. Sarkar, "Computation of inductance of simple vias between two striplines above a ground plane", *IEEE Trans. Microwave Theory and Techniques*, Vol. 33, pp. 268-269, Mar. 1985.

[53] A. E. Ruehli, "Equivalent circuit models for three-dimensional multiconductor systems", *IEEE Trans. Microwave Theory and Techniques*, Vol. 22, pp. 216-221, Mar. 1974.

[54] T. Wang, R. F. Harrington and J. R. Mautz, "Quasi-static analysis of a microstrip via through a hole in a ground plane", *IEEE Trans. Microwave Theory and Techniques*, Vol. 36, No. 6, pp. 1008-1013, 1988.

[55] P. Kok and D. D. Zutter, "Capacitance of a circular symmetric model of a via hole including finite ground plane thickness", *IEEE Trans. Microwave Theory and Techniques*, Vol. 39, pp. 1229-1234, July 1991.

[56] P.A. Kok and D.D. Zutter, "Scalar magnetostatic potential approach to the prediction of the excess inductance of grounded via's and via's through a hole in a ground plane," *IEEE Trans. Microwave Theory and Techniques*, vol. 42, no. 7, pp. 1229-1237, July 1994

[57] J.P. Quine, H.F. Webster, H.H. Glascock and R.O. Carlson, "Characterization of via connections in silicon circuit boards", *IEEE Trans. Microwave Theory and Techniques*, Vol. 36, pp. 21-27, Jan. 1988.

[58] A.W. Mathis, A.F. Peterson and C.M. Butler, "Rigorous and Simplified Models for the Capacitance of a Circularly Symmetric Via", *IEEE Trans. Microwave Theory and Techniques*, Vol. 45, No. 10, pp. 1875-1878, 1997.

[59] J. Tan: G. Pan, "Finite element modeling of 3D interconnection structures", *International Conference on Microwave and Millimeter Wave Technology Proceedings. ICMMT '98.*, 1998, pp957-960

[60] S-G Hsu and R-B Wu, "Full wave characterization of a through hole via using the matrix-penciled moment method", *IEEE Trans. Microwave Theory and Techniques*, Vol. 42, No. 8, pp. 1540-1547, 1994.

[61] S-G Hsu and R-B Wu, "Full-wave characterization of a through hole via in multilayered packaging", *IEEE Trans. Microwave Theory and Techniques*, Vol. 43, No. 5, pp. 1073-1081, 1994.

[62] Q. Gu, Y. E. Yang and M. A. Tassoudji, "Modeling and analysis of vias in multilayered integrated circuits", *IEEE Trans. Microwave Theory and Techniques*, Vol. 41, No. 2, pp. 206-214, 1993.

[63] Q. Gu, A. Tassoudji, S. Y. Poh, R. T. Shin and J. A. Kong, "Coupled noise analysis for adjacent vias in multilayered digital circuits", *IEEE Trans. Circuits and Systems*, Vol. 41, No. 12, pp 796-804, 1994.

[64] E. Laermans, J.D. Geest, D.D. Zutter, F. Olyslager, S. Sercu, and D. Morlion, "Modeling differential via holes," *IEEE Trans. on Advanced Packaging*, vol. 24, no. 3, pp. 357-363, Aug. 2001

[65] D. V. Otto, "The admittance of cylindrical antennas driven from a coaxial line", *Radio Science*, Vol. 2, No. 9, pp. 1031-1042, 1967.

[66] L. Tsang, J. A. Kong, and R. T. Shin, "Theory of Microwave Remote Sensing", Wiley Interscience, 1985.

[67] L. Tsang, J. A. Kong and K. H. Ding, "Scattering of Electromagnetic Waves: Vol. 1 Theory and Applications", Wieley Interscience, New York , 2000

[68] L. Tsang, J. A. Kong, K. H. Ding, and C. Ao, "Scattering of Electromagnetic Waves: Vol. 2 Numerical Simulations", Wiley Interscience, New York, 2001.

[69] L. Tsang, H. Chen, C. Huang and V. Jandhyala, "Modeling of multiple scattering among vias in planar waveguide using foldy-lax equations", *Microwave and Optical Technology Letters*, Vol. 31, No. 3, November 2001, pp 201-208

[70] Y.B. Hua, T.K. Sarkar, "Generalized pencil-of-function method for extracting poles of an EM system from its transient response", *IEEE Trans. Antenna Propagat.*, vol. 37, pp. 229-234, Feb. 1989.

[71] Fang, J.; Zhao, J.; Zhang, J., "Shorting via arrays for the elimination of package resonance to reduce power supply noise in multi-layered area-array IC packages", *IEEE Symposium on IC/Package Design Integration*, 1998. Proceedings. 1998. pp116-119

[72] Ponchak, G.E.; Donghoon Chun; Jong-Gwan Yook; Katehi, L.P.B., "The use of metal filled via holes for improving isolation in LTCC RF and wireless multichip packages", *IEEE Trans. Advanced Packaging*, Vol. 23, Feb. 2000, pp88-99

[73] Araneo, R.; Celozzi, S., "Differential signalling in printed circuit boards: edge effects, radiation patterns and p.u.l. parameters", *International Symposium on Electromagnetic Compatibility, 2001. EMC. 2001*, Vol. 2, 2001, pp1209-1212

[74] Massoud, Y.; Kawa, J.; MacMillen, D.; White, J., "Modeling and analysis of differential signaling for minimizing inductive crosstalk", *Design Automation Conference*, 2001. Proceedings. 2001, pp804-809

[75] Fornberg, P.E.; Kanda, M.; Lasek, C.; Piket-May, M.; Hall, S.H., "The impact of a nonideal return path on differential signal integrity", *IEEE Trans. Electromagnetic Compatibility*, Vol. 44, Feb. 2002, pp11-15

[76] Sercu, J.; Fache, N.; Libbrecht, F.; De Zutter, D., "Full-wave space-domain analysis of open microstrip discontinuities including the singular current-edge behavior", *IEEE Trans. Microwave Theory and Techniques*, Vol. 41, Sept. 1993, pp1581-1588

[77] Roy, T.; Sarkar, T.K.; Swaminathan, M., "Surface integral formulation for calculating conductor and dielectric losses of various transmission structures", *IEEE Trans. Microwave Theory and Techniques*, Vol. 43, Jan. 1995, pp176-185

[78] Uckun, S.; Sarkar, T.K.; Rao, S.M.; Salazar-Palma, M., "A novel technique for analysis of electromagnetic scattering from microstrip antennas of arbitrary shape", *IEEE Trans. Microwave Theory and Techniques*, Vol. 45, April 1997, pp485-491

[79] Tony, E.S.; Chaudhuri, S.K., "Analysis of shielded lossy multilayered-substrate microstrip discontinuities", *IEEE Trans. Microwave Theory and Techniques*, Vol. 49, April 2001, pp701-711

[80] Knockaert, L.; Sercu, J.; De Zutter, D., "Generalized polygonal basis functions for the electromagnetic simulation of complex geometrical planar structures", *IEEE MTT-S International Microwave Symposium Digest*, Vol. 2 , 2001, pp1249-1252

[81] A.W. Glisson and D.R. Wilton, "Simple and Efficient Numerical Methods for Problems of Electromagnetic Radiation and Scattering from Surface", *IEEE Trans. Antennas and Propagat.*, vol. 28, No. 5, pp. 593-603, Sept. 1980.

[82] Harokopus, W.P., Jr.; Katehi, P.B., "Characterization of microstrip discontinuities on multilayer dielectric substrates including radiation losses", *IEEE Trans. Microwave Theory and Techniques*, Vol. 37, Dec. 1989, pp2058-2066

[83] Catedra, M.F.; Gago, E., "Spectral domain analysis of conducting patches of arbitrary geometry in multilayer media using the CG-FFT method", *IEEE Trans. Antennas and Propagation*, Vol. 38, Oct. 1990, pp1530-1536

[84] L. Alatan, M.I. Aksun, K. Mahadevan and M. T. Birand, "Analytical Evaluation of the MoM Matrix Elements", *IEEE Trans. Microwave Theory Tech.*, vol. 44, pp. 519-525, April 1996

[85] J.R. Mosig, "Arbitrarily shaped microstrip structures and their analysis with a mixed potential integral equation" *IEEE Trans. Microwave Theory Tech.*, vol. 36, pp. 314-323, Feb. 1988

[86] D.C. Chang and J.X. Zheng, "Electromagnetic Modeling of Passive Circuit Elements in MMIC", *IEEE Trans. Microwave Theory Tech.*, vol. 40, No.9, pp 1741-1747, Sept. 1992.

[87] Sercu, J.; Fache, N.; Libbrecht, F.; De Zutter, D., "Study of gridding and cell-cell interactions in the method of moments analysis of arbitrarily shaped planar circuits", *IEEE MTT-S International Microwave Symposium Digest*, 1993, pp753-756

[88] Sercu, J.; Devos, H.; Fache, N.; De Zutter, D., "Efficient calculation technique for the impedance matrix equation in the MPIE technique for microstrip and slotline planar structures of arbitrary shape", *Antennas and Propagation Society International Symposium, AP-S. Digest* 1993., pp350-353

[89] Sercu, J.; Fache, N.; Libbrecht, F.; Lagasse, P., "Mixed potential integral equation technique for hybrid microstrip-slotline multilayered circuits using a mixed rectangular-triangular mesh", *IEEE Trans. Microwave Theory and Techniques*, Vol. 43, May 1995, pp1162-1172

[90] T. Yu; B. Zhu; W. Cai, "Mix-RWG current basis function and its simple implementation in MoM", *IEEE MTT-S International Microwave Symposium Digest*, 2000, Vol. 2 , 2000, pp1105-1108

[91] Rius, J.M.; Ubeda, E.; Parron, J., "On the testing of the magnetic field integral equation with RWG basis functions in method of moments", *IEEE Trans. Antennas and Propagation*, Vol. 49, Nov. 2001, pp1550-1553

[92] Cai, W.; Yu, T.; Wang, H.; Yu, Y., "High-order mixed RWG basis functions for electromagnetic applications", *IEEE Trans. Microwave Theory and Techniques*, Vol. 49, July 2001, pp1295-1303

[93] T.S. Bird, "Analysis of mutual coupling in finite arrays of different-sized rectangular waveguides", *IEEE Trans. Antennas and Propagation*, Vol. 38, Feb. 1990, pp166-172

[94] D.R. Wilton, S.M. Rao, A.W. Glisson, D.H. Schaubert, O.M. Al-bundak and C.M. Butler, "Potential Integrals for Uniform and Linear Source Distribution on Polygonal and Polyhedral Domains", *IEEE Trans. Antennas and Propagation*, vol. 32, No. 3, pp 276-281, March, 1984

[95] Jorgenson, R.E.; Mittra, R., "Scattering from structured slabs having two-dimensional periodicity", *IEEE Trans. Antennas and Propagation*, Vol. 39, Feb. 1991, pp151-157

[96] Virga, K.; Rahmat-Samii, Y., "Surface currents on conducting plates with multiple apertures", *Antennas and Propagation Society International Symposium, 1994. AP-S. Digest*, Vol. 2 , 1994, pp684-687

[97] P.B. Katehi and N.G. Alexopoulos, "Frequency-dependent characteristics of microstrip discontinuities in millimeter-wave integrated circuits", *IEEE Trans. Microwave Theory Tech.*, Vol. 33, Oct. 1985, pp1029-1035

[98] W.P. Harokopus and P.B. Katehi, "Characterization of microstrip discontinuities on mulitlayer dielectric substrates including radiation losses", *IEEE Trans. Microwave Theory Tech.*, Vol. 37, Dec. 1989, pp2058-2065

[99] Janhsen, A.; Hansen, V., "Determination of the characteristic impedance of single and coupled lines in layered dielectric media", *IEEE MTT-S International Microwave Symposium Digest*, 1991, pp765-768

[100] Junker, G.P.; Kishk, A.A.; Glisson, A.W., "A novel delta gap source model for center fed cylindrical dipoles", *IEEE Trans. Antennas and Propagation*, Vol. 43, May 1995, 537-540

[101] Freeman, C.L.; Butler, C.M., "Analysis of a strip in a waveguide", *IEEE Trans. Antennas and Propagation*, Vol. 45, Nov. 1997, pp1636-1644

[102] Zhu, L.; Wu, K., "Characterization of unbounded multiport microstrip passive circuits using an explicit network-based method of moments", *IEEE Trans. Microwave Theory and Techniques*, Vol. 45, Dec. 1997, pp2114-2124

[103] I.S. Gradshteyn and I.M. Ryzhik, "Table of integrals, series, and products", New York, Academic Press, 1965

VITA

Houfei Chen was born in Shanghai, China in 1973. He received his Bachelor's degree in Electrical Engineering in 1995 from University of Science and Technology of China (USTC), Hefei, China. He received his Master's degree in Electrical Engineering from the same university in 1998 under the supervision of Prof. Jinren Qian. His Master's thesis is in the title of "Theoretical Research and Numerical Simulation on Fiber Gratings". From September 1998 to July 2002, he pursued doctoral research at the Laboratory of Applications and Computations in Electromagnetics and Optics at the University of Washington as a research assistant under the supervision of Prof. Leung Tsang. The dissertation, entitled "Fast Electromagnetic Simulation for Interconnects on High Speed Circuits", was completed at the end of this period.